System size and energy dependence of dilepton production in heavy-ion collisions at 1-2 GeV/nucleon energies

E. L. Bratkovskaya,[1,2] J. Aichelin,[3] M. Thomere,[3] S. Vogel,[1] and M. Bleicher[1,2]
[1]*Institute for Theoretical Physics, Frankfurt University, 60438 Frankfurt-am-Main, Germany*
[2]*Frankfurt Institut for Advanced Studies, Frankfurt University, 60438 Frankfurt-am-Main, Germany*
[3]*SUBATECH, Laboratoire de Physique Subatomique et des Technologies Associées, Université de Nantes-IN2P3/CNRS-Ecole des Mines de Nantes, 4 rue Alfred Kastler, F-44072 Nantes, Cedex 03, France*
(Received 31 December 2012; revised manuscript received 13 April 2013; published 27 June 2013)

We study the dilepton production in heavy-ion collisions at energies of 1–2 GeV/nucleon as well as in proton-induced pp, pn, pd, and $p + A$ reactions from 1 up to 3.5 GeV where data have been taken by the HADES Collaboration. For the analysis we employ three different transport models: the microscopic off-shell Hadron-String-Dynamics (HSD) transport approach, the Isospin Quantum Molecular Dynamics (IQMD) approach, as well as the Ultra-relativistic Quantum Molecular Dynamics (UrQMD) approach. We find that the HSD and IQMD models describe very reasonably the elementary pp, pn, and πN reactions despite different assumptions on quantities like the excitation function of the Δ multiplicity, where solid experimental constraints are not available. Taking these data on elementary collisions as input, the three models provide a good description of the presently available heavy-ion data. In particular, we confirm the experimentally observed enhancement of the dilepton yield (normalized to the multiplicity of neutral pions N_{π^0}) in heavy-ion collisions with respect to that measured in $NN = (pp + pn)/2$ collisions. We identify two contributions to this enhancement: (a) the pN bremsstrahlung which scales with the number of collisions and not with the number of participants, i.e., pions; (b) the dilepton emission from intermediate Δ's which are part of the reaction cycles $\Delta \to \pi N; \pi N \to \Delta$ and $NN \to N\Delta; N\Delta \to NN$. With increasing system size more generations of intermediate Δ's are created. If such Δ decays into a pion, the pion can be reabsorbed; however, if it decays into a dilepton, the dilepton escapes from the system. Thus, experimentally one observes only one pion (from the last produced Δ), whereas the dilepton yield accumulates the contributions from all Δ's of the cycle. We show as well that the Fermi motion enhances the production of pions and dileptons in the same way. Furthermore, employing the off-shell HSD approach, we explore the influence of in-medium effects like the modification of self-energies and spectral functions of the vector mesons owing to their interactions with the hadronic environment. We find only a modest influence of the in-medium effects on the dilepton spectra in the invariant mass range where data with small error bars exist.

DOI: 10.1103/PhysRevC.87.064907 PACS number(s): 25.75.−q, 25.40.−h

I. INTRODUCTION

According to the theory of strong interactions, the quantum chromodynamics (QCD), hadrons are bound objects of quarks and gluons. The properties of hadrons in vacuum are well known and confirmed by lattice QCD calculations [1] while the properties of hadrons in a strongly interacting environment are the subject of intensive research. QCD-inspired approaches as well as phenomenological models based on phase shifts and SU(3) symmetry [1–14] predict significant changes of hadron properties in a strongly interacting medium. The results of the different models vary substantially. It is therefore one of the challenges of novel experimental heavy-ion physics to study these in-medium modifications of hadrons. Besides the in-medium properties of the antikaon, interesting also for astrophysical reasons, the vector mesons and especially the ρ meson have been in the focus of the theoretical interest because the ρ has the quantum numbers of a photon and can therefore disintegrate into an electron-positron pair. Having only electromagnetic interactions this pair may easily leave the reaction region without further collisions. This makes it possible to reconstruct the invariant mass of the decaying ρ^0. Thus, there is a hope that by measuring the dilepton invariant mass spectra the in-medium mass and width of the ρ meson become experimentally accessible. For this it is necessary to separate the background from known dilepton sources: Dalitz decays of baryonic and mesonic resonances as well as pN and πN bremsstrahlung. At CERN Super Proton Synchrotron energies of 40 and 158 GeV/nucleon such an enhancement above the known background has been measured by the CERES [15] and the NA60 [16] collaborations. The experimental results are compatible with the assumption that in the medium the peak position of the ρ meson mass distribution remains rather unchanged while the width increases considerably (cf. Refs. [17–22]).

At much lower energies, at energies around 1 GeV/nucleon dileptons have been measured in heavy-ion collisions at the LBNL Bevalac in Berkeley by the DLS Collaboration [23–26]. These data led to the so-called "DLS puzzle" because the DLS dilepton yield in C + C and Ca + Ca collisions in the invariant mass range from 0.2 to 0.5 GeV [26] was about five times higher than the results from different transport models at that time using the "conventional" dilepton sources such as bremsstrahlung, π^0, η, ω, and Δ-Dalitz decays and direct decay of vector mesons (ρ, ω, ϕ) [27–29]. This discrepancy remained even after including in the transport calculations the different scenarios for the in-medium modifications of vector meson properties as dropping mass or collisional broadening of the ρ and ω spectral functions [30–33]. To solve this

puzzle was one of the main motivations to build the HADES (High Acceptance Dilepton Spectrometer) detector at GSI in Germany [34–39]. In 2008 the HADES Collaboration confirmed the DLS data [34,35] for C + C at 1.0 GeV/nucleon. In the meantime also the theoretical transport approaches as well as effective models for the elementary NN reactions have been further developed. As it has been suggested in Ref. [40], the DLS puzzle can be solved when incorporating stronger pn and pp bremsstrahlung contributions in line with the updated One-Boson-Exchange (OBE) model calculations from Ref. [41]. The previous OBE approaches [42] used in the old transport calculations for the analysis of the DLS data gave results close to the soft photon approximation. As shown in Ref. [40] the results of the HSD model [off-shell microscopic hadron-string-dynamics (HSD) transport approach] with "enhanced" bremsstrahlung cross sections agree very well with the HADES experimental data for C + C at 1 and 2 GeV/nucleon, as well as with the DLS data for C + C and Ca + Ca at 1 GeV/nucleon, especially when one includes a collisional broadening in the vector-meson spectral functions. Similar results have been obtained by other, independent transport approaches: IQMD [43] and the Rossendorf Boltzmann-Uehling-Uhlenbeck (BUU) method [44].

Despite the fact that theory predicts that the vector meson properties are modified substantially already at energies as low as 1–2 GeV/nucleon, it is quite difficult to observe these changes experimentally. The production yield of ρ^0 and ω mesons is small at these energies and the background from other dilepton sources like Δ-Dalitz decay and pN bremsstrahlung is large in the mass range of interest, $M > 0.4$ GeV. Therefore, the presently available data do not allow for a detailed investigation of the in-medium properties of vector mesons.

This focuses the interest of the present studies to the question whether the invariant mass spectrum below the ρ/ω peak depends on the system size and on the beam energy in a nontrivial way, i.e., whether the dilepton invariant mass spectra can be understood as a superposition of individual pp and pn interactions. In a first publication [37] the HADES Collaboration found that the invariant mass spectra of dileptons, observed in 1 and 2 GeV/nucleon C + C collisions, are practically coincident below $M = 0.4$ GeV if divided by the total number of observed π^0 and after subtracting the η-Dalitz decay contribution. It is strongly suppressed at 1 GeV/nucleon but becomes essential at 2 GeV/nucleon owing to the kinematical threshold for the η production in NN collisions. This scaling with the π^0 number can be interpreted as a scaling with the number of participants $N_{\rm part}$. The HADES Collaboration, comparing the dilepton yield from the light C + C systems with the elementary pp and pd interactions, albeit taken at different energies, has concluded that the dilepton invariant mass spectra in these light systems can be considered as a mere superposition of pn and pp collisions without any "in-medium" enhancement.

In a more recent publication [39] a heavier system, Ar + KCl at 1.75 GeV/nucleon, was investigated and the collaboration came to the conclusion that in this reaction the dilepton invariant mass yield between 0.2 and 0.6 GeV is about 2–3 times larger than expected from a mere superposition of pp and pn collisions [39]. From the analysis of the excess in the transverse-mass slope and from the angular anisotropies the HADES Collaboration concluded that the excess of dileptons in the low invariant mass region scales with the system size very differently than the freeze-out yield of pions and η and that the data are compatible with the assumption that they originate from Δ-Dalitz decays, being suggestive of resonance matter [39].

It is the purpose of the present study to investigate this enhancement within the presently available transport codes—HSD, IQMD, and Ultra-relativistic Quantum Molecular Dynamics (UrQMD)—to explore whether the dilepton production in these systems can be reproduced by the theoretical approaches and to identify eventually the origin of this in-medium enhancement. All these codes have been successfully employed to investigate a multitude of experimental observables. They are, however, not of the same sophistication as far as the dileptons are concerned. The dilepton part of the UrQMD program is still under development and up to now bremsstrahlung is not included. This limits the predictive power to parts of the spectra where bremsstrahlung is not essential. For the study of the in-medium enhancement we limit ourselves to HSD and IQMD calculations. We start out in Sec. II with a short description of the HSD model and of the improvements made compared to the "standard" HSD 2.5 version used for the extended dilepton study in Ref. [40]. Then we come to a brief description of dilepton production in IQMD. In Sec. III the dilepton production in elementary reactions, measured by the HADES and and DLS collaborations, is compared with HSD and IQMD calculations. The fourth section is devoted to the study of dilepton production in heavy-ion collisions. We discuss our calculations for all systems that have been measured by the HADES Collaboration and present also our predictions for Au + Au collision at 1.25 GeV/nucleon which is presently analyzed. After checking that the invariant mass spectra of dileptons in heavy-ion collisions are well reproduced by the HSD as well as by the IQMD approach, we study in Sec. V the enhancement of the dilepton production in heavy-ion collisions as compared to the elementary reactions and identify its origin. In Sec. VI we present our conclusions.

II. THE TRANSPORT MODELS

A. The HSD model

Our analysis of the experimental results is carried out within the off-shell HSD transport model [40,45–47], based on covariant self-energies for the baryons [48]. It has been used for the description of pA and AA collisions from GSI heavy ion synchrotron (SIS) to energies currently available at the BNL Relativistic Heavy Ion Collider. We recall that in the HSD approach nucleons, Δ's, $N^*(1440)$, $N^*(1535)$, Λ, Σ, and Σ^* hyperons, Ξ's, Ξ^*'s, and Ω's, as well as their antiparticles are included on the baryonic side, whereas the 0^- and 1^- octet states are incorporated in the mesonic sector. Inelastic baryon-baryon (and meson-baryon) collisions with energies above $\sqrt{s_{\rm th}} \simeq 2.6$ GeV (and $\sqrt{s_{\rm th}} \simeq 2.3$ GeV) are described by the FRITIOF string model [49], whereas low-energy hadron-hadron collisions are modeled using experimental cross sections.

The dilepton production by the decay of a (baryonic or mesonic) resonance R can be schematically presented in the following way:

$$BB \to RX, \tag{1}$$
$$mB \to RX, \tag{2}$$
$$R \to e^+e^-X, \tag{3}$$
$$R \to mX, \quad m \to e^+e^-X, \tag{4}$$
$$R \to R'X, \quad R' \to e^+e^-X. \tag{5}$$

In a first step a resonance R might be produced in baryon-baryon (BB) or meson-baryon (mB) collisions [Eqs. (1) and (2)]. Then this resonance can either couple directly to dileptons [Eq. (3)] (e.g., Dalitz decay of the Δ resonance: $\Delta \to e^+e^-N$) or produces mesonic [Eq. (4)] or baryonic [Eq. (5)] resonances which then produce dileptons via direct decays (ρ, ω) or Dalitz decays (π^0, η, ω). With increasing energy hadrons are created by nonresonant mechanisms or string decay. This is also true for those that disintegrate into dileptons. The electromagnetic part of all conventional dilepton sources—π^0, η, ω, Δ-Dalitz decays, as well as direct decay of vector mesons ρ, ω, and ϕ—are calculated as described in detail in Ref. [50]. We note that we use here again (as in early HSD dilepton studies [45,46]) the "Wolf" model for the differential electromagnetic decay width of the Δ resonance [51] instead of the "Ernst" description [30] adopted at that time in Ref. [50].

The treatment of the enhanced bremsstrahlung contribution from pp, pn, as well as πN "quasielastic" scattering, based on the OBE calculations by Kaptari and Kämpfer [41], is discussed in detail in Ref. [40] (cf. Sec. 2.6 there), where also a discussion of the different models [42,52,53], which formulate bremsstrahlung in the elementary reactions, can be found. We note here that the OBE models mentioned above [41,42,52,53] provide different results not only for the pN bremsstrahlung contribution (which might be attributed to the different way to realize the gauge invariance) but for the Δ-Dalitz decay, owing to the different form factors. In our transport analysis we use only the bremsstrahlung contribution from Ref. [41], avoiding the uncertainties in the Δ channel in the OBE models and neglecting the quantum mechanical interference between individual contributions which cannot be treated consistently in transport approaches. Also we stress here again that to separate the bremsstrahlung ($pp \to ppe^+e^-$) from a vector-dominance-like dilepton production via the ρ meson ($pp \to pp\rho$, $\rho \to e^+e^-$), we do not employ a vector-dominance form factor when calculating the bremsstrahlung. Thus, the dilepton radiation via the decay of the virtual photon ($pp \to pp\gamma^*$, $\gamma^* \to e^+e^-$) and the direct ρ decay to e^+e^- are distinguished explicitly in the calculations. In the Sec. VI we discuss the model uncertainties concerning the treatment of Δ's and bremsstrahlung.

The off-shell HSD transport approach incorporates the *off-shell propagation* for vector mesons as described in Ref. [54] in extension of early BUU transport models [46,55]. In the off-shell transport description, the hadron spectral functions change dynamically during the propagation through the medium and evolve towards the on-shell spectral functions in the vacuum. As demonstrated in Refs. [20,40], the off-shell dynamics is important for resonances with a rather long lifetime in the vacuum but strongly decreasing lifetime in the nuclear medium (especially ω and ϕ mesons) and has also been proven to be vital for the correct description of the dilepton decay of ρ mesons with masses close to the two-pion decay threshold. For a detailed description of the off-shell dynamics and the implementation of in-medium scenarios (as a collisional broadening and/or dropping mass scenario) in HSD, as well as for an extension of the LUND string model to include "modified" spectral functions, we refer the reader to Refs. [20,40,54].

For the present study we consider the scenario of a "collisional broadening" of the vector meson spectral functions. This is also supported by experimental data in contrast to the "dropping mass" scenario (cf. Refs. [17–22]). We incorporate the effect of collisional broadening of the vector-meson spectral functions by using for the vector meson width

$$\Gamma_V^*(M, |\vec{p}|, \rho_N) = \Gamma_V(M) + \Gamma_{\rm coll}(M, |\vec{p}|, \rho_N). \tag{6}$$

Here $\Gamma_V(M)$ is the total width of the vector mesons ($V = \rho, \omega$) in the vacuum. The collisional width in Eq. (6) is approximated as

$$\Gamma_{\rm coll}(M, |\vec{p}|, \rho_N) = \gamma\ \rho_N \langle v \sigma_{VN}^{\rm tot} \rangle \approx\ \alpha_{\rm coll}\ \frac{\rho_N}{\rho_0}. \tag{7}$$

Here $v = |\vec{p}|/E$, $\vec{p}$, E are the velocity, 3-momentum, and energy of the vector meson in the rest frame of the nucleon current and $\gamma^2 = 1/(1 - v^2)$; ρ_N is the nuclear density; and $\sigma_{VN}^{\rm tot}$ the meson-nucleon total cross section. We use the "broadening coefficients" $\alpha_{\rm coll} \approx 150$ MeV for the ρ and $\alpha_{\rm coll} \approx 70$ MeV for ω mesons as obtained in Ref. [40]. For further details, we refer the reader to Ref. [40].

We use the time integration method to calculate dilepton spectra, which means that vector mesons and resonances can emit dileptons from their production ("birth") up to their absorption ("death"). This is especially important for the study of in-medium effects because this method takes the full in-medium dynamics into account.

We note that it is very important to have an adequate description of the elementary reactions, especially near the threshold where the cross sections grow very rapidly. This rise has a big impact on the description of the experimental data. The comparison of the latest experimental data from the HADES Collaboration on pp collisions at 3.5 GeV [56] with HSD calculations shows that the previous parametrizations of η meson and of vector mesons (ρ, ω) production cross sections from Ref. [40] overestimate the data. The overprediction of the dilepton yield at the ρ peak has been already realized in Ref. [40] from the comparison to the DLS data for pp at 2.09 GeV. Thus, we have modified the HSD model accordingly to obtain a better description of the existing experimental data on elementary reactions (cf. the discussions in the next section).

We note that the HSD model is well tested with respect to the bulk observables at low energy and in light systems, relevant for present study. The pion and η production from C + C collisions at the energies considered here are shown in Sec. 3 of Ref. [40].

1. Particle production from elementary reactions

Here we describe the major changes/improvements made in the HSD model used here compared to the basic HSD version 2.5 used for the dilepton analysis in Ref. [40].

(i) The high-energy part of the $pp \to \eta X$ and the $pn \to \eta X$ cross sections have been newly parametrized. The new parametrization, compared to the experimental data, is shown in Fig. 1 for pp and pn reactions as a function of the center of mass energy above threshold ($\sqrt{s} - \sqrt{s_0}$). The solid and dashed lines represent the inclusive $pp \to \eta X$ and $pn \to \eta X$ cross sections from the HSD model. The experimental data are collected from Refs. [56–60]: The solid squares and the open star stand for the exclusive $pp \to \eta pp$ data, the dots for $pn \to \eta pn$ data. The full diamond and the full star show inclusive data for $pp \to \eta X$. The open and solid stars indicate the exclusive and inclusive cross sections extrapolated from the dilepton data by the HADES Collaboration [56]. It is important to note that in elementary reactions also a deuteron can be produced in the final state via $pn \to \eta d$. The cross section for this channel is indicated by the dash-dotted line in Fig. 1, whereas the dotted line shows the $pn \to \eta X$ cross section including the $pn \to \eta d$ contribution. The open triangles show the experimental data for $pn \to \eta d$ from Refs. [57–59]. The channel $pn \to \eta d$ is not considered in the HSD calculations for $A + A$ and $p + A$ reactions because the probability for deuteron formation in the baryonic medium is negligibly small.

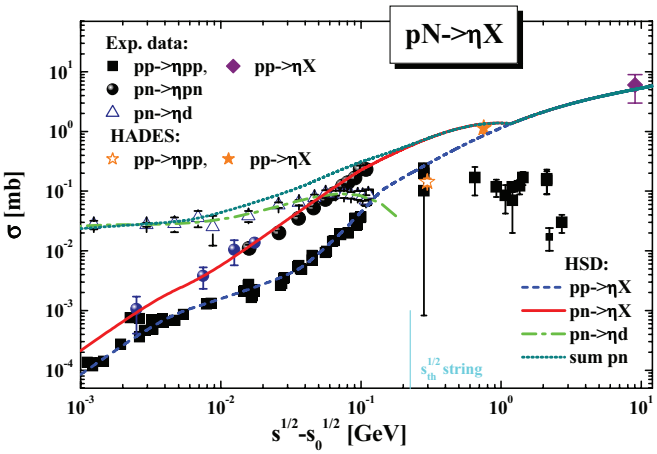

FIG. 1. (Color online) The η production cross section in pp and pn reactions as a function of the invariant energy above threshold ($\sqrt{s} - \sqrt{s_0}$). The solid and dashed lines represent the inclusive $pp \to \eta X$ and $pn \to \eta X$ cross sections from the HSD model, respectively, the dash-dotted line indicates the $pn \to \eta d$ channel, and the dotted line the $pn \to \eta X$ cross section including $pn \to \eta d$. The experimental data are collected from Refs. [56–60]: The solid squares and open star stand for the exclusive $pp \to \eta pp$ experimental data, the dots for $pn \to \eta pn$, and open triangles for $pn \to \eta d$ experimental data; the solid diamond and solid star show inclusive experimental data for $pp \to \eta X$. The open and solid stars indicate the exclusive and inclusive cross sections extrapolated from the dilepton data by the HADES Collaboration [56].

(ii) The HSD model has also been improved concerning the isospin separation of the vector meson production in BB and secondary mB reactions. The isospin averaged cross sections $BB \to VBB$ ($V = \rho, \omega, \phi$) and $mB \to VB$ have been replaced with cross sections that take explicitly the isospin for each channel into account. The new parametrization of the cross section as a function of the center-of-mass energy, $\sqrt{s}$ for the pp reaction is compared in Fig. 2 to the experimental data. The solid lines represent the parametrizations of the inclusive $pp \to VX$ ($V = \rho, \omega$) cross sections, while the dashed lines stand for the exclusive cross sections. We denote these exclusive cross sections for the ρ-meson production as "nonresonant" because in this study we consider explicitly the possible contribution of the baryonic resonance $N(1520)$ to the subthreshold ρ^0 production [$pp \to N(1520)p \to \rho^0 pp$]. It is indicated as the dash-dotted line on the left plot. The dotted line shows the sum of the inclusive nonresonant and exclusive "resonant" contribution. The experimental data [58,61,62] are shown for exclusive $pp \to Vpp$ (dots) and inclusive $pp \to VX$ (squares) vector meson production. The stars indicate the inclusive cross sections extrapolated from the dilepton data by the HADES Collaboration [56].

We note that we do not propagate explicitly the $N(1520)$ resonance in the HSD approach; rather we consider it as an excitation in the amplitude which enhances the ρ-meson production in NN and πN reactions at subthreshold energies. The modeling of the $N(1520)$ production in NN collisions is based on a phase space model with a constant matrix element adopted from Ref. [63]. The contribution of the $N(1520)$ to the ρ cross section is included in line with Ref. [11], which has been used in our previous work [33]. The decay channels of the $N(1520)$ resonance are not well established. Especially the disintegration into a ρ is estimated in between 15% and 25%. Including this contribution from the $N(1520)$ resonance decay presents an upper estimate for the ρ-meson production in NN and πN reactions at subthreshold energies. This model assumption can be checked experimentally via an observation of an enhancement of the dilepton yield near the ρ peak in the elementary reactions at subthreshold energies. In the case of heavy-ion collisions at low bombarding energies, the contribution of the $N(1520)$ resonance to the dilepton spectra can hardly be seen, especially not in reactions of the light nuclei as C + C as measured by the HADES Collaboration at 1.0 GeV/nucleon. The Fermi motion modifies the available energy for meson production and, owing to the rapid rise of the cross section at threshold, the inclusive ρ-meson production mechanism starts to dominate (see Fig. 2), even if the nominal energy is below threshold. However, the $N(1520)$ resonance can be excited by pion-baryon collisions and contribute to the ρ-meson production via the process $\pi N \to N(1520) \to \rho N$. The probability of such processes is larger for heavy nuclei collisions but the pion density is relatively small at subthreshold

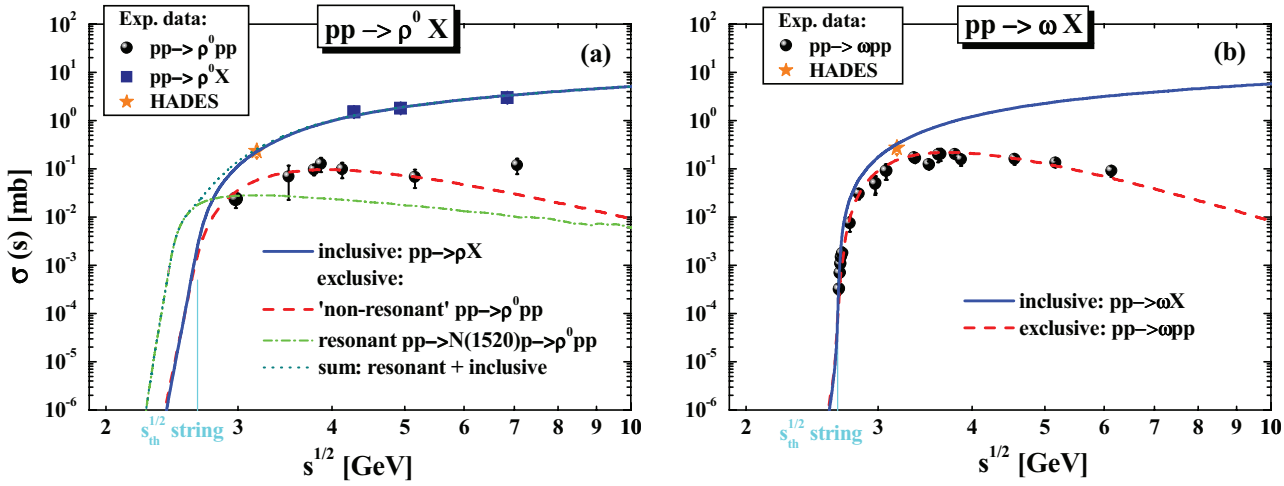

FIG. 2. (Color online) The production cross sections for the channels $pp \to \rho X$ (left plot (a)) and $pp \to \omega X$ [right plot (b)] as a function of the center of mass energy $\sqrt{s}$. The solid lines represent the parametrizations of the inclusive $pp \to VX$ ($V = \rho, \omega$) cross sections, while the dashed lines stand for the exclusive nonresonant cross sections. The dash-dotted line on the left plot shows the contribution from the $N(1520)$ resonance to the ρ^0 production via the process $pp \to N(1520)p \to \rho^0 pp$ and the dotted line indicates the sum of the inclusive nonresonant and exclusive resonant contributions. The experimental data [58,61,62] are shown for exclusive $pp \to Vpp$ (dots) and inclusive $pp \to VX$ (squares) vector meson production. The stars indicate the inclusive cross sections extrapolated from the dilepton data by the HADES Collaboration [56]. The vertical light blue lines show the threshold for meson production by string formation and decay ($\sqrt{s}_{\rm th} = 2.6$ GeV) as implemented in HSD for BB channels.

energies where the possible contribution of $N(1520)$ plays a role. Consequently, the enhancement of the ρ-meson production by accounting for the $N(1520)$ channel is relatively small in the HSD model. This differs from, e.g., the UrQMD model [64,65], where a much larger cross sections for the $N(1520)$ production is used. We come back to this discussion in Sec. IV.

(iii) We improved also the description of multimeson production between the two-pion production threshold and $\sqrt{s} = 2.6$ GeV, where we match the standard HSD description of particle production via strings.

Close to the two-pion threshold the two pions are dominantly produced by the decay of two Δ's created in NN collisions. With increasing energy the available phase space is sufficient for multimeson production and a lot of extra channels become open. However, it is unknown whether the light mesons are produced by the decay of heavy baryonic resonances or directly from the excitation and decay of the strings. Because there is very little experimental information on the exclusive channel decomposition in this "intermediate" energy range, we used the FRITIOF LUND string model as an "event generator" for the production of such "multimeson" channels by adding them to the exclusive channels which are modeled in the HSD explicitly, such that we obtain the inelastic NN cross section, i.e., $\sigma_{\rm inel} = \sigma_{\rm excl} + \Delta\sigma_{\rm incl}$, where $\sigma_{\rm excl}$ stands for the exclusive channels such as $NN \to \Delta N$, $NN \to \Delta Nm$, $m \equiv \pi, \rho, \omega, \phi, \ldots$, and channels with strangeness production such as $NN \to YNK$ ($Y \equiv \Lambda, \Sigma$) and $NN \to NNK\bar{K}$. Here $\Delta\sigma_{\rm incl}$ corresponds to the sum of the two-pion production channels as $NN \to \Delta\Delta$ and multimeson production $NN \to NN(\Delta) + n \times m$ ($n = 2, 3, 4, \ldots$) and channels with the final hyperons and strange mesons. We note that because close to the threshold the FRITIOF model does not provide the correct isospin decomposition for Δ production, because, e.g., an exclusive channel $NN \to \Delta^{++}n$ is missing, we have adjusted the FRITIOF model to correct for the isospin decomposition of produced Δ's: For the exclusive channel $pp \to N\Delta$ we assume now that 3/4 of the produced Δ are in the Δ^{++} state and only 1/4 in the dilepton-producing Δ^+ state. This leads to a reduction of Δ^+ production and an enhancement of Δ^{++} production, respectively.

The excitation function of the multiplicity of the different pions in HSD is shown in Fig. 3: on the left-hand side for pp collisions, on the right-hand side for pn reactions. These multiplicities are compared with the available data, which are very scarce for pn reactions. Additionally to the total pion multiplicity, the multiplicity of Δ's themselves is very important for the dilepton study because the Δ resonances decay into pions as well as into dileptons, whereas other sources of pions do not contribute to the dilepton yield. The Δ production in pp collisions in the HSD approach is shown in Fig. 4 and compared with the available experimental data. Here the production cross sections for the inclusive channels $pp \to \Delta^+ X$ (solid line) and for the exclusive channel $pp \to \Delta^+ p$ (dashed line) from HSD are presented as a function of the invariant energy $\sqrt{s}$. The experimental data [61] are shown for exclusive $pp \to \Delta^+ p$ production. The star indicates the extrapolation for the Δ inclusive cross section from the dilepton spectra by the HADES Collaboration based on the PLUTO simulation program [66] from

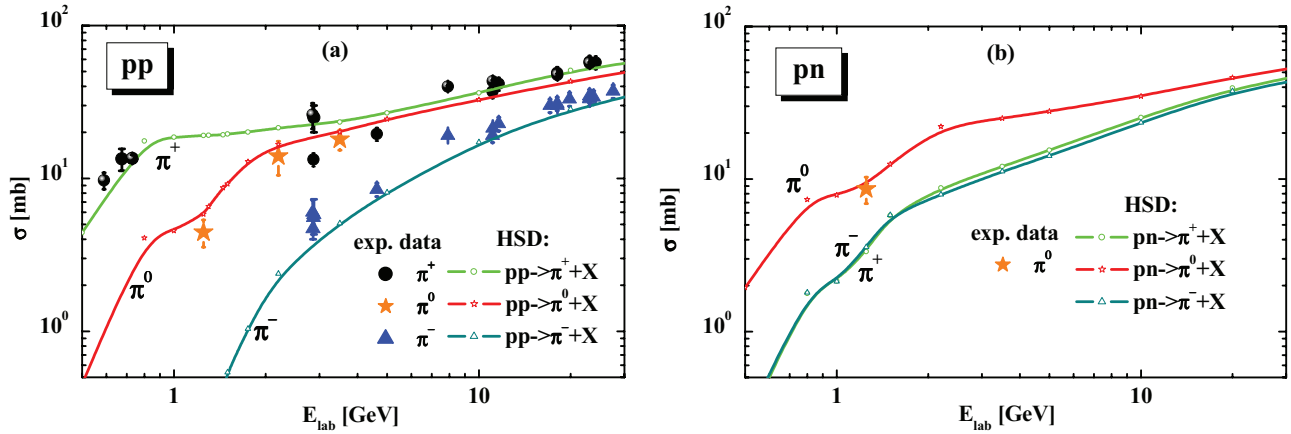

FIG. 3. (Color online) (a) The inclusive pion production cross sections as a function of the proton bombarding energy $E_{\rm lab}$. The HSD results are shown in terms of lines with open symbols whereas the experimental data are indicated by the corresponding solid symbols. That is, for $pp \to \pi^+ + X$: HSD, the solid line with open dots; experimental data, solid dots from Refs. [61,68]. For $pp \to \pi^0 + X$: HSD, the solid line with open stars; the HADES data, full stars from Refs. [56,69]. For $pp \to \pi^- + X$: HSD, the solid line with open triangles; experimental data, full triangles from Refs. [61,68]. (b) The production cross sections for $pn \to \pi X$, $\pi = \pi^+, \pi^0, \pi^-$ from the HSD model, the HADES data; full star from the extrapolation in Ref. [37].

Ref. [56]. One can see from Fig. 4 that the inclusive Δ production dominates the exclusive one already at relatively low $\sqrt{s}$. However, owing to the lack of inclusive experimental data on Δ production it is hard to justify the modeling of Δ dynamics beyond the exclusive channels which are relatively well known experimentally and accurately modeled in transport approaches.

As said, above a kinetic energy of 1.5 GeV there is no experimental information available on whether resonance is involved in the production. This is the reason why different parametrizations have been advanced. For example, in the resonance-based GiBUU model [67] a lower inclusive Δ^+ production cross section is used as compared to HSD. Also the isospin relations are different, which leads to a lower dilepton contribution from Δ-Dalitz decay. Additionally, the different parametrization for the differential dilepton decay width is employed, which, lowering the Δ-Dalitz decay channel substantially compares to the HSD (cf. discussions in Sec. VI).

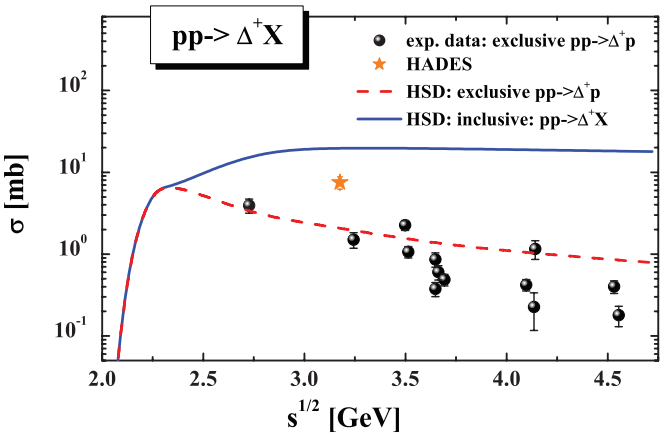

FIG. 4. (Color online) The production cross sections for the inclusive channels $pp \to \Delta^+ X$ (solid line) and the exclusive channel $pp \to \Delta^+ p$ (dashed line) from HSD as a function of the invariant energy $\sqrt{s}$. The experimental data [61] are shown for exclusive $pp \to \Delta^+ p$ production. The star indicates the inclusive cross section extrapolated from the dilepton data by the HADES Collaboration [56].

B. Open questions related to the elementary reactions in transport models

In nucleon-nucleon collisions at low energies, i.e., below $\sqrt{s} < 2.2$ GeV, very seldom more than one meson is produced. The cross sections for these reactions have been measured experimentally (cf. Ref. [58]) and are used in the transport approach. Above $\sqrt{s} \approx 2.2$ GeV the multimeson production starts to dominate, but the experimental information on inclusive as well as exclusive multimeson production channels are very poor. Also it is not known whether the mesons are directly produced or whether they are decay products of intermediate resonances or strings. The theoretical analysis of these data has not produced yet a consistent knowledge on the channel decomposition [70–73]. This introduces large uncertainties for the prediction of the dilepton yield in transport theories because it depends on the formation of specific intermediate resonances. We note that in the UrQMD model the production of mesons at intermediate energies is realized exclusively via excitation and decay of heavy baryonic resonances which are explicitly propagated in the transport model [64,65], whereas in HSD the string mechanism is used (as discussed above) for the description of the same final meson spectra. Thus, one needs more exclusive experimental information to differentiate between the models.

C. The IQMD model

The IQMD model used for the calculations in this study is the same as introduced in the first IQMD paper on dilepton

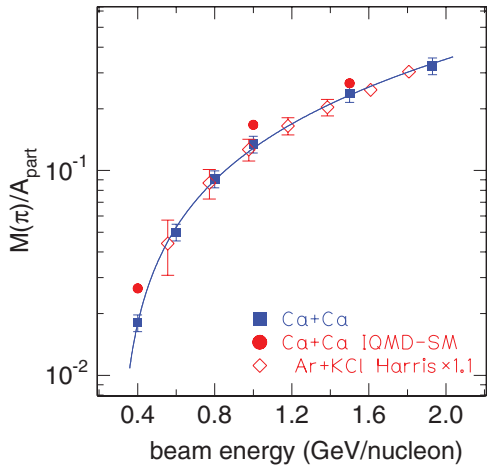

FIG. 5. (Color online) The excitation function of the π multiplicity per participating nucleon ($[N(\pi^+) + N(\pi^-)]/A_{\rm part}$) for Ca + Ca collisions using $A_{\rm part}$ as 0.9 A. Data of the FOPI Collaboration are compared with data of Harris *et al.* [79] and predictions of the IQMD model [74,75].

production [43]. In this model all pions are produced by the decay of Δ resonances. Because no higher mass resonances are included we limit the prediction to beam energies up to 2 GeV/nucleon. The excitation function of the pion yield for the Ca + Ca system, compared with the available data, is shown in Fig. 5. We see that the pion multiplicity, the result of a complicated interplay among Δ creation, absorption, and decay, is quite reasonably reproduced by the IQMD approach [74]. This is also the case for heavier systems [75]. Thus, both the IQMD and the HSD approaches describe the available pion data quite well, a prerequisite for an analysis of the dilepton spectra, which are not only normalized to the pion yield but have an important contribution from the Δ decay. For other models which are used to describe the dilepton production, like that in Ref. [76], it remains to be seen whether they reproduce heavy-ion pion data.

For the calculations of the dilepton spectra the standard IQMD program [77,78] has been supplemented with all elementary cross sections that are important for this process [43]. For that we have used the parametrizations of available experimental data, but for many channels, pp data are only available for low $\sqrt{s}$ values and np data are very scarce. Consequently, in heavy-ion collisions at beam energies larger than 1.5 GeV/nucleon most of the particles that emit dileptons are produced using theoretically calculated cross sections. In Ref. [43] we studied how the uncertainties of the cross sections from elementary reactions influence the dilepton spectra in heavy-ion collisions. For these studies we use the setup in which the $pn \to \omega pn$ cross section is 5 times higher than the $pp \to \omega pp$ cross section. This explains the difference between HSD and IQMD at dilepton invariant masses close to the ρ, ω peak.

In the IQMD approach the dileptons are calculated perturbatively using the "spontaneous decay" method, contrary to the time integration method in HSD and UrQMD. It is based on the assumption that all hadrons which decay into dileptons and which are produced in the heavy-ion collision contribute to the dilepton yield as if they were produced in free space. This implies that a possible later reabsorption of the hadrons is not taken into account. Because in reality some of the Δ's and of the other dilepton-producing hadrons are reabsorbed, the IQMD calculations give an upper limit for the dilepton production in heavy-ion collisions. Consequently, the spontaneous decay method limits the approach to small systems contrary to the time-integration method, which follows the in-medium dynamics of all dilepton sources exactly. However, for the systems studied here the spontaneous decay method is still acceptable. For the details of the cross sections for the creation of dilepton-producing particles, we refer to Ref. [43].

III. DILEPTON PRODUCTION IN ELEMENTARY pp, pd, AND $p + A$ REACTIONS

The first reaction considered here is the dilepton production in elementary reactions like $p + p$, quasifree $p + n(d)$, and $p + Nb$ reactions.

A. Dilepton production in pp and pd at energies around 1.25 GeV

We start our discussion with the HADES and DLS data a 1.25 GeV. Figure 6 shows the differential cross section $d\sigma/dM$ for dileptons as a function of the invariant mass M for pp (left), pn (middle), and pd (right) reactions at 1.25 GeV. The HSD results are presented in comparison to the experimental data from the HADES Collaboration [37,38]. The different lines display the contributions from the various channels in the HSD calculations (for the color coding we refer to the legend). We note here (and that applies to all further plots) that the theoretical calculations passed through the appropriate experimental acceptance filters and that the mass/momentum resolution is taken into account.

As seen in the left panel of Fig. 6 the pp dilepton yield is dominated by the Δ-Dalitz decay, while bremsstrahlung is subleading owing to the destructive interference between initial- and final-state amplitudes in the case of equal charges owing to a different sign in the acceleration. Thus, these HADES data provide a solid constraint on the Δ production whose control will be very important for a robust interpretation of the heavy-ion data. In pn collisions, however, bremsstrahlung is dominating, as can be seen from the middle panel of Fig. 6. Because the form of the dilepton invariant mass spectrum from Δ decay and from bremsstrahlung is not completely the same, the forms of the pp and the pn spectra are not identical and we see in np a slight enhancement close to the kinematic limit. In the right panel of Fig. 6 we compare the HSD results for pd collisions with the so-called quasifree pn HADES data, used later as the "reference" spectra $NN = (pn + pp)/2$ for the interpretation of the heavy-ion data. Experimentally, the quasifree pn events have been separated by measuring the proton spectator in the pd reactions at $1.6 < p_{\rm lab} < 2.6$ GeV/c.

The comparison of the pp and the $pn(d)$ data shows clearly that in $pn(d)$ the proton does not scatter on a quasifree neutron. The kinematical limit for the invariant mass of the dilepton, which is $M_{\rm max} = \sqrt{s_{NN}} - 2m_N = 0.545$ GeV in pp and np

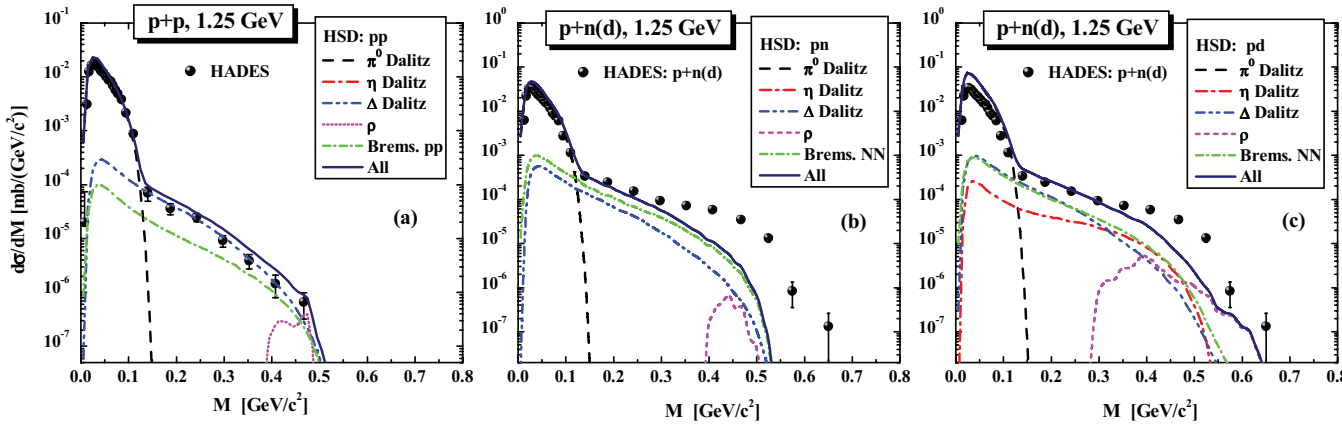

FIG. 6. (Color online) The HSD results for the dilepton differential cross section $d\sigma/dM$ for pp (a), pn (b), and pd (c) reactions at 1.25 GeV in comparison to the experimental data for pp (left) and quasifree pn [(b),(c)] reactions from the HADES Collaboration [37,38]. The individual colored lines display the contributions from the various channels in the HSD calculations (see color coding in the legend). The theoretical calculations passed through the corresponding HADES acceptance filters and mass/momentum resolutions.

collisions, is well exceeded in the pd collisions. The largest invariant mass observed ($M \approx 0.66$ GeV) corresponds to the maximal invariant mass which is kinematically allowed in the *three*-body pd system under the condition that the outgoing proton has at least a momentum of 1.6 GeV/c. Therefore, at the upper end of the invariant mass spectra we have a collision of the proton with the deuteron with a center-of-mass energy of $\sqrt{s_{pd}} = \sqrt{(p_p + p_d)^2}$. One has to keep this observation in mind for the interpretation of dilepton production in heavy-ion collisions, when the pd results are used as a reference to discuss the in-medium enhancement of the dilepton yield.

In semiclassical transport calculations, like HSD, one simulates the deuteron as a bound system of a proton and a neutron that are redistributed in coordinate and momentum space according to the wave function of the Paris potential [80]. The energy of each nucleon (in the deuteron rest frame) is taken as $E_N = m_N + \varepsilon/2$, where $\varepsilon = -2.2$ MeV is the binding energy of the deuteron. We use the energy-momentum relation for free particles to determine the effective mass of the nucleon and then the energy-momentum 4-vector to describe the collision. An incoming nucleon scatters with one or subsequently with both nucleons of the deuteron but never with the two at the same time. This gives another kinematic as compared to a true three-body collision and therefore HSD calculations underpredict the dilepton production close to the kinematical limit of pd collisions.

Another problem with the quasifree pn scattering is related to the possibility of deuteron formation in the final state. This is not probable in heavy-ion collisions (cf. Ref. [81]) and not included in HSD. However, as seen from the Fig. 1, the process $pn \to \eta d$ might be important for the η production at threshold energies. Thus, we include this contribution as an enhanced cross section for η production in pn (this was not included in our previous work [40]) but we do not treat the deuteron formation explicitly in the code. As seen from the right panel of Fig. 6 in np collisions around $M = 0.4$ GeV the η contribution turns out to be of the same order of importance as Δ-Dalitz decays and bremsstrahlung.

Figure 6 (right) shows that in pd collisions the HSD model underestimates the dilepton yield between $0.35 < M < 0.5$ GeV, a region which is accessible in two-body collisions at this energy. A possible candidate to explain this enhancement is the contribution of subthreshold ρ-meson production via excitation and decay of the $N(1520)$ resonance shown as the dash-dotted line in Fig. 2. A very small contribution of this resonant ρ production channel is even seen in pp collisions (dotted line on the left plot). However, this contribution is not sufficient to describe the experimental data. This is in line with a recent study by the GiBUU group [67]. Also IQMD calculations fail to describe this part of the spectrum.

Figure 7 shows the IQMD predictions for pp and np collisions as well compared to pp and pd HADES data. We see a very good agreement between HSD and IQMD predictions for the elementary pp and pn reactions.

The cross section $d\sigma/dM$ at 1.27 GeV, calculated in the HSD model, is compared in Fig. 8 to the pp (left) and pd (right) DLS data [24]. The theoretical calculations passed through the corresponding DLS acceptance filter and mass resolution. While the agreement between HSD and the data looks reasonable, one has to keep in mind that, owing to the very broad mass resolution, the spectra are strongly distorted at large invariant masses. There seems to be an underestimation of the last experimental point for pd; however, the quality of the data does not allow for robust conclusions.

B. Dilepton production in pp and pd at energies around 2.2 GeV

The differential cross section $d\sigma/dM$ from HSD calculations for e^+e^- production in pp reactions at bombarding energies of 2.2 GeV in comparison to the HADES data [69] is presented in Fig. 9 (left panel). The right panel of Fig. 9 shows for the same reaction the HSD results for the differential transverse momentum cross sections for pp at 2.2 GeV separated for different invariant mass bins: $M \leqslant 0.15$ GeV, $0.15 \leqslant M \leqslant 0.55$ GeV, and $M \geqslant 0.55$ GeV. Also at an energy

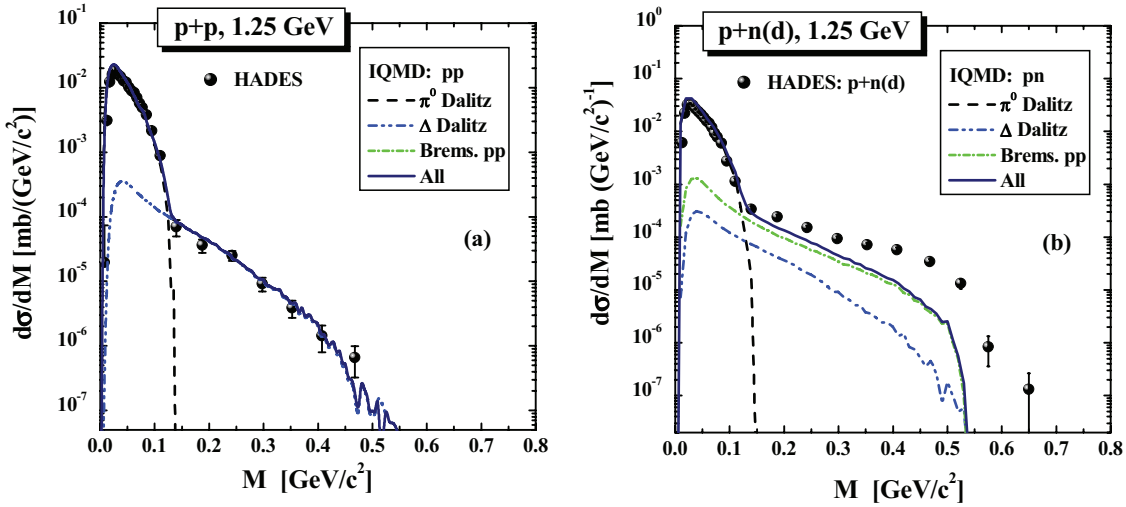

FIG. 7. (Color online) The IQMD results for the dilepton differential cross section $d\sigma/dM$ for pp (a) and pn (b) reactions at 1.25 GeV in comparison to the experimental data for pp (a) and quasifree $pn(d)$ (b) reactions from the HADES Collaboration [37,38]. The individual colored lines display the contributions from the various channels in the IQMD calculations (see color coding in the legend). The theoretical calculations passed through the corresponding HADES acceptance filters and mass/momentum resolutions.

of 2.2 GeV we see a quite satisfying agreement between theory and experiment.

Figure 10 shows the dilepton differential cross section $d\sigma/dM$ for the pp (left panel) and pd (right panel) at 2.09 GeV from HSD calculations in comparison to the DLS data [24]. We see also here a good agreement and the fact that the DLS as well as the HADES data are reproduced with the same theory underlines the consistency of both data sets, which have quite different acceptance cuts.

C. Dilepton production in pp at 3.5 GeV

Finally we come to the HADES pp data at 3.5 GeV. Although HADES has not measured heavy-ion collisions at this energy we include these results for completeness. Figure 11 shows the differential cross section $d\sigma/dM$ from HSD calculations for dilepton production in pp reactions at a bombarding energy of 3.5 GeV in comparison to the HADES data [56]. We present the results including and excluding the bremsstrahlung contribution because at this energy there exist no solid bremsstrahlung calculations. The validity of our approach, to take the Kaptari and Kaempfer matrix element and to adjust only the phase space, as described in detail in Ref. [40], becomes questionable at such a high energy. The thick lines, labeled in the legend as "All wo Brems," show the sum of all channels (labeled as "All") without pp bremsstrahlung. For the distribution of the invariant masses of the dileptons, bremsstrahlung does not play a major role at this energy in pp, as expected.

In Fig. 12 we compare the HSD results for pp at 3.5 GeV and for four different mass bins: $M \leqslant 0.15$ GeV, $0.15 \leqslant M \leqslant 0.47$ GeV, $0.47 \leqslant M \leqslant 0.7$ GeV, and $M \geqslant 0.7$ GeV to the HADES data [56]. The upper four plots show the rapidity distribution and the lower four plots the transverse momentum spectra. As in Fig. 11 the thick lines, labeled in the legend as "All wo Brems," show the sum of all channels (labeled as "All") without pp bremsstrahlung. We observe that the

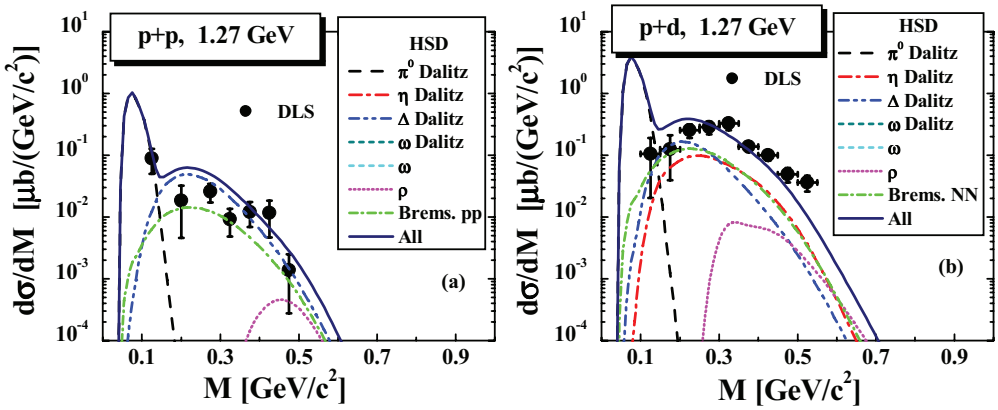

FIG. 8. (Color online) The dilepton differential cross section $d\sigma/dM$ for pp (a) and pd (b) at 1.27 GeV in comparison to the DLS data [24]. The HSD calculations passed through the corresponding DLS acceptance filter and mass resolution.

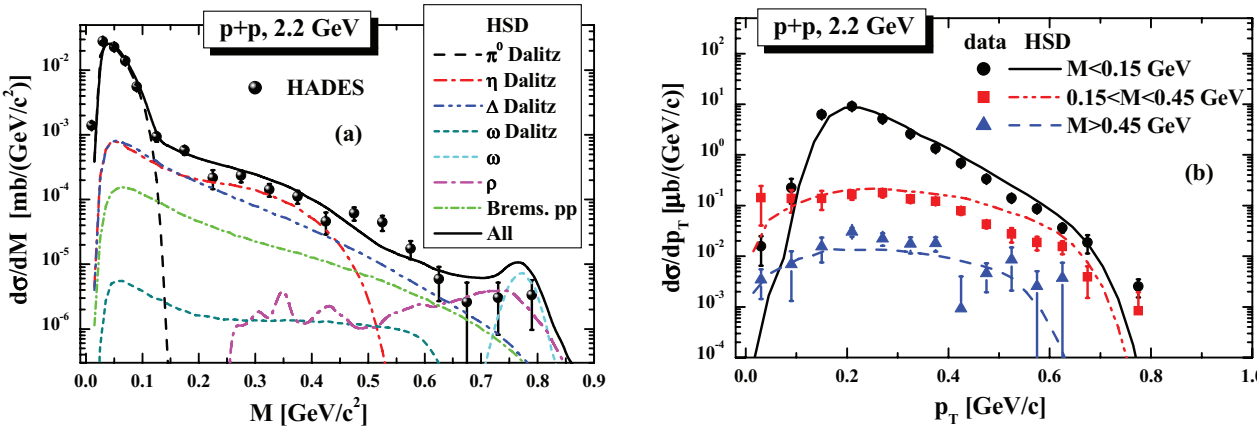

FIG. 9. (Color online) (a) The differential cross section $d\sigma/dM$ from HSD calculations for e^+e^- production in pp reactions at a bombarding energy of 2.2 GeV in comparison to the HADES data [69]. The individual colored lines display the contributions from the various channels in the HSD calculations (for the color coding, see legend). (b) HSD results for the differential dilepton transverse momentum cross section for pp at 2.2 GeV and for different mass bins: $M \leqslant 0.15$ GeV, $0.15 \leqslant M \leqslant 0.55$ GeV, and $M \geqslant 0.55$ GeV. The theoretical calculations passed through the corresponding HADES acceptance filter and mass/momentum resolution.

rapidity distribution is well described except for invariant masses around the ρ peak, where we overpredict the data by a constant factor. Also the transverse momentum distribution is well described by theory with the exception of a region around $M \approx 0.6$ GeV, where our calculations overpredict the data.

We note that the present result is in a better agreement with the HADES p_T data as compared to the early HSD predictions [40,56] owing to the following reasons: a lowering of the η-Dalitz dilepton contribution owing to the reduction of the η production cross section in line with the new HADES data [cf. discussion in Sec. II A1(1)]; a lowering of the direct ρ, ω-dilepton decay contributions owing to the modification of the vector meson production cross section [cf. discussion in Sec. II A1(2)]; a lowering of the Δ-Dalitz dilepton contribution owing to the adjustment of the isospin decomposition in the exclusive channel $NN \to \Delta^{++}n$ from FRITIOF [cf. discussion in Sec. II A1(3)]. The latter reduces the total (inclusive) Δ^+ production by a factor up to 1.4 at 3.5 GeV and correspondingly the dilepton yield. This reduction is even larger (more than a factor of 3) for dileptons with high invariant masses and high p_T because they stem dominantly from the Dalitz decay of exclusive Δ's simply owing to kinematical reasons; a lower amount of associated particles leaves more energy for the generation of high-mass Δ's. An addition reduction of the Δ dilepton yield stems from the different parametrizations used for the differential electromagnetic decay width of the Δ resonance (cf. discussion in Sec. VI): presently, "Wolf" [51] instead of the original "Ernst" description [30] with a coupling constant $g = 3$ instead of $g = 2.7$, which is consistent with the "photon" ($M \to 0$) limit. Without these modifications the present HSD version reproduces the results of Refs. [40,56].

We speculate that HSD produces slightly too many Δ's at 3.5 GeV. Because the elementary cross section for inclusive Δ production in pp reactions at this energy is not available, the repartition of the pion yield between Δ resonances (which

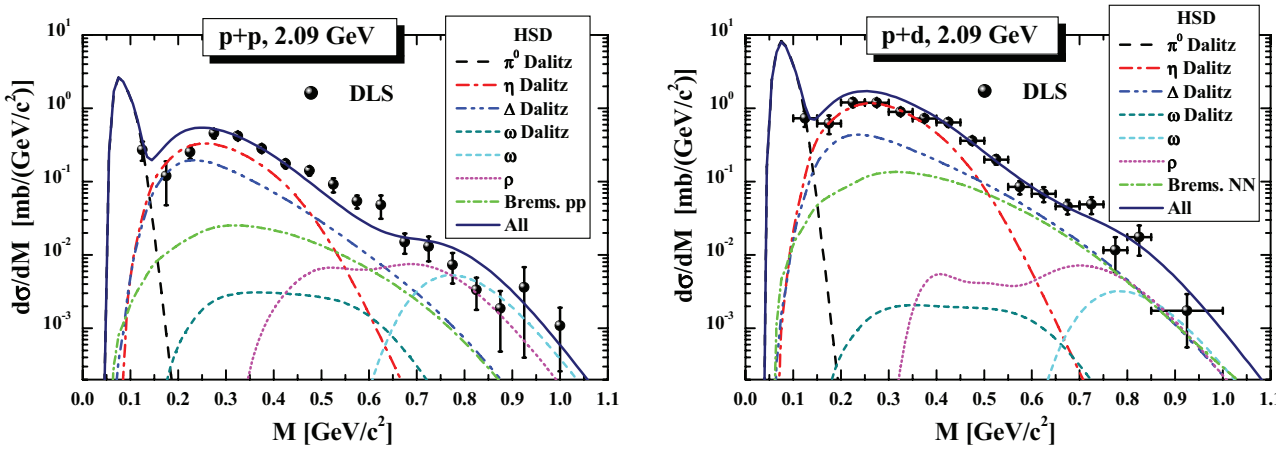

FIG. 10. (Color online) The dilepton differential cross section $d\sigma/dM$ for the pp (a) and pd (b) at 2.09 GeV in comparison to the DLS data [24]. The theoretical calculations passed through the corresponding acceptance filters and mass resolutions.

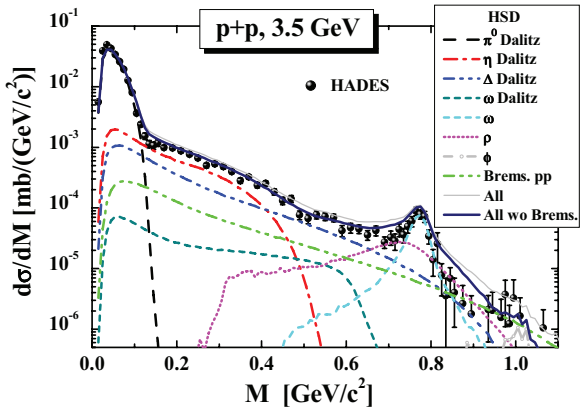

FIG. 11. (Color online) The differential cross section $d\sigma/dM$ from HSD calculations for e^+e^- production in pp reactions at a bombarding energy of 3.5 GeV in comparison to the HADES data [56]. The individual colored lines display the contributions from the various channels in the HSD calculations (see color coding in the legend). The thick line, labeled as All wo Brems, shows the total sum of all channels (labeled as All) without pp Bremsstrahlung. The theoretical calculations passed through the corresponding HADES acceptance filters and mass/momentum resolutions.

produce dileptons) and other resonances (which do not produce dileptons) is not well known and may be the origin of the deviation obtained in the p_T spectra. For the mass bin $0.47 < M < 0.7$ GeV we see that above $p_T = 0.7$ GeV/c bremsstrahlung is the dominating source of dilepton production. We plot the sum of all contributions without bremsstrahlung as well.

D. Dilepton production in pA collisions at 3.5 GeV

We are coming now to $p + A$ reactions. Figure 13 compares the differential cross section $d\sigma/dM$ from HSD calculations for e^+e^- production in $p + Nb$ reaction at a bombarding energy of 3.5 GeV to the HADES data [82]. The upper part shows the case of the "free" vector-meson spectral functions while the lower part gives the result for the collisional broadening scenario. Again the thick lines, labeled in the legend as All wo Brems, show the sum of all channels (labeled as All) without NN bremsstrahlung. We display both cases because the treatment of bremsstrahlung using the extrapolation of the OBE model to such high energy is questionable, as discussed above. For the same reason the πN bremsstrahlung presented in Fig. 13 has to be considered with care. The collisional broadening scenario comes closer to the experimental results in the region around the ρ peak. We thus find a nice agreement between theory and experiment also for proton-nucleus collisions.

IV. DILEPTON PRODUCTION IN HEAVY-ION COLLISIONS

A. Dileptons from the HSD and IQMD models

Now we come to the heavy-ion results and start with showing in Fig. 14 the mass differential dilepton spectra—normalized to the π^0 multiplicity—of HSD calculations for C + C at 1.0 GeV/nucleon in comparison to the HADES data [34]. The HADES Collaboration has obtained the π^0 multiplicity by the average of the multiplicity of charged pions [83] and we apply the same method for the theoretical calculations. The top panel displays the results for free vector-meson spectral functions while the bottom panel shows the result for the collisional broadening scenario. We note here—and this holds for all dilepton spectra normalized to the number of π^0's—that the normalization is done by the total number of π^0's in 4π, i.e., without applying an experimental acceptance. This allows for a direct comparison with the published HADES results.

The Δ-Dalitz decay and bremsstrahlung contributions are the dominant channels and contribute with about the same weight to the invariant mass spectra. For invariant masses $M > 0.3$ GeV also the subthreshold η channel contributes in an important way. The different descriptions of the ρ meson become important only at large invariant masses where no experimental data are available. The figure shows as well the contribution from direct ρ decays when including the $N^*(1520)$ resonance, which may enhance the ρ meson production at subthreshold energies as discussed in Sec. II B. As seen in the figure, there is, indeed, a small contribution but not larger than the experimental error bars. At higher energies other channels dominate. Therefore, the $N^*(1520)$ resonance is not an important source for dilepton production in heavy-ion reactions. Also the in-medium effects owing to the collisional broadening of the spectral functions for ρ and ω mesons is not visible in the final spectra owing to the strong contributions from other dilepton sources at low invariant masses where this effect is most pronounced and partly attributable to the limited experimental mass resolution at high invariant masses which smears out the spectra.

Figure 15 shows the results of IQMD calculations, including acceptance in the same way as the HSD calculations. It is remarkable that the two quite sophisticated transport theories predict results that are that similar. Even the channel decomposition is very similar, which is all but trivial because the invariant mass spectra depend on many details of the reaction. They include the Δ dynamics in a nucleus, which we discuss in Sec. V in more detail, the number of collisions and hence of the spatial distributions of the nucleons in the colliding nuclei, the Fermi momentum, and the Pauli blocking of reactions if final-state nucleons would be placed in already occupied phase-space regions.

Figure 16 shows the mass differential dilepton spectra—normalized to the π^0 multiplicity from HSD calculations for C + C—at 2 GeV/nucleon in comparison to the HADES data [37]. The theoretical calculations passed through the corresponding HADES acceptance filters and mass/momentum resolutions, which leads to a smearing of the spectra at high invariant mass and particularly in the ω peak region. The upper part shows again the case of free vector-meson spectral functions while the lower part presents the result for the collisional broadening scenario. Also, here the difference between the in-medium scenarios is of minor importance, partly owing to the limited mass resolution, which smears out the spectra. Nevertheless, one can conclude that the free calculations predict an enhancement in the region of the ρ

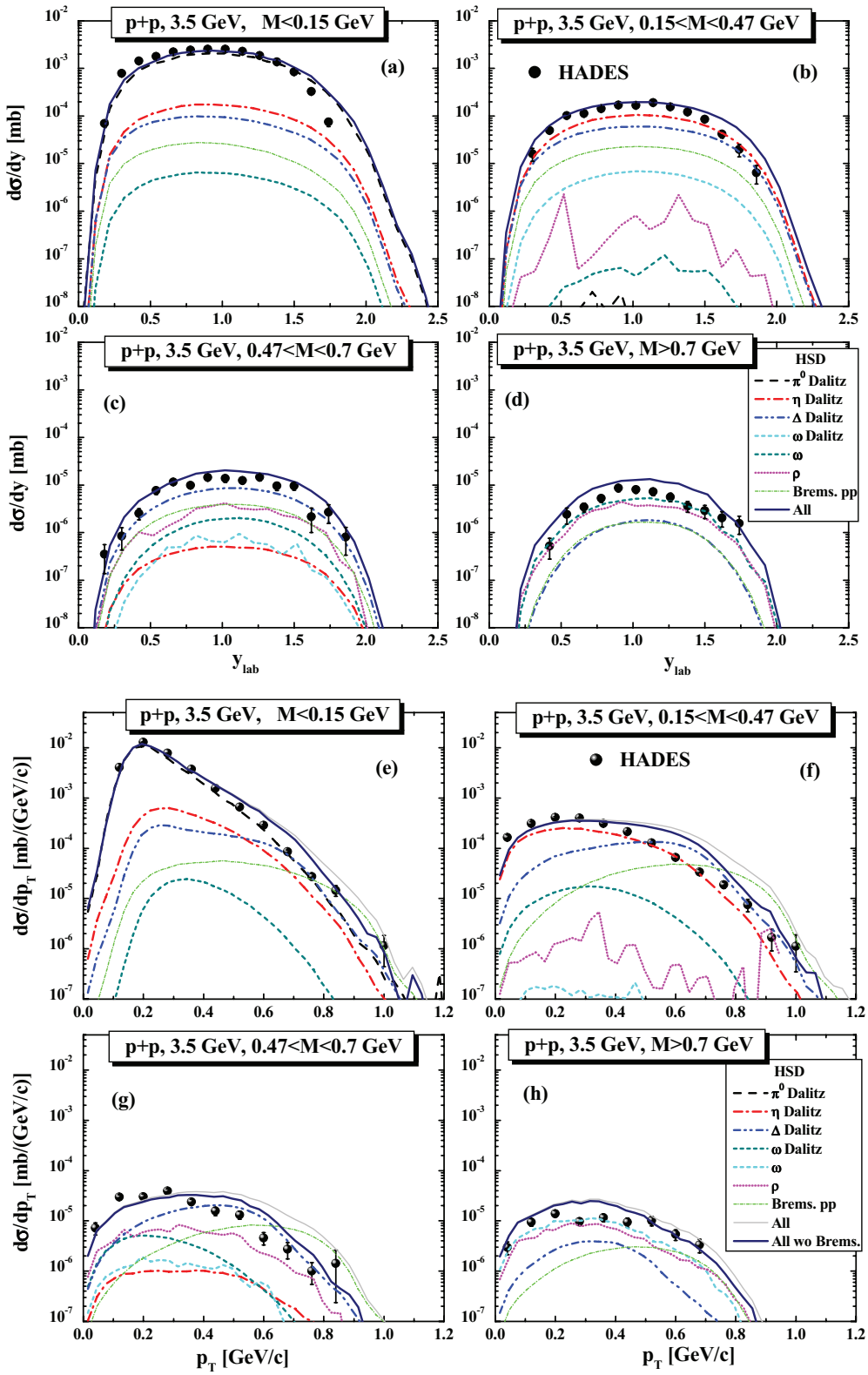

FIG. 12. (Color online) The HSD results for the rapidity distribution [upper four plots (a)–(d)] and the transverse momentum spectra [lower four plots (c)–(h)] for pp at 3.5 GeV and for four different mass bins: $M \leqslant 0.15$ GeV, $0.15 \leqslant M \leqslant 0.47$ GeV, $0.47 \leqslant M \leqslant 0.7$ GeV, and $M \geqslant 0.7$ GeV in comparison to the HADES data [56]. The individual colored lines display the contributions from the various channels in the HSD calculations (see color coding in the legend). The tick lines, labeled in the legend as All wo Brems, show the sum of all channels (labeled as All) without pp bremsstrahlung. The theoretical calculations passed through the corresponding HADES acceptance filters and mass/momentum resolutions.

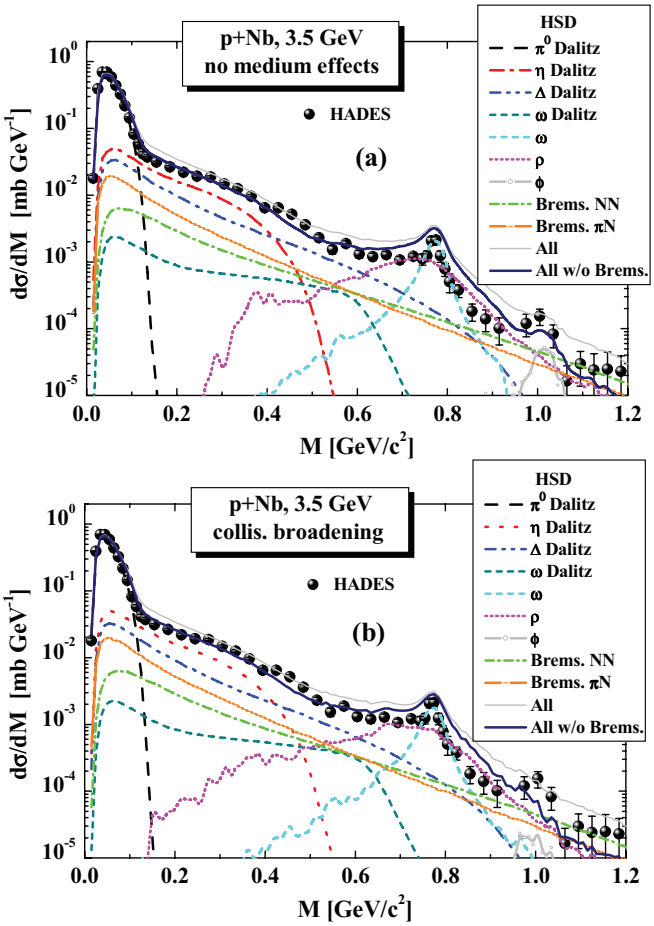

FIG. 13. (Color online) The differential cross section $d\sigma/dM$ from HSD calculations for e^+e^- production in the $p + Nb$ reaction at a bombarding energy of 3.5 GeV/nucleon in comparison to the HADES data [82]. Panel (a) shows the case of free vector-meson spectral functions while panel (b) gives the result for the collisional broadening scenario. The individual colored lines display the contributions from the various channels in the HSD calculations (see color coding in the legend). The tick lines, labeled in legend as All wo Brems, show the sum of all channels (labeled as All) without pp bremsstrahlung. The theoretical calculations passed through the corresponding HADES acceptance filters and mass/momentum resolutions.

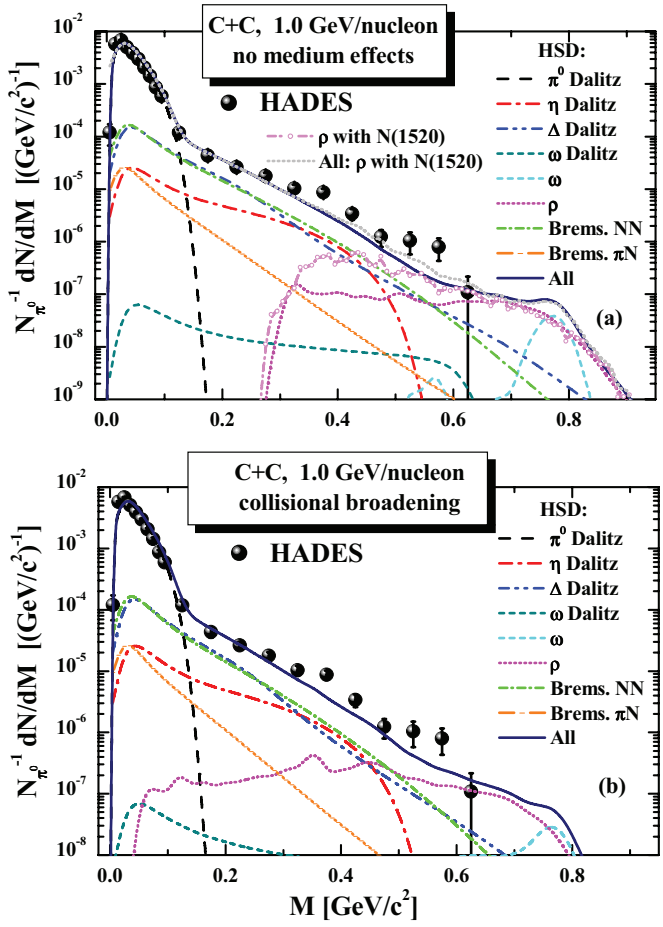

FIG. 14. (Color online) The results of the HSD transport calculation for the mass differential dilepton spectra—normalized to the π^0 multiplicity—for C + C at 1.0 GeV/nucleon in comparison to the HADES data [34]. Panel (a) shows the case of free vector-meson spectral functions, while panel (b) gives the result for the collisional broadening scenario. In both scenarios the HADES acceptance filter and mass/momentum resolution have been incorporated. The different color lines display individual channels in the transport calculation (see legend).

mass which is not seen in the experimental data, which are more in favor to the collisional broadening scenario.

Figure 17 compares the same data with the results from IQMD calculations for C + C at 2 GeV/nucleon, which have been acceptance corrected in the same way as the HSD data. Again we see a very good agreement between the two theoretical approaches. Only the different parametrizations of the ω cross section yield deviations at invariant masses around 0.77 GeV.

Figure 18 displays the mass differential dilepton spectra—normalized to the π^0multiplicity—from HSD calculations for Ar + KCl at 1.76 GeV/nucleon in comparison to the HADES data [39]. The top panel shows again the case of free vector-meson spectral functions while the lower panel gives the result for the collisional broadening scenario. Also in this data set the enhancement around the ρ mass is clearly visible. For this heavier system the collisional broadening scenario shows a slightly better agreement with experiment than the free result and we expect that for larger systems the difference between the two approaches increases.

Figure 19, which presents the IQMD results for this reaction, shows that the agreement between both theories continues also for heavier systems. Again up to invariant masses of 0.7 GeV both invariant mass spectra are almost identical and agree with data. Also the channel decomposition is rather similar. Here one can see again the overestimation of the dilepton yield by IQMD at the ρ/ω peak, which is related to the enhance ω production cross section in elementary pn collisions relative to pp collisions owing to the isospin model used in IQMD (cf. Sec. II C).

The transverse momentum spectra—normalized to the π^0 multiplicity—for Ar + KCl at 1.75 GeV/nucleon have been measured by the HADES Collaboration for five different mass

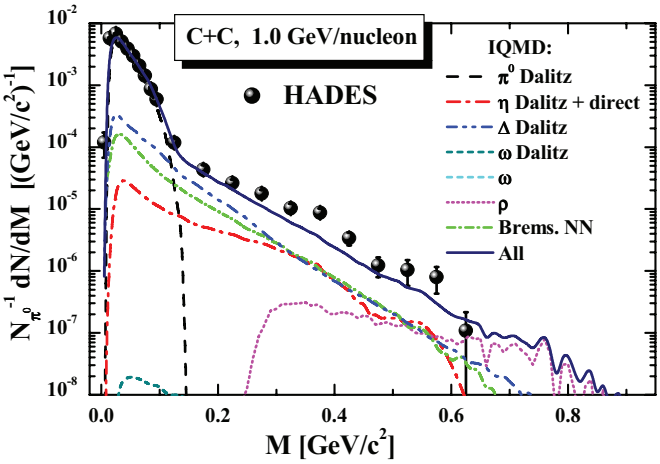

FIG. 15. (Color online) The mass differential dilepton spectra—normalized to the π^0 multiplicity from IQMD calculations for C + C—at 1 GeV/nucleon in comparison to the HADES data [34]. The different color lines display individual channels in the transport calculation (see legend). The theoretical calculations passed through the corresponding HADES acceptance filter and mass/momentum resolutions.

bins [39]: bin 1, $M \leqslant 0.15$ GeV; bin 2, $0.13 \leqslant M \leqslant 0.3$ GeV; bin 3, $0.3 \leqslant M \leqslant 0.45$ GeV; bin 4, $0.45 \leqslant M \leqslant 0.65$ GeV; bin 5, $M \geqslant 0.65$ GeV. Figure 20 presents the HADES data in comparison with HSD calculations, on the top without medium effect and on the bottom for the dropping mass scenario. We see also here a good agreement between theory and experiment. Thus, one can conclude that the agreement between theory and experiment (Figs. 14–20) up to $M \approx 0.5$ GeV is of such a quality that we can use the theory to study the physical processes involved.

The HADES Collaboration has recently measured also the dilepton invariant mass spectra for the reaction Au + Au at 1.25 GeV/nucleon. The analysis is not completed yet. Figure 21 presents the HSD predictions for the mass differential dilepton spectra—normalized to the π^0 multiplicity—for this reaction. The top panel shows the case of free vector-meson spectral functions, while the bottom panel gives the result for the collisional broadening scenario.

B. Dileptons from the UrQMD model

In this section we present the results from the UrQMD (v. 2.3) transport model [64,65]. In this model the dilepton afterburner does not contain bremsstrahlung. It is, however, useful to verify whether it agrees with HSD and IQMD calculations as far as all hadronic dilepton sources are concerned. For the details of the dilepton treatment in UrQMD at SIS energies, we refer the reader to Refs. [84,85].

Figure 22 shows the mass differential dilepton spectra—normalized to the π^0 multiplicity from UrQMD calculations for C + C—at 2 GeV/nucleon in comparison to the HADES data [37] and Fig. 23 shows that for Ar + KCl at 1.76 GeV/nucleon in comparison to the HADES data [39]. As one can see from Figs. 22 and 23 the UrQMD v. 2.3 substantially overestimates the dilepton yield from the vector

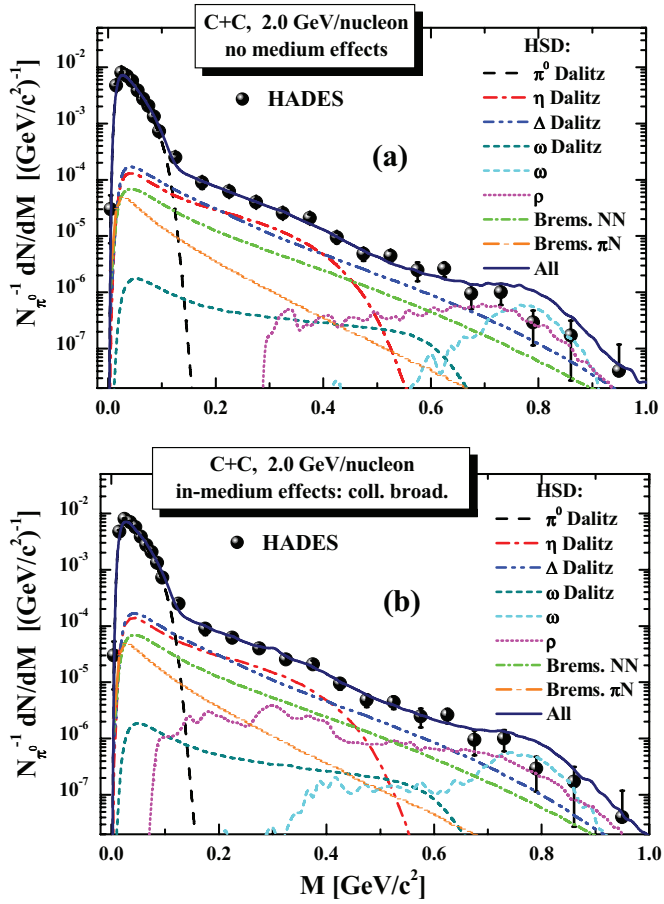

FIG. 16. (Color online) The mass differential dilepton spectra—normalized to the π^0 multiplicity—from HSD calculations for C + C at 2 GeV/nucleon in comparison to the HADES data [37]. Panel (a) shows the case of free vector-meson spectral functions, while the panel (b) gives the result for the collisional broadening scenario. The different color lines display individual channels in the transport calculation (see legend). The theoretical calculations passed through the corresponding HADES acceptance filter and mass/momentum resolutions.

mesons. The problem can be traced back to the description of ρ production in elementary NN collisions, which proceeds via an excitation and decay of heavy baryonic resonances $N(1520)$, $N(1770)$, ... Their coupling to the ρ channel is not well known and may therefore be overestimated. However, the dilepton yield at low invariant masses is underestimated for both systems. This is, first of all, attributable to the lack of the bremsstrahlung contributions but also to an underprediction of the η yield in UrQMD.

We note that the UrQMD model is presently under improvement and extension; updated results for the dileptons at SIS energies are expected soon [86].

V. RATIOS OF DILEPTON YIELDS $R(AA/NN)$

A. Comparison with experimental data

The primary interest of measuring dilepton production in heavy-ion collisions is to see whether it is a mere superposition of the production in elementary $[pp + pn(d)]$ collisions. Of

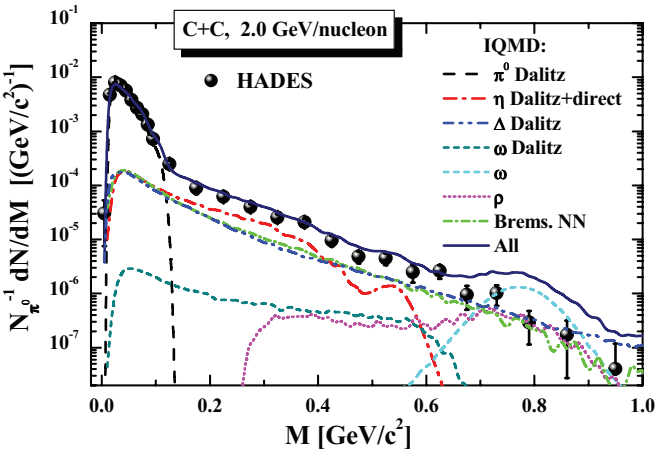

FIG. 17. (Color online) The mass differential dilepton spectra—normalized to the π^0 multiplicity—from IQMD for C + C at 2 GeV/nucleon in comparison to the HADES data [37]. The different color lines display individual channels in the transport calculation (see legend). The theoretical calculations passed through the corresponding HADES acceptance filter and mass/momentum resolutions.

course, in this threshold energy regime the Fermi motion of the nucleons inside a nucleus plays an important role and therefore the question has to be formulated more precisely: Is there an in-medium enhancement beyond the Fermi motion? This question we address in this section.

The HADES Collaboration has measured the elementary reactions at different beam energies than the heavy-ion reactions, i.e., pp and quasifree pn reactions at 1.25 GeV and the C + C collisions at 1.0 and 2.0 GeV/nucleon and Ar + KCl at 1.75 GeV/nucleon. Thus, a comparison of elementary reaction data with those of heavy ions at the same energy was not possible experimentally. Therefore, we also have to calculate the "reference spectrum" $NN = (pp + pn)/2$ at 1.25 GeV to compare with experimental AA/NN ratios. Then we show the sensitivity of the ratio AA/NN to the energy selection of reference spectra NN, which finally might influence the interpretation of in-medium modifications in $A + A$ collisions relative to the NN. All calculations presented here have been performed with free vector meson spectral functions.

Figure 24 (left panel) shows the mass differential dilepton spectra—normalized to the multiplicity of π^0's and after η-Dalitz yield subtraction—from HSD calculations for C + C at 1.0 GeV/nucleon (solid line), for the isospin-averaged reference spectra $NN = (pp + pn)/2$ at 1.25 GeV (short-dashed line) and at 1.0 GeV (dashed line), as well as for pd at 1.25 GeV (dot-dashed line). These calculations are compared to the corresponding HADES data from Refs. [37] for C + C at 1.0 GeV/nucleon and the reference spectra taken as an averaged sum of pp and quasifree $pn(d)$ (denoted as $[pp + pn(d)]/2$) measured at 1.25 GeV. The theoretical calculations passed through the HADES acceptance filter for C + C at 1.0 GeV/nucleon (denoted as "acc:CC@1AGeV") and mass/momentum resolutions, which smears out the high-mass region. The theoretical reference spectra are taken as the averaged sum of dilepton spectra from $p + p$ and free

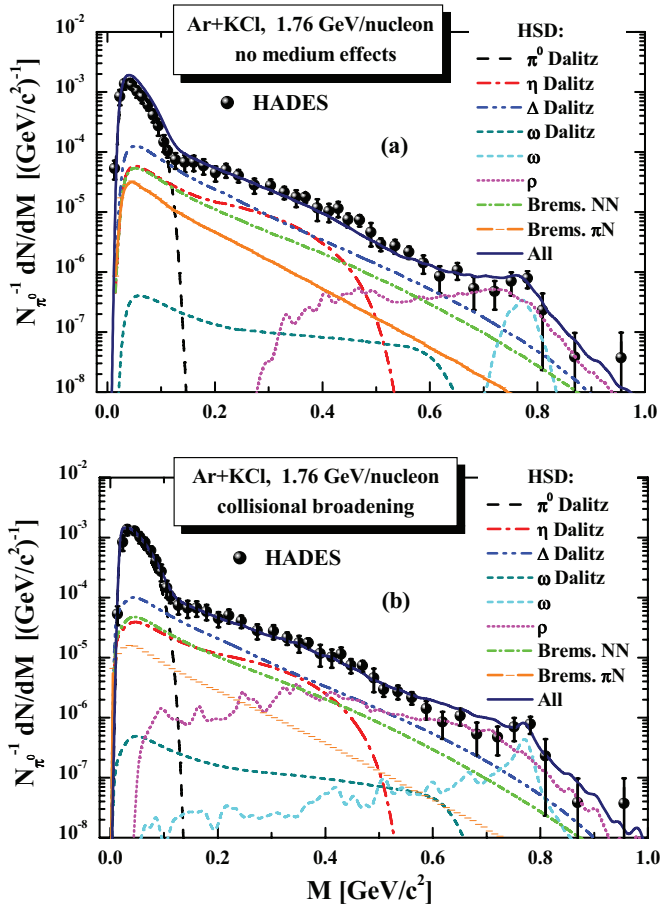

FIG. 18. (Color online) The mass differential dilepton spectra—normalized to the π^0 multiplicity—from HSD for Ar + KCl at 1.76 GeV/nucleon in comparison to the HADES data [39]. Panel (a) shows the case of free vector-meson spectral functions, while panel (b) gives the result for the collisional broadening scenario. The individual colored lines display the contributions from the various channels in the HSD calculations (see color coding in the legend). The theoretical calculations passed through the corresponding HADES acceptance filter and mass/momentum resolutions.

$p + n$ collisions. As seen from the figure there is no essential difference between our theoretical pd and NN spectra up to $M \approx 0.5$ GeV and only for larger invariant masses the enhanced "open" phase space for pd compared to NN becomes important.

Figure 24 (right panel) shows the ratio of the dilepton differential spectra for C + C at 1.0 GeV/nucleon to the isospin-averaged $NN = (pp + pn)/2$. Both spectra are normalized to the π^0 multiplicity and the η-Dalitz yield has been subtracted. The solid and short-dashed line present the ratio of C + C at 1.0 GeV/nucleon to NN at 1.25 GeV in the acceptance region and in 4π, respectively. The dash-dotted and dashed lines are the corresponding ratios of C + C at 1.0 GeV/nucleon to NN at 1.0 GeV. If we divide the spectra of C + C at 1.0 GeV/nucleon by the NN spectra at 1.25 GeV the ratio is quite flat, as the experiments show as well. The enhancement in the theory at the upper end of the π^0 peak and hence around $M = 0.15$

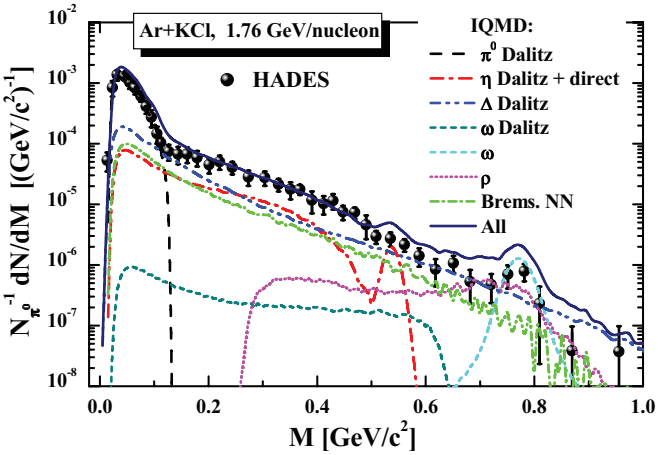

FIG. 19. (Color online) The mass differential dilepton spectra—normalized to the π^0 multiplicity—from IQMD for Ar + KCl at 1.76 GeV/nucleon in comparison to the HADES data [39]. The individual colored lines display the contributions from the various channels in the IQMD calculations (see color coding in the legend). The theoretical calculations passed through the corresponding HADES acceptance filter and mass/momentum resolutions.

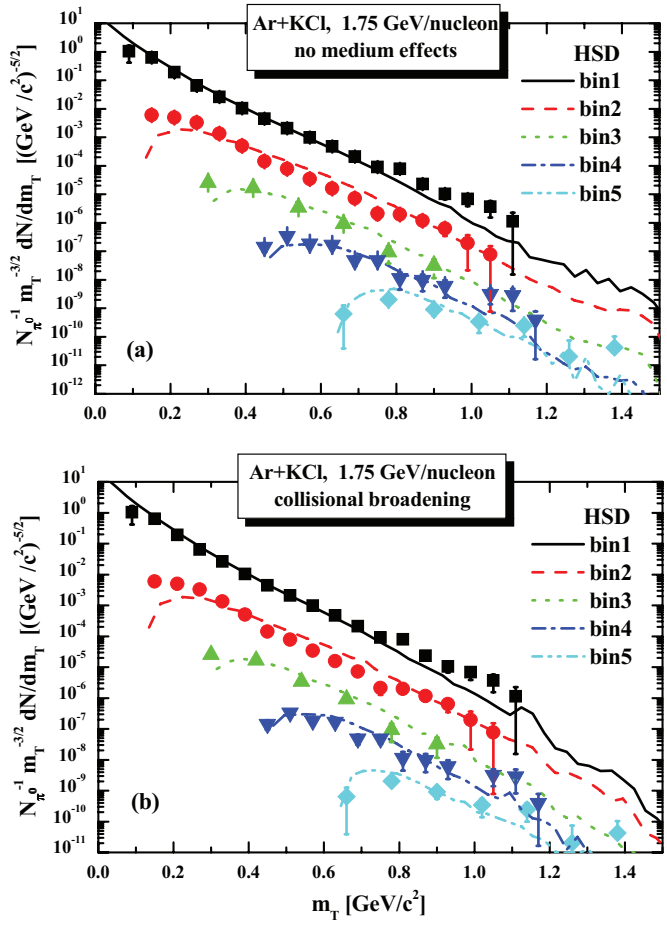

FIG. 20. (Color online) The HSD results for the transverse momentum spectra—normalized to the π^0 multiplicity—for Ar + KCl at 1.75 GeV/nucleon for five different mass bins in comparison to the HADES data [39]: bin 1, $M \leqslant 0.15$ GeV; bin 2, $0.13 \leqslant M \leqslant 0.3$ GeV; bin 3, $0.3 \leqslant M \leqslant 0.45$ GeV; bin 4, $0.45 \leqslant M \leqslant 0.65$ GeV; bin 5, $M \geqslant 0.65$ GeV. Panel (a) shows the case of free vector-meson spectral functions, while panel (b) gives the result for the collisional broadening scenario. The individual colored lines display the contributions from the various channels in the HSD calculations (see color coding in the legend). The theoretical calculations passed through the corresponding HADES acceptance filter and mass/momentum resolutions.

GeV comes in about equal parts from bremsstrahlung and Δ-Dalitz decay. We observe as well that the acceptance cuts do not change the enhancement. Therefore, we can discuss it in the next section using 4π yields. In this figure we display as well that the true enhancement, obtained by comparing C + C and NN at the same energy, is much larger. For 0.125 GeV $< M <$ 0.3 GeV it is about a factor of two.

We note that the HADES Collaboration used pp and quasifree $pn(d)$ spectra at 1.25 GeV as a reference $NN^d = [pp + pn(d)]/2$ spectrum for the ratios of the dilepton yields from AA to NN. To avoid the additional uncertainties of dilepton production in pd collision, a system that cannot be modeled reasonably well in semiclassical approaches, we use the reference spectra $NN = (pn + pp)/2$. As Fig. 24 shows, both methods are equivalent up to invariant masses of $M =$ 0.4 GeV. Above this value the ratio increases very quickly because in the elementary reactions the limitation owing to phase space is more severe than in heavy-ion collisions, where the Fermi motion can provide larger invariant masses. These HSD results are confirmed by the IQMD calculations shown in Fig. 25 in a form equivalent to that of Fig. 24.

Now we step to the energy 2.0 GeV/nucleon. To compare the experimental data for C + C, measured at two different energies 1.0 and 2.0 GeV/nucleon, the HADES Collaboration transformed the C + C data measured at 2.0 GeV/nucleon to the acceptance of C + C at 1.0 GeV/nucleon by using—owing to lack of statistics—a one-dimensional transformation (see Ref. [37]). We denote this transformation as "1D-acc:CC@1AGeV" to distinguish it from the standard three-dimensional filtering procedure using the "3D" (defined above as "acc:CC@1AGeV") experimental acceptance matrix (which depends on M, p_T, and y), provided by the HADES Collaboration [87] for the filtering of theoretical 4π results.

Figure 26 presents for C + C at 2.0 GeV/nucleon the same quantities as Fig. 24 for C + C at 1.0 GeV/nucleon. The solid line on the left is the result of the HSD calculations; the short-dashed line and the dash-dotted line are the isospin-averaged reference spectra $NN = (pp + pn)/2$ at 1.25 GeV and pd at 1.25 GeV. The dashed line is the reference NN spectrum at 2.0 GeV; the corresponding HADES data are taken from Refs. [37]. Note that the simulated HSD mass distribution for C + C at 2.0 GeV/nucleon has been transformed to the corresponding acceptance in the same way as done for the experimental data using the "1D-acc:CC@1AGeV" transformation. Fluctuations introduced by this procedure result, in part, from the limited statistics of the relevant HADES C + C data set and in part from the necessary rebinning of the latter.

The right panel of Fig. 26 shows the ratio of the dilepton differential spectra—normalized to the π^0 multiplicity and

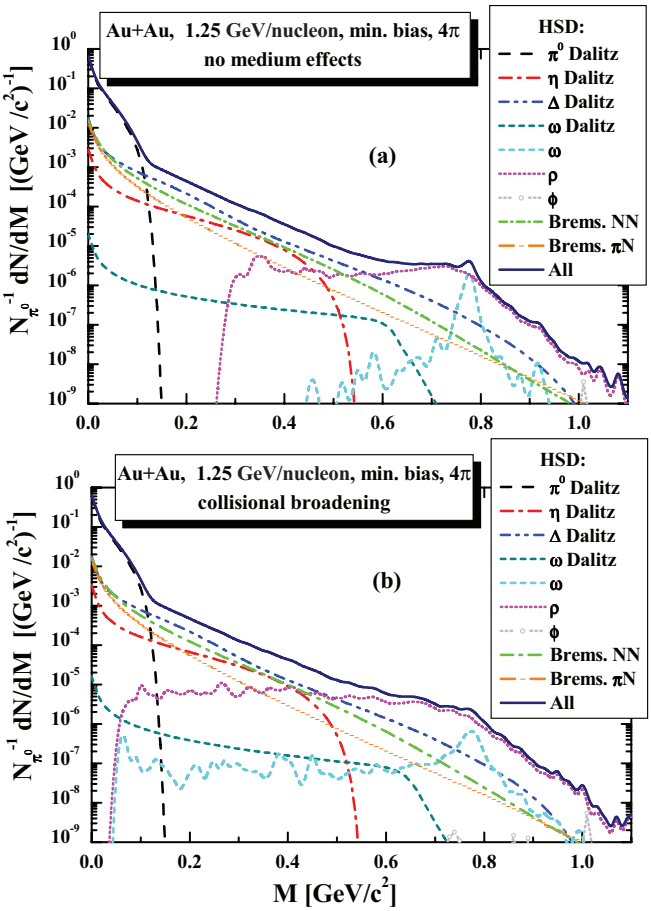

FIG. 21. (Color online) The mass differential dilepton spectra—normalized to the number of π^0's—from HSD for minimal bias Au + Au collisions at 1.25 GeV/nucleon. Panel (a) shows the case of free vector-meson spectral functions, while panel (b) gives the result for the collisional broadening scenario. The different color lines display individual channels in the transport calculation (see legend).

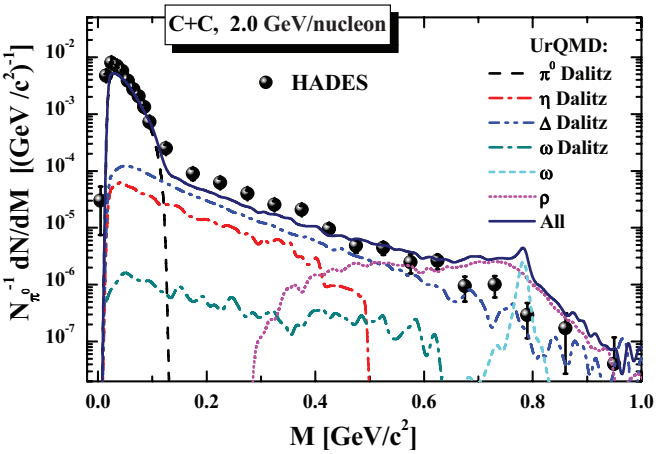

FIG. 22. (Color online) The mass differential dilepton spectra—normalized to the number of π^0's from UrQMD for C + C—at 2 GeV/nucleon in comparison to the HADES data [37]. The different color lines display individual channels in the transport calculation (see legend). The theoretical calculations passed through the corresponding HADES acceptance filter including mass/momentum resolutions.

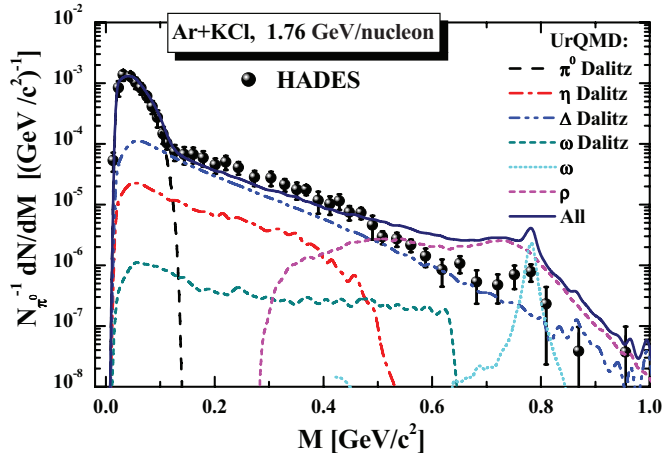

FIG. 23. (Color online) The mass differential dilepton spectra—normalized to the number of π^0's—from UrQMD for Ar + KCl at 1.76 GeV/nucleon in comparison to the HADES data [39]. The individual colored lines display the contributions from the various channels in the HSD calculations (see color coding in the legend). The theoretical calculations passed through the corresponding HADES acceptance filter including mass/momentum resolutions.

after η-Dalitz yield subtraction—of C + C at 2.0 GeV/nucleon to the isospin-averaged reference spectra $NN = (pp + pn)/2$ taken at 1.25 GeV, applying the C + C at 2.0 GeV/nucleon "1D-acc:CC@1AGeV" experimental acceptance (solid line) and in 4π result with the default Wolf differential electromagnetic width for Δ-Dalitz decay (short-dashed line) and "Krivoruchenko" width (dash-dot-dotted line) to demonstrate the model uncertainties (cf. discussion in Sec. VI). Also the HSD results for the ratio of C + C at 2.0 GeV/nucleon to the reference NN spectra, taken at 2.0 GeV, are shown, including the full 3D experimental acceptance (dash-dotted line) and in 4π (dashed line). These results show that the experimental data measured up to an invariant mass of $M \approx 0.5$ GeV are compatible with a ratio of one and hence with no in-medium enhancement. The theoretical results are more complicated. Up to an invariant mass of $M \approx 0.3$ GeV theory predicts a enhancement factor of about 1.8 for 4π. The ratio at the same nominal energy shows this enhancement even up to invariant masses of $M \approx 0.6$ GeV before the influence of the Fermi motion sets in.

The IQMD calculations for C + C at 2.0 GeV/nucleon are presented in Fig. 27, which shows the same quantities as Fig. 26. We see that the both models agree quite well and the form of the ratio is identical in both approaches.

Figure 28 (left panel) displays the mass differential dilepton spectra for Ar + KCl at 1.76 GeV/nucleon (solid line), normalized to the π^0 multiplicity and after η-Dalitz yield subtraction. We compare HSD calculations for Ar + KCl at 1.76 GeV/nucleon, for the isospin-averaged reference spectra $NN = (pp + pn)/2$ at 1.25 GeV (short-dashed line) and at 1.76 GeV (dashed line) as well as for pd at 1.25 GeV (dot-dashed line) to the corresponding HADES data, taken from Ref. [39]. The theoretical calculations for Ar + KCl and for NN passed through the HADES acceptance filter for Ar + KCl and mass/momentum resolutions. The right

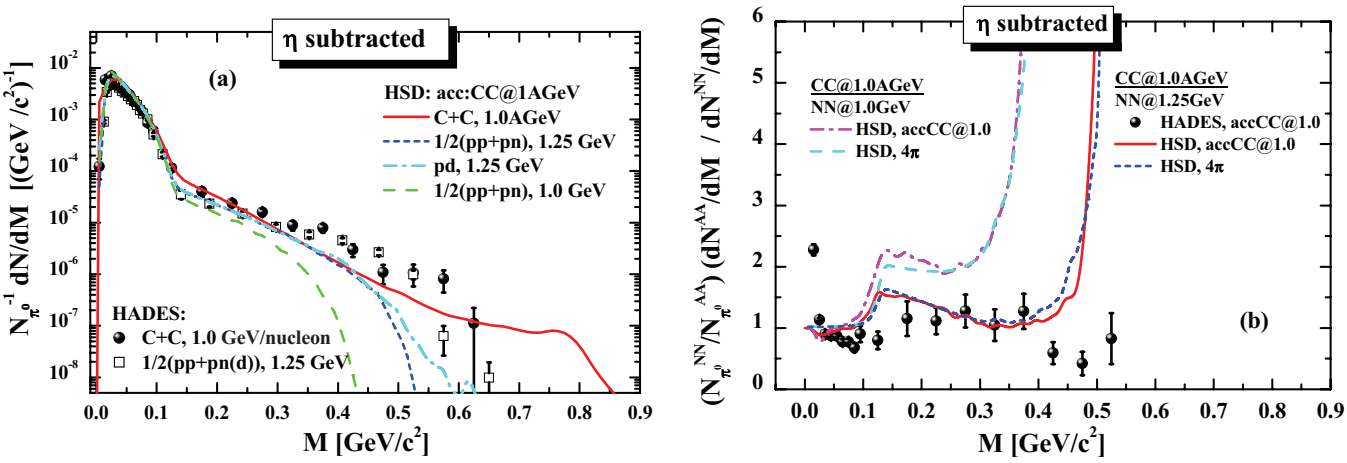

FIG. 24. (Color online) (a) The mass differential dilepton spectra—normalized to the π^0 multiplicity and after η-Dalitz yield subtraction—from HSD calculations for C + C at 1.0 GeV/nucleon (solid line), for the isospin-averaged reference spectra $NN = (pp + pn)/2$ at 1.25 GeV (short-dashed line) and that at 1.0 GeV (dashed line), as well as for pd at 1.25 GeV (dot-dashed line) in comparison to the corresponding HADES data [37] for C + C at 1.0 GeV/nucleon and the reference spectra taken as an averaged sum of pp and quasifree $pn(d)$ (denoted as $[pp + pn(d)]/2$) measured at 1.25 GeV. The theoretical calculations passed through the HADES acceptance filter for C + C at 1.0 GeV/nucleon (denoted as "acc:CC@1AGeV") and mass/momentum resolutions. (b) Ratio of the dilepton differential spectra—normalized to the π^0 multiplicity and after η-Dalitz yield subtraction—to the isospin-averaged reference spectra $NN = (pp + pn)/2$ taken at 1.25 GeV employing C + C at 1.0 GeV/nucleon experimental ("acc:CC@1AGeV") acceptance (solid line) and in 4π (short-dashed line). Also the HSD results for the ratio of C + C at 1.0 GeV/nucleon to the reference NN spectra at 1.0 GeV are shown with experimental ("acc:CC@1AGeV") acceptance corrections (dash-dotted line) and in 4π (dashed line).

panel of Fig. 28 shows the ratio of the dilepton differential spectra—normalized to the π^0 multiplicity and after η-Dalitz yield subtraction—to the isospin-averaged reference spectra $NN = (pp + pn)/2$ taken at 1.25 GeV and employing the Ar + KCl experimental acceptance (solid line) and in 4π (short-dashed line). We display as well the HSD results for the ratio of Ar + KCl at 1.76 GeV/nucleon to the reference NN spectrum at the same energy, including the experimental Ar + KCl acceptance (dash-dotted line) and in 4π (dashed line). These results show clearly that for invariant masses of 0.1 GeV $< M <$ 0.35 GeV the data as well as theory are not a mere superposition of the elementary spectra. The comparison also excludes that this enhancement, observed in heavy-ion collisions, is attributable to acceptance because the results with acceptance and in 4π are very similar. At larger invariant masses theory and data do not agree because of the bump at the invariant masses around $M \approx 0.5$ GeV, seen in the experimental pd reactions, is not reproduced by theory.

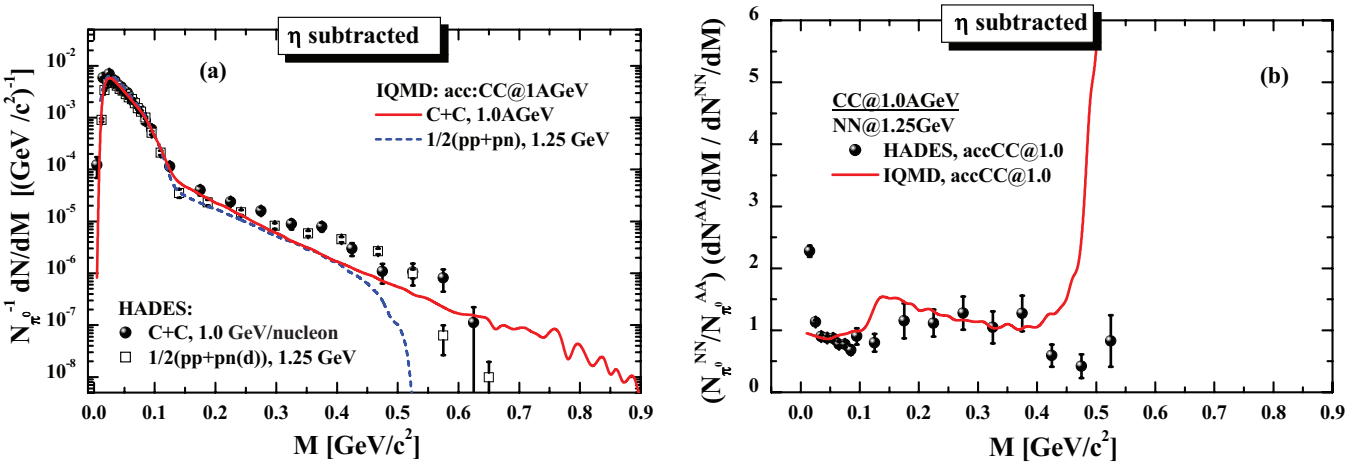

FIG. 25. (Color online) (a) The mass differential dilepton spectra—normalized to the π^0 multiplicity and after η-Dalitz yield subtraction—from IQMD calculations for C + C at 1.0 GeV/nucleon (solid line) and for the isospin-averaged reference spectra $NN = (pp + pn)/2$ at 1.25 GeV (short-dashed line) in comparison to the HADES data [37]. The theoretical calculations passed through the HADES acceptance filter for C + C at 1.0 GeV/nucleon and mass/momentum resolutions. (b) Ratio of the dilepton differential spectra—normalized to the π^0 multiplicity and after η-Dalitz yield subtraction—of C + C at 1.0 GeV/nucleon [employing C + C at 1.0 GeV/nucleon experimental ("'acc:CC@1AGeV"') acceptance] to the isospin-averaged reference spectra $NN = (pp + pn)/2$ taken at 1.25 GeV.

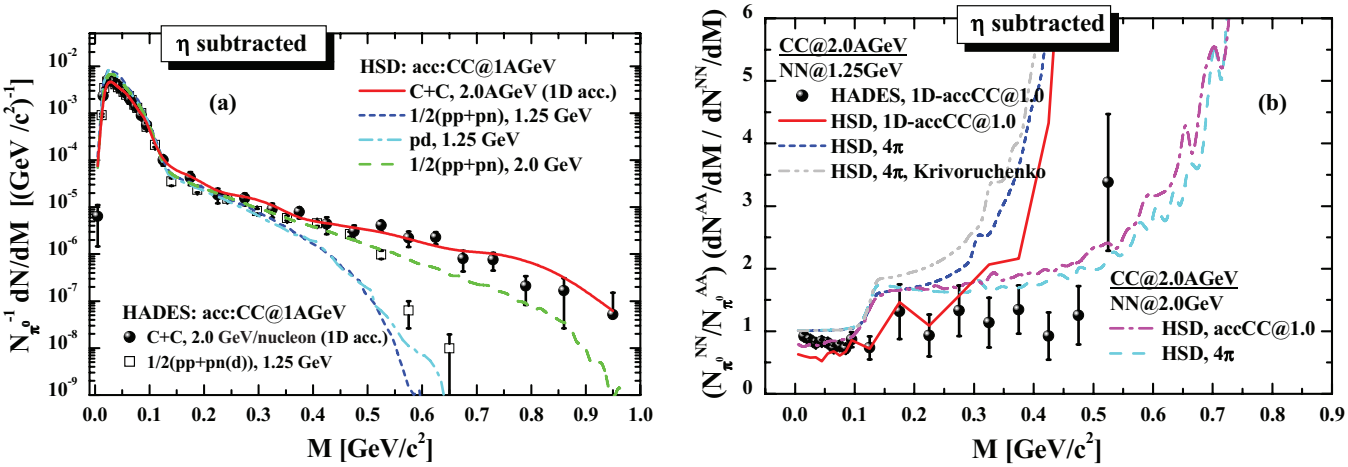

FIG. 26. (Color online) (a) The mass differential dilepton spectra—normalized to the π^0 multiplicity and after η-Dalitz yield subtraction—from HSD calculations for C + C at 2.0 GeV/nucleon (solid line) and for the isospin-averaged reference spectra $NN = (pp + pn)/2$ at 1.25 GeV (short-dashed line) and at 2.0 GeV (dashed line) as well as for pd at 1.25 GeV (dot-dashed line) in comparison to the HADES data [37] - for C + C measured at 2.0 GeV/nucleon and $[pp + pn(d)]/2$ at 1.25 GeV and transformed to the acceptance for C + C at 1.0 GeV/nucleon (see the discussion in the text). The theoretical calculations passed through the HADES acceptance filter for C + C at 1.0 GeV/nucleon ("1D-acc:CC@1AGeV") and mass/momentum resolutions. Right (b): Ratio of the dilepton differential spectra of C + C at 2.0 GeV/nucleon—normalized to the π^0 multiplicity and after η-Dalitz yield subtraction—to the isospin-averaged reference spectra $NN = (pp + pn)/2$ at 1.25 GeV with experimental ("1D-acc:CC@1AGeV") acceptance (solid line) and in 4π result with the default Wolf differential electromagnetic width for Δ-Dalitz decay (short-dashed line) and Krivoruchenko width (dash-dot-dotted line). Also the HSD results for the ratio of C + C at 2 GeV/nucleon to the reference NN spectra at 2.0 GeV are shown: with experimental ("acc:CC@1AGeV") acceptance for C + C at 1.0 GeV/nucleon (dash-dotted line) and in 4π (dashed line).

Taking the reference spectra at the same nominal energy theory predicts that this enhancement is constant up to energies of $M \approx 0.5$ GeV. Then the Fermi motion becomes important and yields a strong increase of the ratio.

Consequently, the experimental ratios of the invariant mass spectra measured in heavy-ion collisions to the isospin-averaged reference spectra $NN = (pp + pn)/2$ taken at 1.25 GeV reveals an in-medium enhancement in Ar + KCl collisions at 1.75 GeV/nucleon, whereas in C + C collisions at 2 GeV/nucleon this ratio is compatible with one and therefore no in-medium enhancement is seen. The transport models show an enhancement in all heavy-ion reactions when the reference spectrum is taken at the same energy. It shows as well that acceptance cuts do not modify this enhancement.

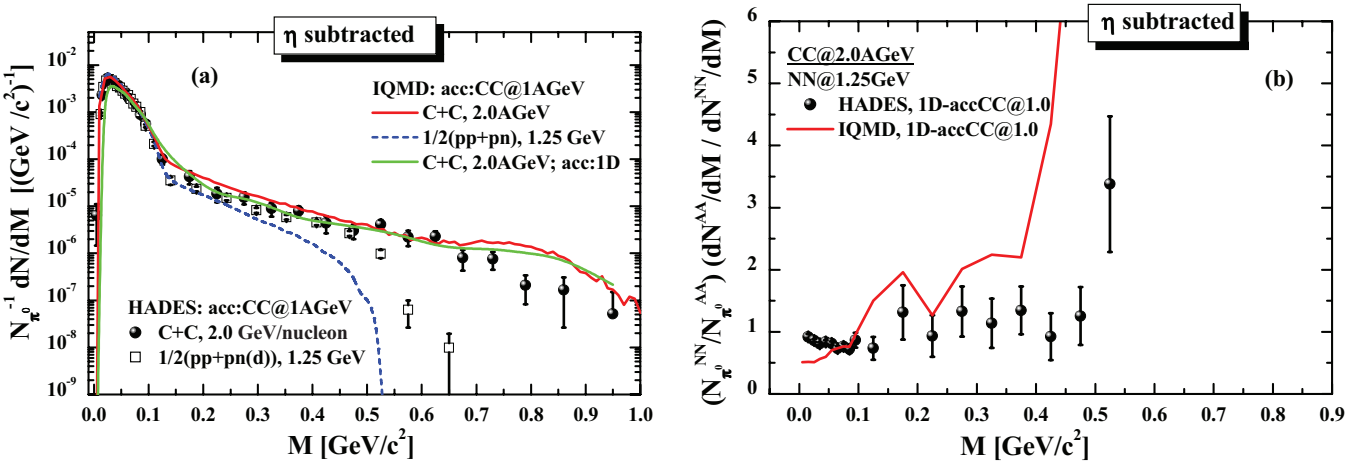

FIG. 27. (Color online) (a) The mass differential dilepton spectra—normalized to the π^0 multiplicity and after η-Dalitz yield subtraction—from IQMD calculations for C + C at 2.0 GeV/nucleon (solid line) and for the isospin-averaged reference spectra $NN = (pp + pn)/2$ at 1.25 GeV (short-dashed line) in comparison to the HADES data [37]. The theoretical calculations passed through the corresponding HADES acceptance filter for C + C at 1.0 GeV/nucleon ("1D-acc:CC@1AGeV") and mass/momentum resolutions (see the discussion in the text). (b) Ratio of the dilepton differential spectra for C + C at 2.0 GeV/nucleon—normalized to the π^0 multiplicity and after η-Dalitz yield subtraction—to the isospin-averaged reference spectra $NN = (pp + pn)/2$ taken at 1.25 GeV with experimental ("1D-acc:CC@1AGeV") acceptance for C + C at 1.0 GeV/nucleon (solid line).

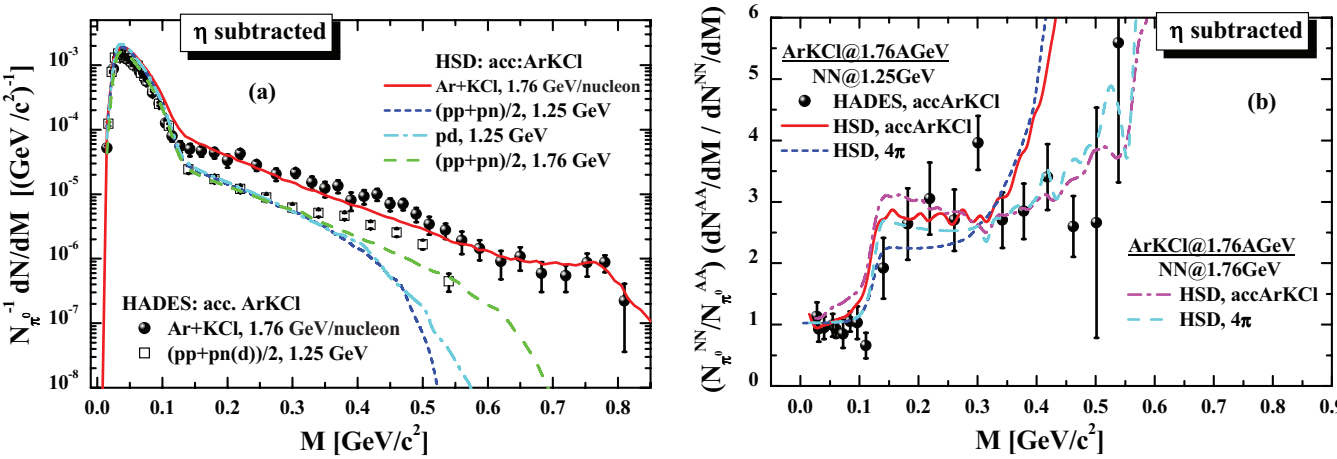

FIG. 28. (Color online) (a) The mass differential dilepton spectra—normalized to the π^0 multiplicity and after η-Dalitz yield subtraction—from HSD calculations for Ar + KCl at 1.76 GeV/nucleon (solid line) and for the isospin-averaged reference spectra $NN = (pp + pn)/2$ at 1.25 GeV (short-dashed line) and at 1.76 GeV (dashed line), as well as for pd at 1.25 GeV (dot-dashed line) in comparison to the corresponding HADES data [39]. The theoretical calculations for Ar + KCl and for NN passed through the HADES acceptance filter for Ar + KCl and mass/momentum resolutions. (b) Ratio of the dilepton differential spectra—normalized to the π^0 multiplicity and after η-Dalitz yield subtraction—to the isospin-averaged reference spectra $NN = (pp + pn)/2$ taken at 1.25 GeV, involving Ar + KCl experimental acceptance (solid line) and for 4π (short-dashed line). Also, the HSD results for the ratio to the reference NN spectra taken at 1.76 GeV are shown, with the Ar + KCl experimental acceptance (dash-dotted line) and in 4π (dashed line).

The origin of this enhancement is discussed in the next section.

In Fig. 29 we display the same quantities as in Fig. 28 but for IQMD calculations. The enhancement of the experimental ratio is confirmed by IQMD calculations, which are in quantitative agreement with the HSD results.

B. Energy and system size dependence of the dilepton yield

In this section we present the energy and system size dependence of the dilepton yield in 4π as predicted by the HSD calculations to study the question of a possible in-medium enhancement and to identify eventually its physical origin.

Figure 30 shows the HSD calculations for the mass differential dilepton spectra—normalized to the π^0 multiplicity—for pn (left) and pp (right) collisions at 1.0, 1.25, 1.75, 2.0, and 3.5 GeV in 4π acceptance. Whereas the normalization renders the low-invariant mass part to one, independent of the beam energy, the spectra at high-invariant masses show a strong beam energy dependence, as expected. Bremsstrahlung is not coupled to the number of pions (or the number of participants which is often assumed to be proportional to the number of

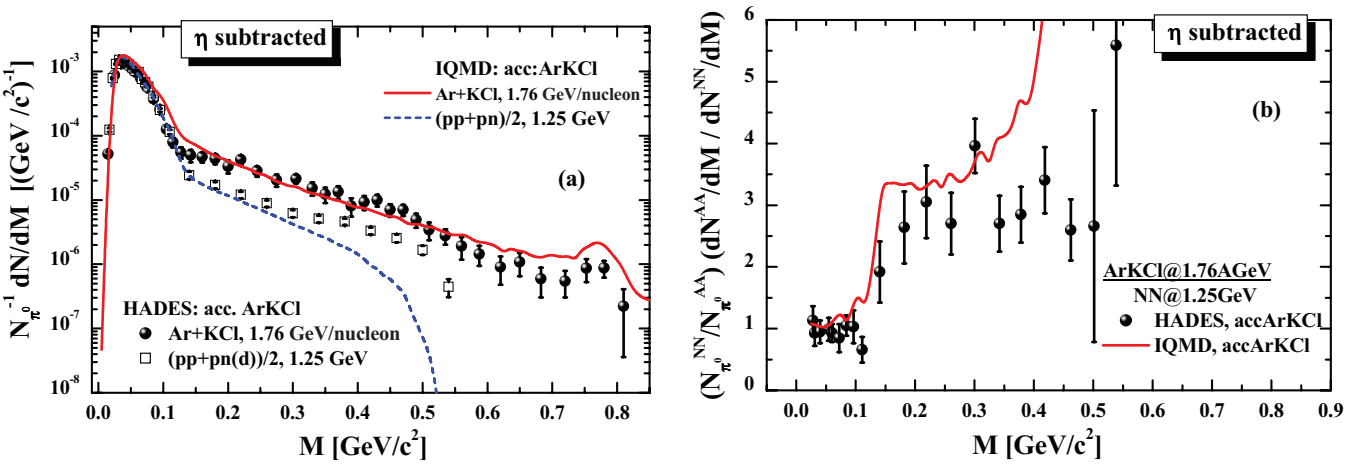

FIG. 29. (Color online) (a) The mass differential dilepton spectra—normalized to the π^0 multiplicity and after η-Dalitz yield subtraction—from IQMD calculations for of Ar + KCl at 1.76 GeV/nucleon (solid line) and for the isospin-averaged reference spectra $NN = (pp + pn)/2$ at 1.25 GeV (short-dashed line) in comparison to the corresponding HADES data [39]. The theoretical calculations for Ar + KCl and for NN passed through the HADES acceptance filter for Ar + KCl and mass/momentum resolutions. (b) Ratio of the dilepton differential spectra—normalized to the π^0 multiplicity and after η-Dalitz yield subtraction—to the isospin-averaged reference spectra $NN = (pp + pn)/2$, taken at 1.25 GeV, employing the Ar + KCl experimental acceptance (solid line).

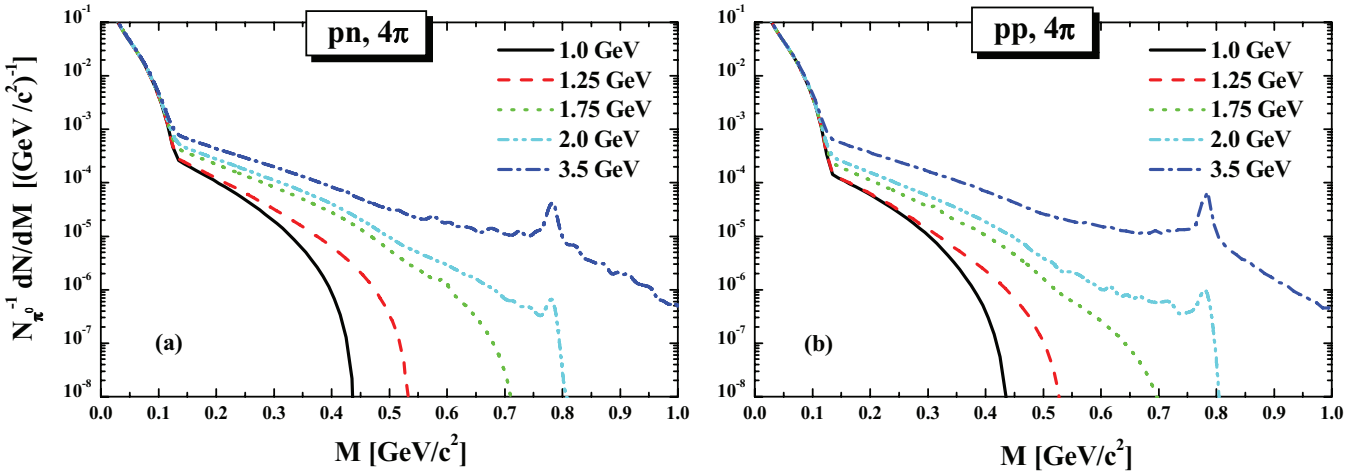

FIG. 30. (Color online) The 4π mass differential dilepton spectra—normalized to the π^0 multiplicity—obtained in HSD calculations for pn (a) and pp (b) collisions at 1.0, 1.25, 1.75, 2.0, and 3.5 GeV.

π's) but to the number of collisions. Also the production of heavier mesons increases at these energies close to the meson thresholds, either because it becomes easier to produce them directly or because the baryonic resonances which decay into these resonances are more frequently populated. Last but not least, the phase space limitation of the invariant mass changes with energy, which makes ratios between invariant mass spectra at different energies complicated. Owing to the isospin dependence of different processes the pp and pn invariant mass spectra differ in detail but are generally determined by phase space. We can conclude from Fig. 30 that the comparison of dilepton data of heavy ions and of elementary reactions suffer substantially if both are measured at different energies. This renders quantitative conclusions difficult.

Figure 31 displays the results of HSD calculations for the 4π mass differential dilepton spectra—normalized to the π^0 multiplicity—for the minimal bias symmetric heavy-ion collisions as compared to the isospin-averaged reference spectra $NN = (pn + pp)/2$. We display calculations for C + C, Ar + KCl, and Au + Au at 1.0, 1.25, 1.75, and 2.0 GeV/nucleon. The top panel corresponds to the total dilepton $A + A$ spectra, whereas the bottom panel shows the dilepton spectra after η-Dalitz yield subtraction. The thick lines in the bottom panel stand for the $A + A$ dilepton yields, whereas the thin lines show the NN spectra at the same energies. We see clearly that the dilepton spectra do not scale with the π^0 multiplicity for invariant masses $M > 0.11$ GeV. There is a strong energy and system size dependence of this invariant mass region owing to the complicated dynamics of baryon resonances and mesons. Generally, the invariant mass spectra in $A + A$ collisions are smoother owing to the Fermi motion.

Figure 32 presents the ratio $(1/N_{\pi^0}^{AA} dN^{AA}/dM)/(1/N_{\pi^0}^{NN} dN^{NN}/dM)$ of the mass differential dilepton spectra—normalized to the π^0 multiplicities—obtained in HSD calculations. Displayed are the ratios of minimal bias C + C, Ar + KCl, and Au + Au collisions and of the isospin-averaged reference spectra $NN = (pn + pp)/2$ at the same energy. The bottom panel depicts the same ratios but for the dilepton spectra after η-Dalitz yield subtraction. Clearly,

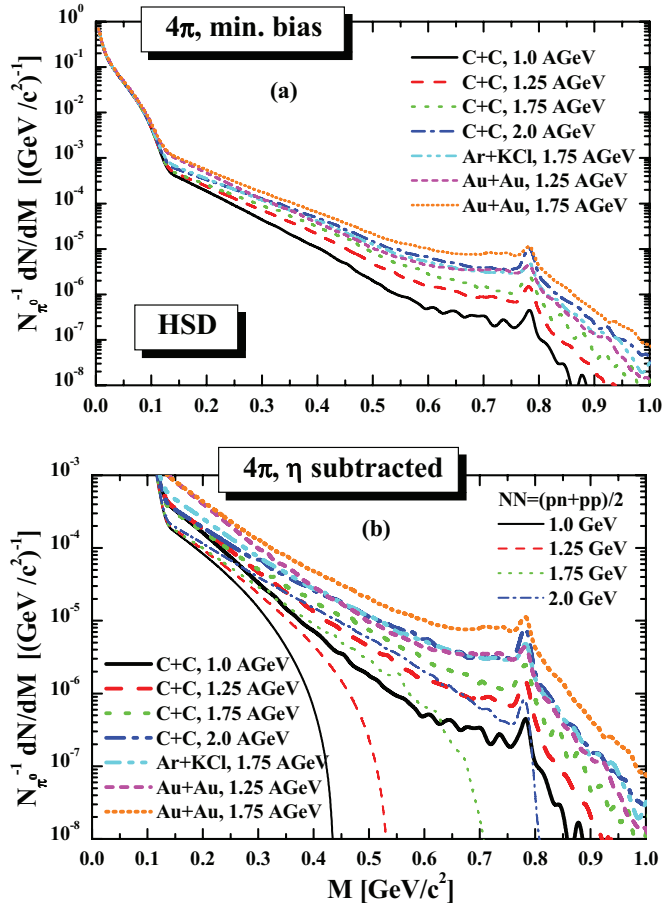

FIG. 31. (Color online) The invariant mass differential dilepton spectra—normalized to the π^0 multiplicity—obtained in HSD calculations for the minimal bias C + C, Ar + KCl, and Au + Au collisions and for the isospin-averaged reference spectra $NN = (pn + pp)/2$ at 1.0, 1.25, 1.75, and 2.0 GeV/nucleon in 4π acceptance. Panel (a) corresponds to the total dilepton $A + A$ spectra, whereas panel (b) shows the dilepton spectra after η-Dalitz yield subtraction. The thick lines on the lower plot stand for the $A + A$ dilepton yields, whereas the thin lines show the NN spectra at the same energy.

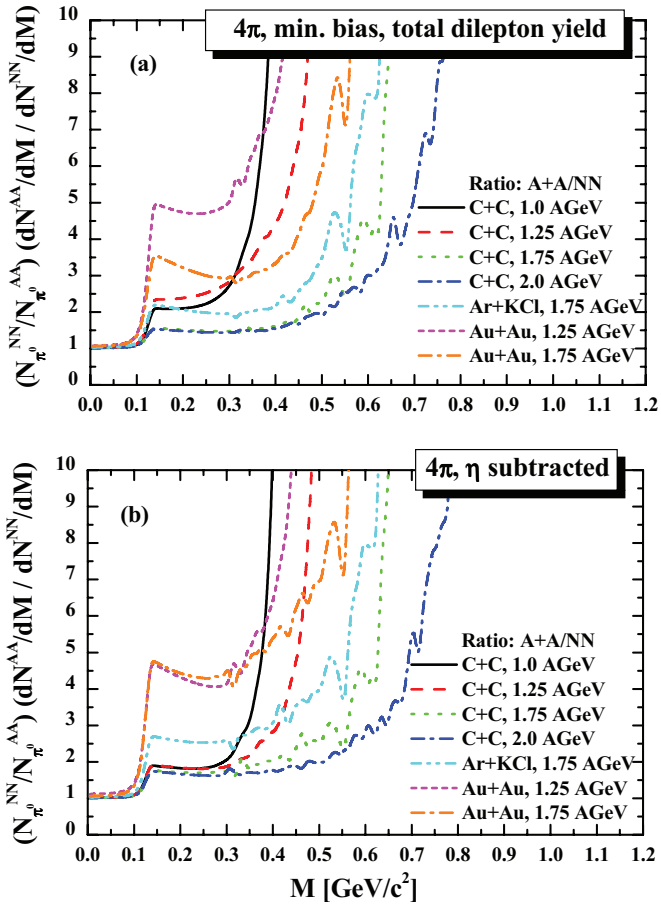

FIG. 32. (Color online) (a) The ratio $(1/N_{\pi^0}^{AA} dN^{AA}/dM)/(1/N_{\pi^0}^{NN} dN^{NN}/dM)$ of the invariant mass differential dilepton 4π spectra—normalized to the π^0 multiplicity—from HSD calculations for minimal bias $A + A$ collisions: We display C + C, Ar + KCl, and Au + Au collisions in comparison to the isospin-averaged reference spectra $NN = (pn + pp)/2$ at 1.0, 1.25, 1.75, and 2.0 GeV/nucleon. (b) The same ratios but for the dilepton spectra after η-Dalitz yield subtraction.

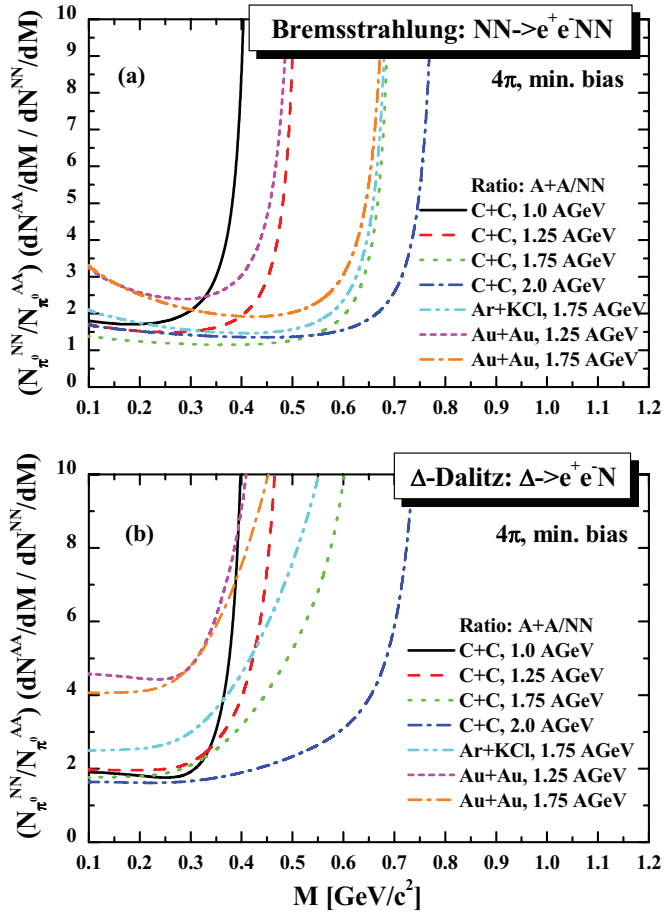

FIG. 33. (Color online) The ratio $(1/N_{\pi^0}^{AA} dN^{AA}/dM)/(1/N_{\pi^0}^{NN} dN^{NN}/dM)$ of the dilepton yield from the bremsstrahlung channel (a) and Δ-Dalitz decay (b), normalized to the multiplicity of π^0. We display HSD calculations for the ratio of the minimal bias C + C, Ar + KCl, and Au + Au collisions and the isospin-averaged reference spectra $NN = (pn + pp)/2$ at the same energy.

we see a quite complex structure. We start with the energy dependence of the ratio, which decreases with energy. Including the η production this can be clearly seen by comparing the Au + Au collisions at 1.75 and at 1.25 GeV/nucleon as well as by comparing the C + C system at different energies; η subtraction modifies some details but does not change the tendency. It is also obvious that the ratio increases with the system size. The ratio for Au + Au at 1.25 GeV/nucleon is about 4.5, that of C + C at the same energy around 2.5. We study now the origin of this enhancement in detail.

In Fig. 33 we display the enhancement factor in heavy-ion collisions for two different processes: bremsstrahlung and Δ-Dalitz decay. We show the ratio $(1/N_{\pi^0}^{AA} dN^{AA}/dM)/(1/N_{\pi^0}^{NN} dN^{NN}/dM)$ of the dilepton yield from HSD calculations of the minimal bias $A + A$ collisions: C + C, Ar + KCl, and Au + Au and of the isospin-averaged reference spectra $NN = (pn + pp)/2$ at the same energy. The top panel shows the contribution from bremsstrahlung; the bottom panel shows that from the Δ-Dalitz decay.

We do not expect that bremsstrahlung, one of the dominant sources at beam energies around 1 GeV/nucleon, scales with the number of pions; therefore, the ratio should deviate from one. It has to be systematically larger than one owing to multiple collisions of incoming nucleons in heavy-ion collisions. We see that the ratio depends on the mass but depends little on the energy of the system. In Au + Au collisions where the number of elementary collisions is large the enhancement can reach a factor of 3. At higher energies the bremsstrahlung contribution is not really settled because there are no reliable calculations for the elastic and inelastic elementary channels.

The other dominant source for dilepton production at beam energies around 1 GeV/nucleon is Δ-Dalitz decay. One may assume that the Δ-Dalitz decay scales with the number of pions because the relative ratio is given by the branching ratio but this is not the case. First of all, we are here in a threshold region where the Fermi momentum can lead only to a substantial enhancement of the production. Second, pions from Δ decay can be reabsorbed by nucleons and can form again a Δ which may later disappear in a $\Delta N \rightarrow NN$ collisions. This process

TABLE I. Ratio of π^0 mesons and the integrated dilepton yield $[N(\Delta \to e^+e^-) = \int dM \frac{dN(\Delta \to e^+e^-)}{dM}]$ from Δ-Dalitz decays for C + C and Au + Au at $b = 0.5$ fm and 1 GeV/nucleon and that from the "elementary" NN reactions for different scenarios: with/without Fermi motion ("Fermi m."), with/without secondary mB collisions ("mB col.")

1 Fermi m.	2 mB col.	3 System	4 $N(\pi^0)$	5 $N(\Delta \to e^+e^-)$	6 $R(\pi^0) = \frac{N^{AA}(\pi^0)}{N^{NN}(\pi^0)}$	7 $R(e^+e^-) = \frac{N^{AA}(\Delta \to e^+e^-)}{N^{NN}(\Delta \to e^+e^-)}$	8 $\frac{R(e^+e^-)}{R(\pi^0)} = \frac{(7)}{(6)}$
−	−	CC	0.743	0.565×10^{-4}	6.74	5.56	0.83
−	−	AuAu	18.76	1.688×10^{-3}	170.08	166.3	0.98
+	−	CC	1.407	1.16×10^{-4}	12.76	11.42	0.89
+	−	AuAu	31.07	2.75×10^{-3}	281.69	270.93	0.97
−	+	CC	0.633	0.86×10^{-4}	5.74	8.47	1.47
−	+	AuAu	10.75	3.45×10^{-3}	97.46	339.8	3.49
+	+	CC	1.07	1.77×10^{-4}	9.70	17.44	1.80
+	+	AuAu	16.62	6.32×10^{-3}	150.68	622.66	4.13

is even important in systems as small as C + C. Dileptons, on the contrary, cannot be reabsorbed and are seen in the detector. Table I shows quantitatively the consequences of these processes for reactions at 1 GeV/nucleon. We compare there the pion and dilepton yield for C + C and Au + Au for different conditions. If there is neither a Fermi momentum (Fermi m.) nor meson absorption on baryons (mB col.) the ratio of π^0's to dileptons corresponds to the branching ratios and the enhancement factor (last column) is one, independent of the system size of the heavy-ion reaction. The Fermi motion alone increases the pion yield (sixth column) as well as the dilepton yield (seventh column) by almost a factor of two. Because in the ratio displayed in Fig. 33 one divides by the number of pions this ratio remains one for small invariant masses, whereas the Fermi motion makes the ratio explode for invariant masses close to the phase space boundary. Meson-baryon interactions (mB coll) lower the number of pions in heavy-ion collisions, by 15% in C + C collisions and by 47% in Au + Au collisions because they can lead to a disappearance of the pions if the $\pi N \to \Delta$ collision is followed by a $\Delta N \to NN$ collision. At the same time they enhance the dilepton yield because dileptons do not get reabsorbed and therefore every Δ that is produced contributes to the dilepton yield. The mB interactions are therefore the reason that dileptons behave differently than pions. This cycle of Δ production, Δ decay, and π reabsorption in $\pi N \to \Delta$ collisions, which leads in heavy system to the creation of several generations of Δ's, was studied already 20 years ago as one of the key elements to the pion dynamics in heavy-ion collision which allows the pions to equilibrate with the system and to serve as a measure of the number of participants [88]. The last two lines of Table I show that the pion absorption enhances the dilepton production as compared to the pions by a factor of about 1.5–1.7 in C + C collisions and by a factor of 3.5–4.1 for Au + Au collisions; i.e., the enhancement grows with the size of the system.

The system size effect is demonstrated explicitly in Fig. 34: The left plot shows the ratio of the mass differential dilepton spectra $(1/N_{\pi^0}^{AA} dN^{AA}/dM)/(1/N_{\pi^0}^{NN} dN^{NN}/dM)$—normalized to the π^0 multiplicity and after η-Dalitz yield subtraction–from HSD calculations for the minimal bias C + C, Ar + KCl, Cr + Cr, Ti + Pb, and Au + Au collisions and of the isospin-averaged reference spectra $NN = (pn + pp)/2$ at 1.75 GeV/nucleon. The right plot shows the same but for the Δ-Dalitz decay contributions only. We see also here that the different ratios are separated by a factor which is (almost) independent of invariant mass and depends basically on the size of the colliding nuclei because the effect of multiple Δ regeneration increases with the atomic number of the colliding ions.

Thus, the dilepton enhancement observed in Fig. 32 (and hence also in the experimental spectra) is attributable to bremsstrahlung and the Δ dynamics in the medium. Both are not related to collective effects like the in-medium modifications of spectral functions but are a mere consequence of the presence of other nucleons in the nuclei. They also appear if no potential but only collisional interactions between the nucleons exist. This effect grows with the nuclear size which is directly related to an increase of the high baryon density phase from light to heavy-ion collisions. This is demonstrated in Fig. 35, which shows the time evolution of the baryon density from HSD in the central cell $\rho(0, 0, 0, t)$ in units of the normal nuclear density $\rho_0 = 0.168$ fm^{-3} for central ($b = 0$ fm) Au + Au (left panel) and Ar + KCl (right panel) at different energies: 1.25, 1.7, 2.0, and 3.5 GeV/nucleon. By comparing the Ar + KCl and Au + Au density profiles one sees that the maximum density reached in the central cell is approximately the same in both cases, up to $3\rho_0$, and grows only slightly with increasing energy. However, the high baryon density phase for the heavy Au + Au nuclei collisions is much longer than for the intermediate Ar + KCl system, which implies a longer reaction time and a stronger influence of secondary reactions on observables, as discussed above.

C. In-medium effects in vector meson production

Now we come to the question of how the in-medium effects in vector meson production can influence the ratios. The dilepton spectra for $p + Nb$ at 3.5 GeV/nucleon, C + C at 1.0, 2.0 GeV/nucleon, and Ar + KCl at 1.75 GeV/nucleon within the collisional broadening scenario for the vector meson spectral functions have been already presented in Secs. III and IV (cf. Figs. 13, 14, 16, and 18) in comparison to

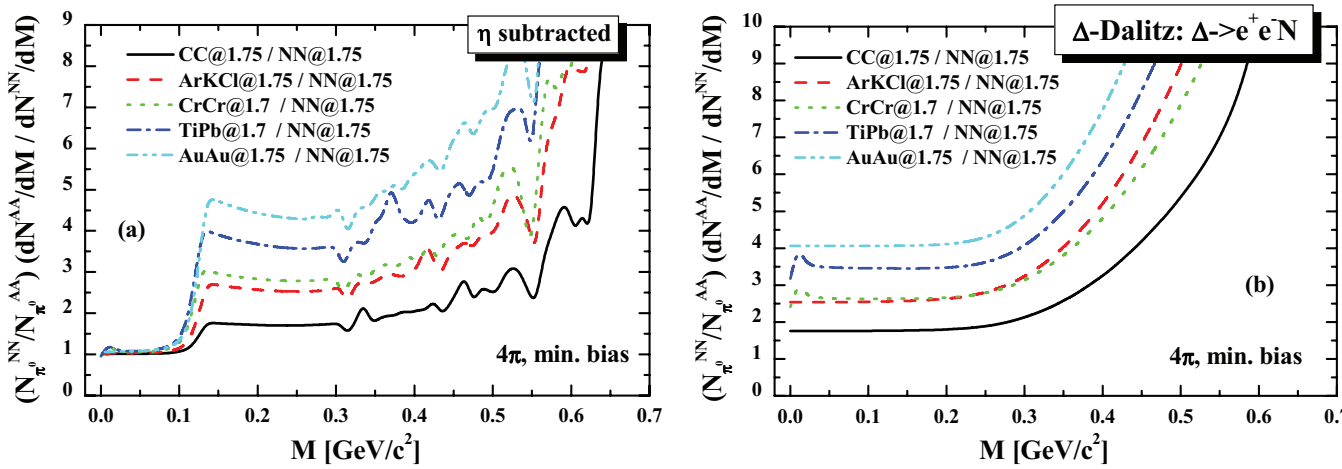

FIG. 34. (Color online) (a) The 4 π ratio $(1/N_{\pi^0}^{AA} dN^{AA}/dM)/(1/N_{\pi^0}^{NN} dN^{NN}/dM)$ of the mass differential dilepton spectra—normalized to the π^0 multiplicity and after η-Dalitz yield subtraction—from HSD calculations for the minimal bias C + C, Ar + KCl, Cr + Cr, Ti + Pb, and Au + Au collisions to the isospin-averaged reference spectra $NN = (pn + pp)/2$ at 1.75 GeV/nucleon. (b) Same as the left plot but for the Δ-Dalitz decay contributions, only.

the HADES data as well as our predictions for Au + Au at 1.25 GeV/nucleon (cf. Fig. 21).

In Fig. 36 we display for reactions at 1.70 GeV/nucleon the system size dependence of the 4π mass differential dilepton spectra—normalized to the π^0 multiplicity—from HSD calculations for minimal bias $A + A$ reactions. We display the result for the symmetric Cr + Cr and Au + Au systems as well as for the asymmetric Ti + Pb system. The solid lines stand for the "no medium effects" scenario, whereas the dashed lines show the dilepton yield for the collisional broadening scenario. The bottom panel is a magnification of the top one for the mass range $0.4 < M < 1.0$ GeV. First of all, we note the growth of the dilepton yield for $0.15 \leqslant M \leqslant 0.6$ GeV when going from the intermediate Cr + Cr to the heavy system Au + Au. The larger the system mass, the more important is the aforementioned Δ reaction cycle and the more the dilepton production is enhanced as compared to pion production. As we have discussed already in Secs. III and IV, for the collisional broadening scenario one sees clearly the influence of the larger width of the vector meson resonances (the peaks get smaller and broader).

What would be the consequence of this in-medium effect on the dilepton ratio of AA spectra to the reference spectrum? Would this observable yield information on the underlying dynamical processes? Previously we concentrated on the ratio $R(AA/NN)$, where the reference spectrum is constructed as an average of pp and pn yields: $NN = (pp + pn)/2$. However, such a ratio would not be well suited for studying in-medium effects in the vector meson mass region owing to the limited open phase space in NN collisions relative to AA collisions—taken at the same energies—because the Fermi motion in AA extends the kinematical limits, which leads to a fast rise of $R(AA/NN)$ at larger invariant masses M. Moreover, as has been discussed in Sec. III A, there is a general problem with NN as a reference spectrum because, experimentally, pn are usually quasifree pd reactions. For the beam energies discussed here, in the interesting invariant mass region, $M > 0.5$ GeV there are no

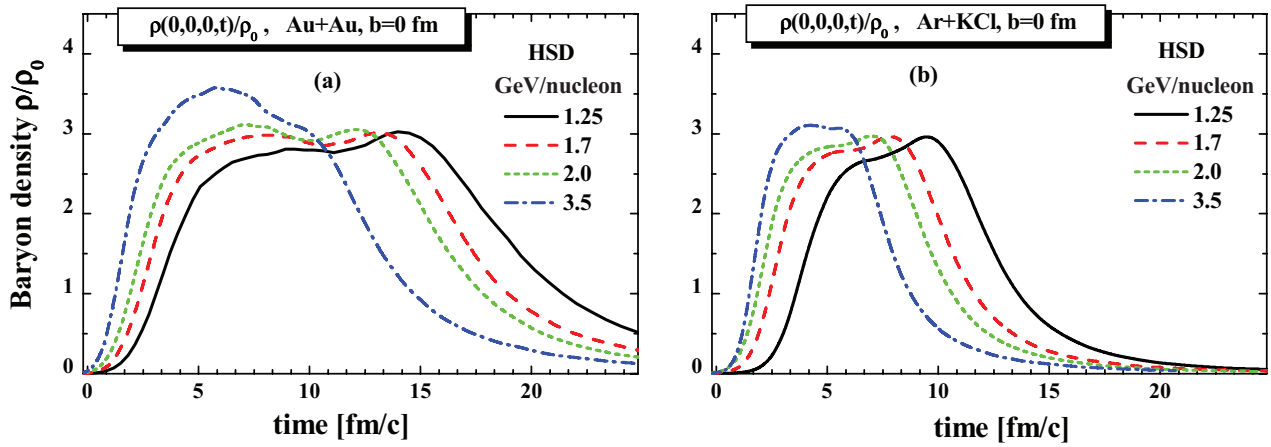

FIG. 35. (Color online) The time evolution of the baryon density from HSD in the central cell $\rho(0, 0, 0, t)$ in units of the normal nuclear density $\rho_0 = 0.168$ fm^{-3} for central ($b = 0$ fm) Au + Au (a) and Ar + KCl (b) at different energies: 1.25, 1.7, 2.0 and 3.5 GeV/nucleon.

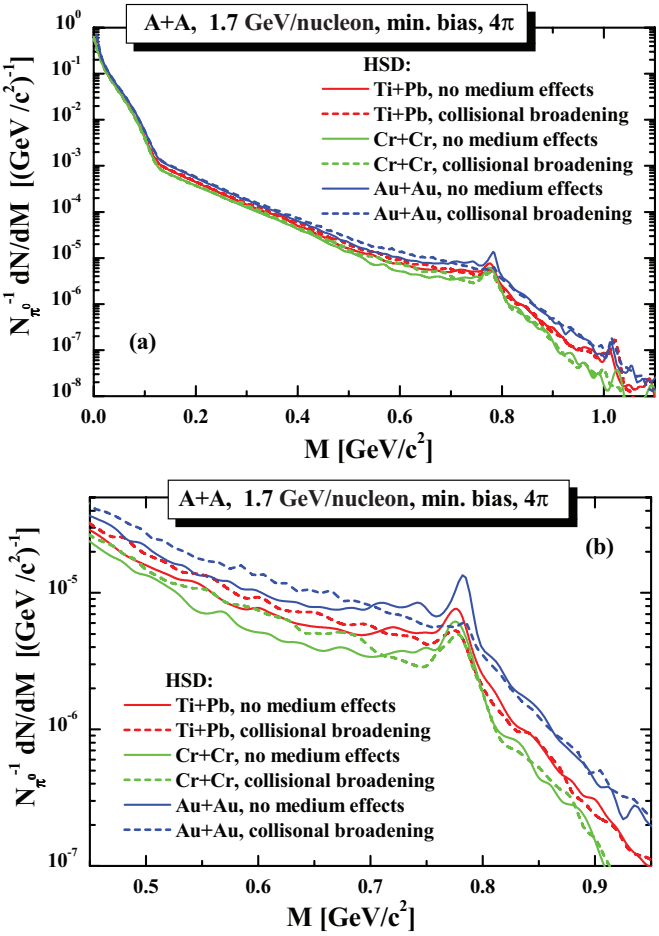

FIG. 36. (Color online) The 4 π mass differential dilepton spectra—normalized to the π^0 multiplicity—from HSD calculations for minimal bias Ti + Pb, Cr + Cr, and Au + Au collisions at 1.7 GeV/nucleon. The solid lines stand for the no medium effects scenario, whereas the dashed lines show the dilepton yield for the collisional broadening scenario. Panel (b) is a magnification of panel (a) for the mass range $0.4 < M < 1.0$ GeV.

quasifree pn collisions anymore but genuine three-body pd collisions.

Alternatively, the in-medium enhancement can be studied by comparing the yield of a heavy system to that of a light system. Figure 37 displays for a beam energy of 1.7 GeV/nucleon the ratio of the invariant mass differential dilepton spectra for intermediate Cr + Cr and heavy Au + Au nuclei and of the light nuclei C + C, which is chosen as a reference spectrum. We study two scenarios: the no medium effects and the collisional broadening scenarios. One clearly sees that the enhancement for $M \leqslant 0.5$ GeV owing to the multiple Δ production and bremsstrahlung persists when one compares collisions of heavy and light nuclei and can become as large as a factor of two. Thus, C + C collisions can also be used as reference spectra to study such nuclear effects. Moreover, we observe as well that the difference between the two scenarios is small for low invariant masses and becomes noticeable only at invariant masses close to the ρ mass. However, even there the differences remain moderate. Therefore, high-precision data

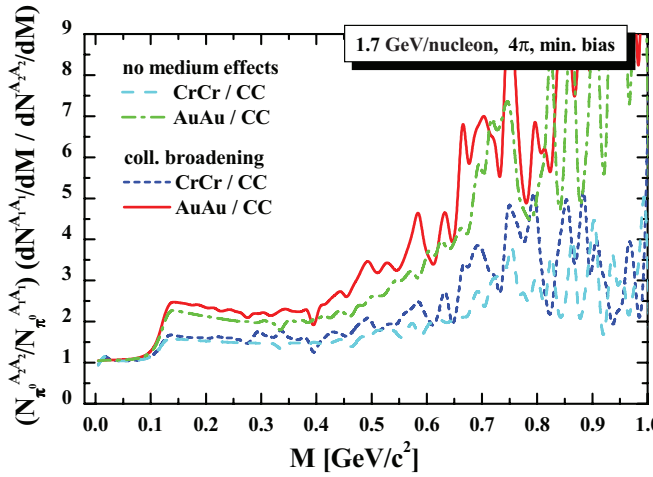

FIG. 37. (Color online) The 4 π ratio $(1/N_{\pi^0}^{A-2A_2} dN^{A_2A-2}/dM)/(1/N_{\pi^0}^{A_1A_1} dN^{A_1A_1}/dM)$ of the mass differential dilepton spectra—normalized to the π^0 multiplicity—from HSD calculations for minimal bias Au + Au (Cr + Cr) collisions and C + C collisions. This ratio is displayed for the no medium effects and for the collisional broadening scenario.

are required to study the question of whether vector mesons are modified by the strongly interacting medium in this energy region. However, the ratio for AuAu/CC grows much faster (for both the no medium and the in-medium scenario) than for CrCr/CC. This is attributable to the enhancement of the vector meson productions by secondary mB and meson-meson interactions in a heavy system relative to the light system. This effect is hence easy to observe experimentally.

VI. UNCERTAINTIES OWING TO DIFFERENT ASSUMPTIONS IN THE TRANSPORT MODELS

In this section we discuss the different assumptions in different transport approaches owing to the lack of experimental information and theoretical knowledge and the consequences for the prediction of these approaches. The uncertainties related to the production cross sections in elementary reactions have been addressed in Sec II. There are, however, other sources of uncertainties, in particular for the dilepton production by Δ-Dalitz decay: the lack of knowledge of the electromagnetic decay width of the Δ resonance, of the mass distribution of the Δ resonance in elementary NN collisions, and of its total decay width, as well as different assumptions on how the total decay width is related to the Δ lifetime.

A. Electromagnetic decay width of Δ resonance

The differential electromagnetic decay width of a Δ resonance into dileptons of an invariant mass M, $\Delta \to Ne^+e^-$, can be related to the Δ decay into a nucleon and a virtual photon, $\Delta \to N\gamma^*$, by (cf. Ref. [51])

$$\frac{d\Gamma}{dM}^{\Delta \to N\, l+l-}(M) = \frac{2\alpha}{3\pi} \frac{\Gamma^{\Delta \to N\gamma^*}(M, M_\Delta)}{M}, \qquad (8)$$

where $\alpha = 1/137$ and M_Δ is the current mass of the Δ resonance. Unfortunately, there is no direct measurement of the $\Delta \to N\gamma^*$ width and starting from the pioneering work

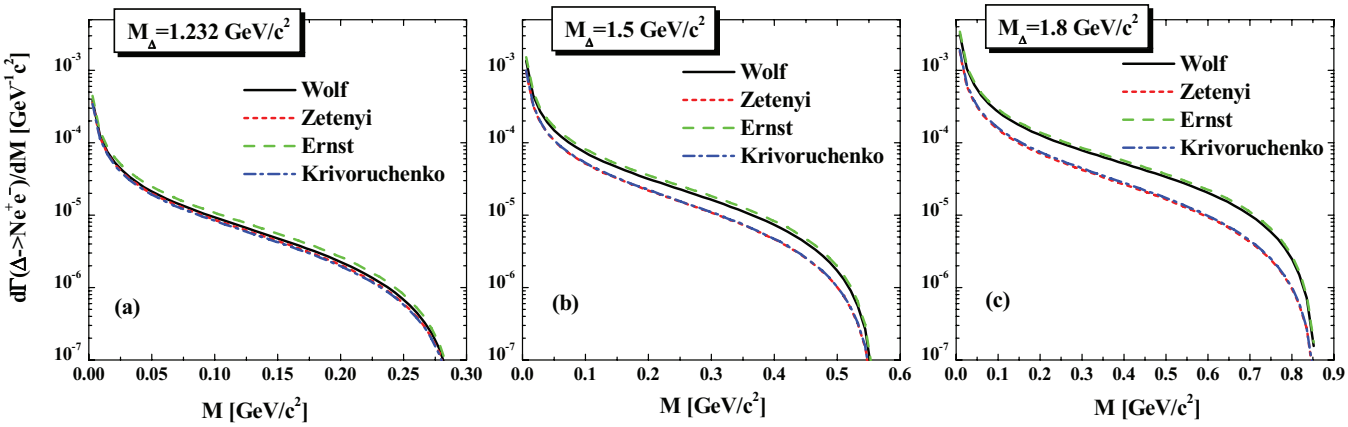

FIG. 38. (Color online) The electromagnetic decay width of Δ resonance to dileptons $\Delta \to Ne^+e^-$ for different models denoted as "Wolf" [51], "Zetenyi" [91], "Ernst" [30], and "Krivoruchenko" [90] for different Δ masses of 1.232 GeV (a), 1.5 GeV (b), and 1.8 GeV (c).

of Jones and Scadron [89] there is a series of different models [30,51,90,91]. In the present versions of the HSD, IQMD, and UrQMD transport approaches the "Wolf" model is employed for the electromagnetic decay width [51]:

$$
\begin{aligned}
\Gamma^{\Delta\to N\gamma^*}(M, M_\Delta) &= \frac{\lambda^{1/2}\left(M^2, m_N^2, M_\Delta^2\right)}{16\pi M_\Delta^2}\cdot m_N \\
&\quad\cdot [2m_T(M, M_\Delta) + m_L(M, M_\Delta)], \\
m_L(M, M_\Delta) &= (efg)^2\frac{M_\Delta^2}{9m_N}M^2\cdot 4(M_\Delta - m_N - q_0), \\
e^2 &= 4\pi\alpha, \quad g = 5.44, \\
m_T(M, M_\Delta) &= (efg)^2\frac{M_\Delta^2}{9m_N}\left\{q_0^2[5M_\Delta - 3(q_0 + m_N)]\right. \\
&\quad \left. - M^2(M_\Delta + m_N + q_0)\right\}, \\
f &= -1.5\frac{M_\Delta + m_N}{m_N[(m_N + M_\Delta)^2 - M^2]}, \\
q_0 &= \left(M^2 + p_f^2\right)^{1/2}, \\
p_f^2 &= \frac{\left[M_\Delta^2 - (m_N + M)^2\right]\left[M_\Delta^2 - (m_N - M)^2\right]}{4M_\Delta^2}, \\
\lambda\left(M^2, m_N^2, M_\Delta^2\right) &= M^4 + m_N^4 + M_\Delta^4 \\
&\quad - 2\left(M^2m_N^2 + M^2M_\Delta^2 + m_N^2M_\Delta^2\right). \qquad (9)
\end{aligned}
$$

There is a variety of models for the electromagnetic decay width of Δ resonance to dileptons $\Delta \to Ne^+e^-$; cf. Refs. [30,51,90,91]. Figure 38 shows $\Gamma^{\Delta\to N\ e+e-}(M, M_\Delta)$ for different models denoted as "Wolf" [51], Zetenyi [91], Ernst [30], and Krivoruchenko [90] and for three different Δ masses: 1.232 GeV (a), 1.5 GeV (b), and 1.8 GeV (c). One can see that in the low-mass region, i.e., around the Δ pole mass 1.232, all approaches give similar results, whereas with increasing M_Δ the differences grow. The models "Wolf" and "Ernst" lead to a similar dilepton yield which is, however, up to a factor of 3 higher then that from the models "Krivoruchenko" and "Zatenyi". This introduces a systematic error for the prediction of the dilepton yield for large mass dileptons.

B. Total decay width and the lifetime of Δ resonance

The population of high-mass Δ's in NN reactions depends on the shape of the differential mass distribution which is given by the Δ spectral function. The spectral function of a Δ resonance of mass M_Δ is usually assumed to be of the relativistic Breit-Wigner form,

$$
A_\Delta(M_\Delta) = C_1\cdot\frac{2}{\pi}\,\frac{M_\Delta^2\Gamma_\Delta^{\rm tot}(M_\Delta)}{\left(M_\Delta^2 - M_{\Delta 0}^2\right)^2 + \left[M_\Delta\Gamma_\Delta^{\rm tot}(M_\Delta)\right]^2}, \qquad (10)
$$

with $M_{\Delta 0}$ being the pole mass of the Δ. The factor C_1 is fixed by the normalization condition,

$$
\int_{M_{\rm min}}^{M_{\rm lim}} A_\Delta(M_\Delta)dM_\Delta = 1, \qquad (11)
$$

where $M_{\rm lim} = 2$ GeV is chosen as an upper limit for the numerical integration. The lower limit for the vacuum spectral function corresponds to the nucleon-pion decay, $M_{\rm min} = m_\pi + m_N$. In NN collisions the Δ's can be populated up to the $M_{\rm max} = \sqrt{s} - m_N$ and hence the available part of spectral function is defined by the beam energy.

The shape of spectral function (and correspondingly the production of high-mass Δ's) depends strongly on the total width $\Gamma_\Delta^{\rm tot}$. Owing to the lack of experimental information this total width has to be assumed and different parametrizations exist.

For the present HSD calculations we adopt the "Monitz" model [92] (cf. also Ref. [51]):

$$
\Gamma_\Delta^{\rm tot}(M_\Delta) = \Gamma_R\frac{M_{\Delta 0}}{M_\Delta}\cdot\left(\frac{q}{q_r}\right)^3\cdot F^2(q), \qquad (12)
$$

$$
q^2 = \frac{\left[M_\Delta^2 - (m_N + m_\pi)^2\right]\left[M_\Delta^2 - (m_N - m_\pi)^2\right]}{4M_\Delta^2},
$$

$$
\Gamma_R = 0.11\ \text{GeV}, \quad M_{\Delta 0} = 1.232\ \text{GeV};
$$

$$
F(q) = \frac{\beta_r^2 + q_r^2}{\beta_r^2 + q^2}, \qquad (13)
$$

$$
q_r^2 = 0.051936, \quad \beta_r^2 = 0.09.
$$

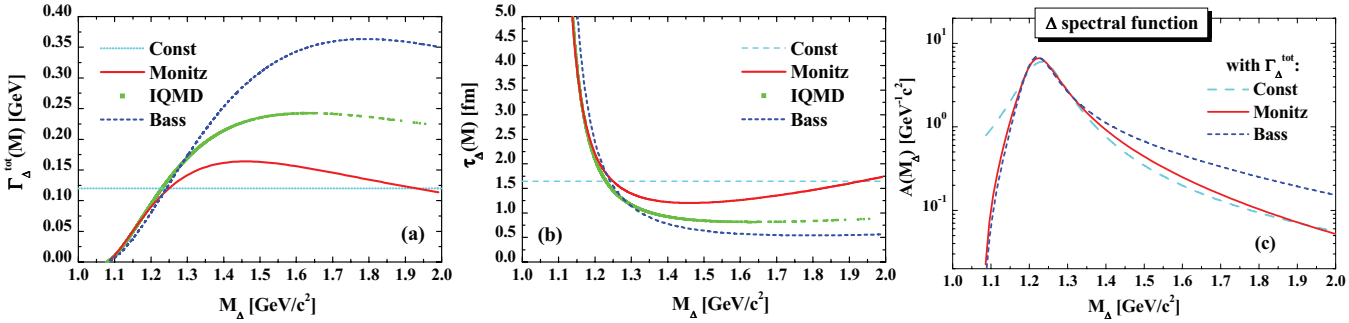

FIG. 39. (Color online) The mass dependence of the total width $\Gamma^{\rm tot}_\Delta(M_\Delta)$ (a), lifetime (b), and the spectral function (c) from different models: Const, the constant width $\Gamma^{\rm tot}_{\Delta 0} = 0.12$ GeV; Monitz, from Eq. (12) (cf. Ref. [92]); Bass, from Eq. (14) (cf. Ref. [64]); IQMD, from Refs. [77,78].

In the UrQMD model one employs the "Bass" parametrization [64], which differs from the Monitz model (12) by the form factor (13):

$$F_B(q) = 1.2\,\frac{\tilde\beta_r^2}{\tilde\beta_r^2 + q^2}, \qquad \tilde\beta_r^2 = q_r^2/0.2. \tag{14}$$

In panel (a) of Fig. 39 we show the mass dependence of the total width $\Gamma^{\rm tot}_\Delta(M_\Delta)$ from different models: Const, a constant width $\Gamma^{\rm tot}_\Delta = 0.12$ GeV; Monitz, from Eq. (12) (cf. Ref. [92]); Bass, from Eq. (14) (cf. Ref. [64]); as well as the parametrization used in the IQMD model [77,78] denoted as "IQMD." We observe substantial differences between the models, especially for large mass Δ. These differences become more important at higher energies. For lower energies, especially for the 1 GeV/nucleon data, phase space limits the Δ masses to $M_\Delta < 1.4$ GeV.

The total decay width is related to the lifetime of the resonances—another important quantity for the transport approaches—by

$$\tau_\Delta(M_\Delta) = \frac{\hbar c}{\Gamma^{\rm tot}_\Delta(M_\Delta)}. \tag{15}$$

The lifetime as a function of M_Δ is illustrated in panel (b) of Fig. 39. The lifetime of large mass Δ is in the Bass parametrization up to three times lower than in the Monitz parametrization. Δ's of such a high mass are rare, however, as can be seen from panel (c) of Fig. 39, which shows the mass dependence of the spectral function for different parametrizations of the width.

C. Consequences for the dilepton yield

Now we show how the uncertainties in the modeling of the total Δ width and of the electromagnetic decay width affect the final results for the dilepton yield.

1. Convolution model

We start out with a simple example: The dilepton yield from the Δ-Dalitz decay is a convolution of the mass distribution of the Δ resonances—which we take for our model study to be defined by the spectral function $A_\Delta(M_\Delta)$ [Eq. (10)]—and the Δ mass-dependent branching ratio for the electromagnetic decay into dileptons, which is defined as a ratio of electromagnetic partial width $\frac{d\Gamma}{dM}^{\Delta\to Ne^+e^-}(M, M_\Delta)$ and the total width $\Gamma^{\rm tot}_\Delta(M_\Delta)$,

$$\frac{dN}{dM}^{e^+e^-}(M) = \int dM_\Delta \cdot A_\Delta(M_\Delta) \cdot \frac{d\Gamma}{dM}^{\Delta\to Ne^+e^-}(M, M_\Delta) \cdot \frac{1}{\Gamma^{tot}_\Delta(M_\Delta)} \tag{16}$$

$$= \int dM_\Delta \cdot A_\Delta(M_\Delta) \cdot \frac{d\Gamma}{dM}^{\Delta\to Ne^+e^-} \times (M, M_\Delta) \cdot \tau_\Delta(M_\Delta), \tag{17}$$

where the expression (16) has been rewritten in terms of the Δ lifetime using relation (15).

In panel (a) of Fig. 40 we show the dilepton yield for two different assumptions for $\Gamma^{\rm tot}_\Delta(M_\Delta)$ and for $\frac{d\Gamma}{dM}^{\Delta\to \rm Ne^+e^-}(M, M_\Delta)$: (1) solid line: total width - "Bass", electromagnetic - "Wolf"; (2) dot-dashed line: total width - "Bass", electromagnetic - "Krivoruchenko"; (3) dashed line: total width - "Const", electromagnetic - "Wolf"; (4) dot-dot-dashed line: total width - "Const", electromagnetic - "Krivoruchenko". The variation of $\Gamma^{\rm tot}_\Delta(M_\Delta)$ changes the dilepton yield only marginally as long as the same electromagnetic decay width is used: cases (1), (3) and (2), (4). The reason can easily be seen from Eq. (16): The total width $\Gamma^{\rm tot}_\Delta(M_\Delta)$ enters in the numerator of spectral function [Eq. (10)] and in the denominator of the branching ratio and thus cancels. The only remaining dependence comes from the denominator of Eq. (10), but far from the pole mass $\Gamma^{\rm tot}_\Delta(M_\Delta)$ this term is small as compared to the other part of the denominator. Oppositely, for a fixed total width $\Gamma^{\rm tot}_\Delta(M_\Delta)$ the variation of $\frac{d\Gamma}{dM}^{\Delta\to Ne^+e^-}(M, M_\Delta)$ leads to differences of the dilepton yield up to the factor of 3 for high-invariant masses: cases (1), (2) and (3), (4).

Thus, we can conclude that different assumptions on the total width $\Gamma^{\rm tot}_\Delta(M_\Delta)$ have little influence on the invariant mass distribution of dileptons, whereas the lack of knowledge of $\frac{d\Gamma}{dM}^{\Delta\to Ne^+e^-}(M, M_\Delta)$ introduces an uncertainty of up to a factor of three for the dilepton yield from Δ decay at large invariant masses.

Different assumptions have been made of how to relate $\Gamma^{\rm tot}_\Delta(M_\Delta)$ to the lifetime of the Δ. We do not discuss here

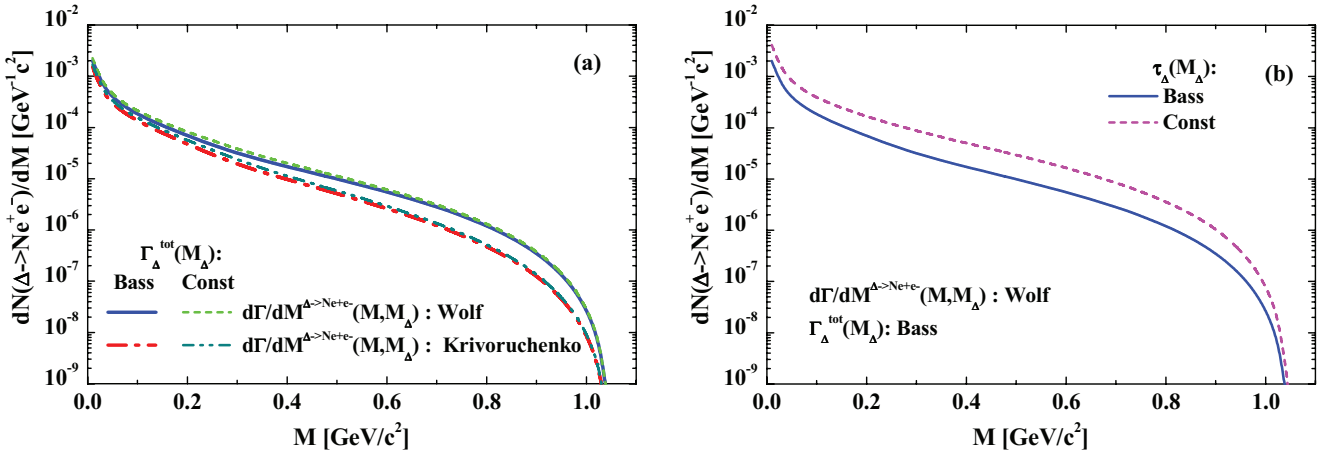

FIG. 40. (Color online) (a) The dilepton yield as a function of invariant dilepton mass for the two parametrizations of the total width $\Gamma^{\rm tot}_\Delta(M_\Delta)$ and two models for the partial electromagnetic decay width $\frac{d\Gamma}{dM}^{\Delta\to Ne^+e^-}(M, M_\Delta)$: (1) solid line: total width - "Bass", electromagnetic- "Wolf"; (2) dot-dashed line: total width - "Bass", electromagnetic - "Krivoruchenk"; (3) dashed line: total width - "Const", electromagnetic - "Wolf" (4) dot-dot-dashed line: total width - "Const", electromagnetic - "Krivoruchenko". (b) The dilepton yield as a function of invariant dilepton mass for the two assumptions of the lifetime $\tau_\Delta(M_\Delta)$: solid line - "Bass"; dashed line - "Const" lifetime, while using the "Bass" total width for spectral function and the "Wolf" model for the partial electromagnetic decay width in both cases.

the rationale behind the different approaches. Rather we concentrate on the consequences for the dilepton yield. In HSD the total width for the Δ production [i.e., that which enters the spectral function $A_\Delta(M_\Delta)$] is the same as the width used to determine the lifetime Eq. (15). In this case, we have a cancellation of the total width in Eq. (16) as discussed above, which leads to the low sensitivity of dilepton spectra to different $\Gamma^{\rm tot}_\Delta(M_\Delta)$. In the UrQMD model (cf., e.g., the corresponding discussion in Ref. [64], Sec. 3.3.4), on the contrary, the width used for the Δ production differs from that in the lifetime definition (15), so there is no cancellation of the widths anymore; rather the ratios of the two widths enters the Eq. (16).

In panel (b) of Fig. 40 we demonstrate the consequences of the different lifetime definitions. We employ in all cases the "Wolf" parametrization of $\frac{d\Gamma}{dM}^{\Delta\to Ne^+e^-}(M, M_\Delta)$ and $\Gamma^{\rm tot}_\Delta(M_\Delta)$ of Bass but vary the description of the lifetime. The solid blue line shows the dilepton yield under the assumption that $\Gamma^{\rm tot}_\Delta(M_\Delta)$ of Bass determines the lifetime [Eq. (15)], whereas the dashed red line shows the result assuming that for the calculation of the lifetime [Eq. (15)] a constant width of 120 MeV is employed. For a constant width we observe a strong enhancement, which is mainly related to the large contribution of the high-mass Δ's to the dilepton yield. This is illustrated in Fig. 41, where we show the contribution of Δ's from different mass ranges to the dilepton yield. The sum of all four bins gives the solid curve of Fig. 40. One has to keep in mind, however, that in real NN collisions at low energies the high-mass tail of the Δ distribution is strongly suppressed owing to the limitation of the phase space.

2. *pp and heavy-ion collisions*

Now we extend our study of systematic errors to pp and heavy-ion calculations. For this purpose we use the HSD model.

The Δ resonances can be produced dominantly in NN or πN collisions. The mass distribution of the produced Δ's, $dN/dM_\Delta(s, M_\Delta)$, is defined by the spectral function $A_\Delta(M_\Delta)$ [Eq. (10)] integrated over the corresponding phase space which depends on the invariant energy $\sqrt{s}$ of the NN or πN collisions and the masses of the final associated particles M_X (e.g., $NN \to \Delta + X$). At low energies the phase space leads to the suppression of high-mass Δ's.

We start with the time-integrated Δ mass distribution dN/dM_Δ. It is shown in Fig. 42 for central C + C collisions at 2 GeV/nucleon. We display the mass distribution for two choices for the total width: The solid line displays the calculation for the Monitz width; the short-dashed line displays the calculation for the Bass width. For compar-

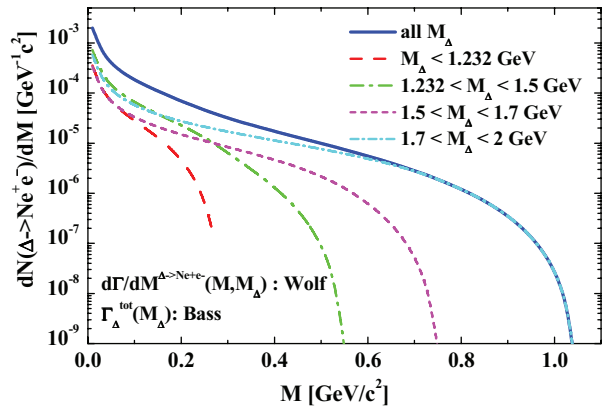

FIG. 41. (Color online) The contribution of Δ's from the four mass bins to the dilepton yield $dN/dM(\Delta \to Ne^+e^-)$: (1) $M_\Delta \leqslant$ 1.232 GeV, (2) $1.232 \leqslant M_\Delta \leqslant 1.5$ GeV, (3) $1.5 \leqslant M_\Delta \leqslant 1.7$ GeV, (4) $1.7 \leqslant M_\Delta \leqslant 2.0$ GeV. Calculations are done using the "Bass" total width for spectral function and the "Wolf" model for the partial electromagnetic decay width.

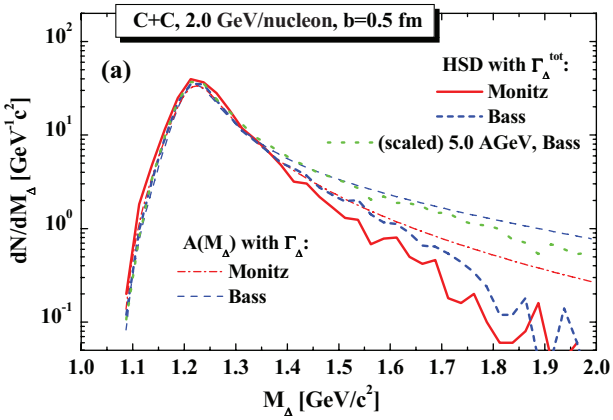

FIG. 42. (Color online) The Δ mass distribution from HSD for the central C + C collisions at 2 GeV/nucleon for the two model cases for the total width: solid line - "Monitz", short-dashed line, "Bass" width. The thin dash-dotted and dashed lines show the spectral function $A_\Delta(M_\Delta)$ calculated with "Monitz" and "Bass" widths, correspondingly. The dotted line stands for dN/dM_Δ from HSD for C + C collisions at 5.0 GeV/nucleon with "Bass" width (scaled to the maximum of dN/dM_Δ at 2 GeV/nucleon for easy comparison of the shape of mass distributions).

ison we also show the spectral function $A_\Delta(M_\Delta)$ (scaled to the maximum of dN/dM_Δ) for both widths. Owing to the limited available energy in low-energy heavy-ion collisions, only a part of the full spectral function can be explored (the absorption and rescattering effects for C + C collisions do not distort the initial production shape of Δ mass distribution too much). This lowers the uncertainties of the predicted dilepton yields related to the very high-mass tail of the distribution. Going to higher energies the phase space opens more and more and the high-mass tail of spectral function can be populated. This is shown by the dotted line which displays dN/dM_Δ for C + C collisions at 5.0 GeV/nucleon employing the Bass width which we scaled to the maximum of dN/dM_Δ for C + C at 2 GeV/nucleon for easy comparison of the shape of corresponding mass distributions.

Similar to panel (a) of Fig. 40 we demonstrate in Fig. 43 the consequences of the variation of the electromagnetic decay width on the differential cross section $d\sigma/dM$ [panel (a)] and the transverse momentum spectra [right column, panels (b)–(e)] for four different mass bins ($M \leqslant 0.15$ GeV, $0.15 \leqslant M \leqslant 0.47$ GeV, $0.47 \leqslant M \leqslant 0.7$ GeV, and $M \geqslant 0.7$ GeV) from HSD calculations for e^+e^- production in pp reactions at a bombarding energy of 3.5 GeV. The dash-dot-dotted and the dashed lines show the Δ-Dalitz contribution and the corresponding total sum of all channels without pp Bremsstrahlung as in Figs. 11 and 12, for the "Wolf" electromagnetic decay width. The dash-dotted line stands for the parametrization using Krivoruchenko width; the solid line is the corresponding sum. We point out that we have selected the pp reaction at 3.5 GeV here because at this high energy the open phase space is large enough to populate the high-mass Δ's. Thus, one expects a large deviation in the dilepton mass spectra coming from the high-mass tail of the Δ spectral function—as follows from Figs. 38 and 40 (left)—compared to the low-energy reactions where the available energy limits the production of heavy Δ's. Furthermore, Fig. 43 (right column) demonstrates the sensitivity of p_T distribution to the form of the electromagnetic decay width. Despite the deviation being bigger for the bin with the largest dilepton masses ($M > 0.7$ GeV), this effect is not visible in the final p_T spectra owing to the dominant contributions from the direct decay of vector mesons. For the lower mass bins ($0.15 \leqslant M \leqslant 0.47$ GeV and $0.47 \leqslant M \leqslant 0.7$ GeV) the difference is better observed in the final p_T spectra. Thus, the measurement of the p_T distributions at various mass bins can help in distinguishing of different models.

We continue with the comparison of the final mass differential dilepton spectra for central C + C collisions at 2 GeV/nucleon [Fig. 44(a)]. The legend for the individual lines is the same as in Fig. 43. We observe similar deviations as obtained within the "convolution" model; see panel (a) of Fig. 40.

Thus, we conclude that the uncertainty of the electromagnetic decay width of the Δ resonance translates to an uncertainty of about a factor of 1.5 in the dilepton yield from Δ decays in heavy-ion collisions. For large invariant masses of the Δ this uncertainty reaches even a factor of 3. However, these large invariant masses are only populated at beam energies at which η production becomes important with the consequence that the η-Dalitz decay and bremsstrahlung are the dominant sources for dilepton production. Therefore, the uncertainty of the dilepton yield from large mass Δ decay has little influence on the measured total dilepton yield at large invariant masses or on the ratio $R(AA/NN)$; cf. dash-dot-dotted line in Fig. 26(b).

The simulations for the different assumptions about the lifetime for the central C + C at 2 GeV/nucleon are presented in panel (b) of Fig. 44. The assumptions correspond to that of panel (b) of Fig. 40. The solid line, "Const", displays the results assuming a constant lifetime, whereas the dashed line shows the result assuming the "Bass" lifetime. In both cases the "Bass" total width has been employed for the Δ spectral function and the "Wolf" model has been used for the partial electromagnetic decay width. One can see that the two assumptions about the lifetime yield an uncertainty of a factor of 2, slightly less than the factor we obtained for elementary reactions (Fig. 42).

We would like to stress here that the uncertainties in the electromagnetic decay width of Δ resonance as well as that of total width/lifetime of the Δ can be reduced by measuring the dilepton yield in πN reactions at different energies. Such a measurement would allow for more precise predictions than presently possible.

D. Electromagnetic Δ − N transition form factor

The introduction of the electromagnetic $\Delta - N$ transition form factor $F_{\Delta N}$ for the Δ-Dalitz decay has been studied in Ref. [67] within the GiBUU transport model for NN and pNb reactions. The model from Refs. [93] has been chosen for the $\Delta - N$ transition form factor, which is based on the

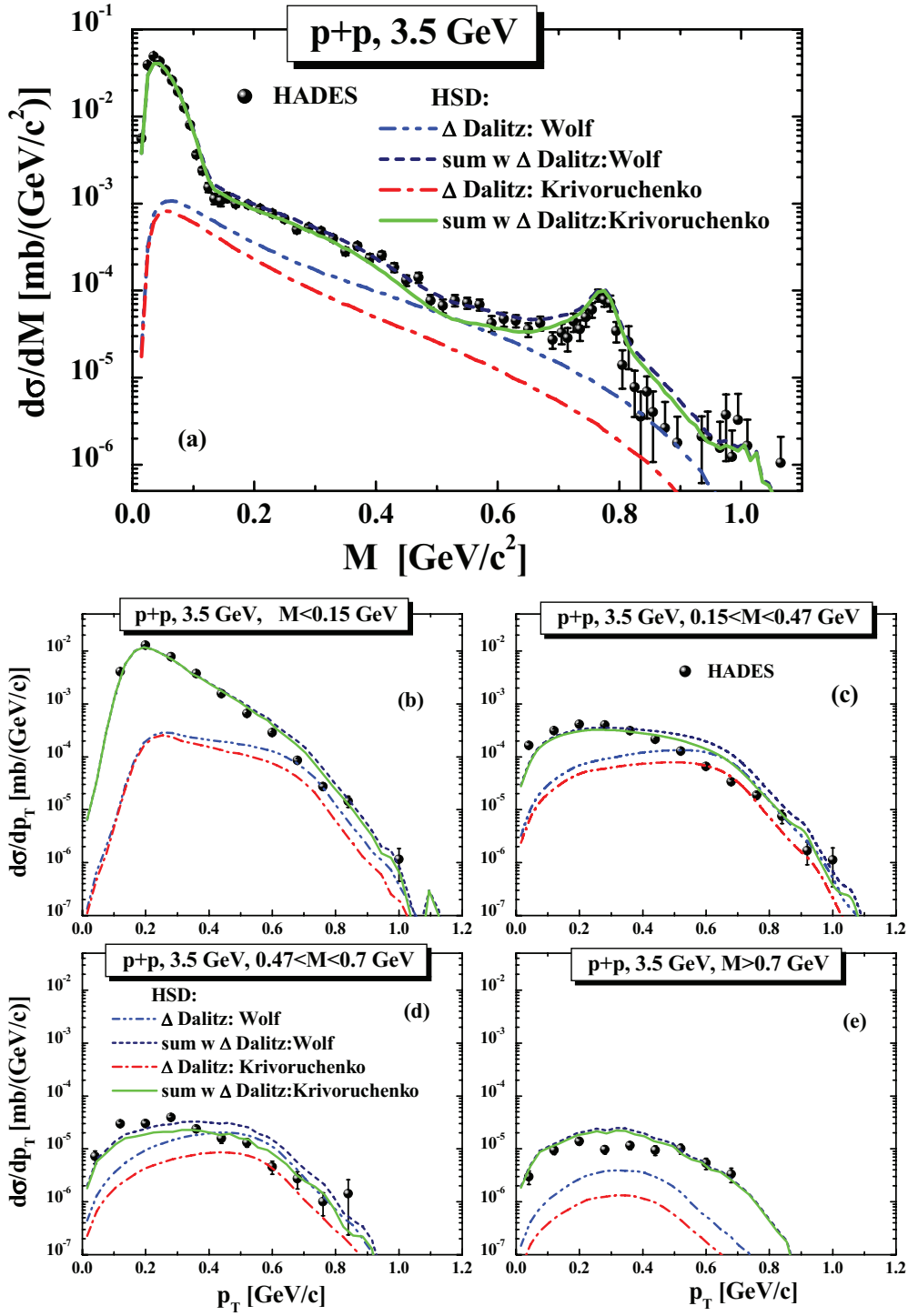

FIG. 43. (Color online) (a) The differential cross section $d\sigma/dM$ from HSD calculations for e^+e^- production in pp reactions at a bombarding energy of 3.5 GeV in comparison to the HADES data [56]. (b)–(e) The HSD results for the transverse momentum spectra for pp at 3.5 GeV and for four different mass bins: $M \leqslant 0.15$ GeV, $0.15 \leqslant M \leqslant 0.47$ GeV, $0.47 \leqslant M \leqslant 0.7$ GeV, and $M \geqslant 0.7$ GeV in comparison to the HADES data [56]. The individual lines are similar to those in the left column. The dash-dot-dotted and the dashed lines show the Δ-Dalitz contribution and the corresponding total sum of all channels without pp Bremsstrahlung as in Figs. 11 and 12, for the "Wolf" electromagnetic decay width. The dash-dotted line stands for the parametrization using "Krivoruchenko" width; the solid line is the corresponding sum.

Vector Dominance Model (VDM), assuming that the virtual photon is converted first to a ρ_0 meson; that is, the transition $\Delta \to \gamma * N \to Ne^+e^-$ can be considered as $\Delta \to \gamma^* N \to \rho_0 N \to e^+e^- N$. For that one needs to extrapolate the $\Delta - N$

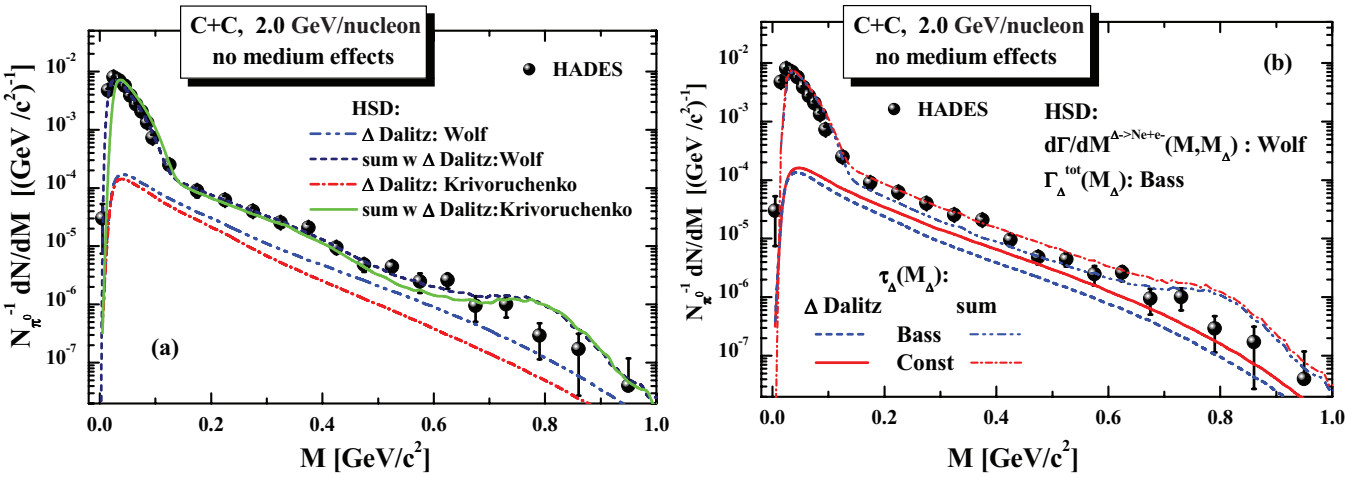

FIG. 44. (Color online) (a) The mass differential dilepton spectra—normalized to the π^0 multiplicity—from HSD calculations for central ($b = 0.5$ fm) C + C collisions at 2 GeV/nucleon in comparison to the HADES data [37]. The dash-dot-dotted and the dashed lines show the Δ-Dalitz contribution and the corresponding total sum of all channels as in Fig. 16, for the "Wolf" electromagnetic decay width. The dash-dotted line stands for the parametrization using "Krivoruchenko" width, the solid line is the corresponding sum. (b) Similar to the left column - the mass differential dilepton spectra as a function of invariant dilepton mass for the two model cases of lifetime $\tau_\Delta(M_\Delta)$: solid line - "Const", dashed line - "Bass" life time, while using the "Bass" total width for the Δ production and dynamics and "Wolf" model for the partial electromagnetic decay width in both cases.

transition form factor from the spacelike region to the timelike region, where its strength is unknown experimentally.

In Fig. 45 we demonstrate the effect of the electromagnetic $\Delta - N$ transition form factor: panel (a) shows the electromagnetic decay width of the Δ resonance into dileptons $\Delta \to Ne^+e^-$ using the "Krivoruchenko" model for different Δ masses of 1.232 GeV (dot-dashed line), 1.5 GeV (dashed line), and 1.8 GeV (solid line); the thick (thin) lines, with (without) the $\Delta - N$ form factor $F_{\Delta N}$ from Ref. [93]. Panel (b) displays the dilepton yield using the "convolution" model [Eq. (16)] with the "Bass" total width. One can see that the inclusion of the form factor leads to an enhancement of the dilepton yield up to a factor of 10 at $M \sim 0.6$ GeV.

We have investigated the consequences of the electromagnetic $\Delta - N$ transition form factor for heavy-ion collisions for C + C reactions at 2 GeV/nucleon, where the Δ channel is one of the dominant channels. Figure 46 shows the results of the HSD calculations for two different models (in line with our discussion above on the model uncertainties) for the electromagnetic decay width, "Krivoruchenko" (dashed lines) and "Wolf" (dash-dotted lines), which provide the lower and upper limit for the effects of the form factor for the final spectra (solid lower and upper lines). One can conclude that the introduction of the $\Delta - N$ transition form factor [93] leads to overestimation of the dilepton yield in heavy-ion collisions, i.e., is not in line with the HADES data.

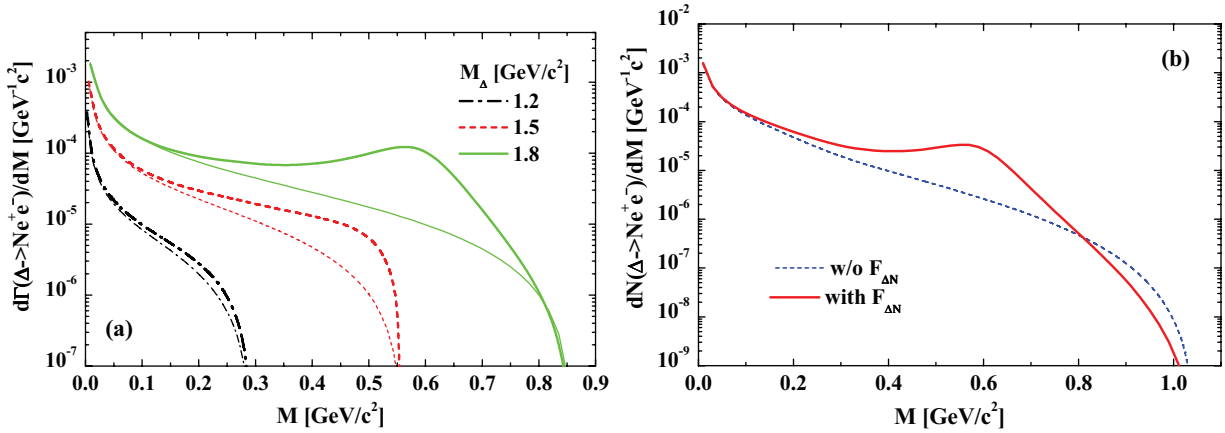

FIG. 45. (Color online) (a) The electromagnetic decay width of the Δ resonance to dileptons $\Delta \to Ne^+e^-$ using the "Krivoruchenko" model for different Δ masses of 1.232 GeV (a), 1.5 GeV (b), and 1.8 GeV (c). Thick lines - with the $\Delta - N$ form factor $F_{\Delta N}$ from Ref. [93], thin lines - without the $\Delta - N$ form factor. (b) The dilepton yield as a function of the invariant dilepton mass using the "Krivoruchenko" model for the electromagnetic decay width and the "Bass" model for the total width. Solid lines - with including the $\Delta - N$ form factor $F_{\Delta N}$, dashed line - without the $\Delta - N$ form factor.

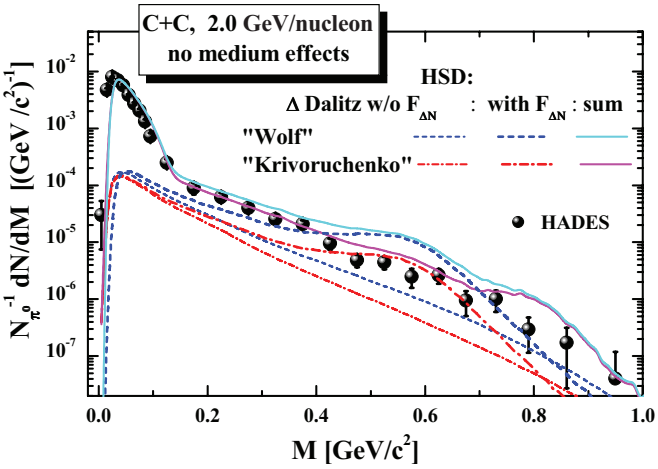

FIG. 46. (Color online) The results of the HSD transport calculation for the mass differential dilepton spectra—normalized to the π^0 multiplicity—for C + C at 2.0 GeV/nucleon. Thick lines, with the $\Delta - N$ form factor $F_{\Delta N}$ from Ref. [93]; thin lines, without the $\Delta - N$ form factor. Here the dashed lines correspond to the "Wolf" model for the electromagnetic decay width; the dash-dotted lines correspond to the Krivoruchenko model.

E. Electromagnetic pion form factor for the *pn* bremsstrahlung

Here we discuss the uncertainties related to the implementation of the electromagnetic pion form factor $F_\pi(M)$ motivated by the VDM for the *pn* bremsstrahlung contribution, as advocated in the OBE model in Ref. [94]. With the help of this form factor one hopes to account for the dilepton radiation from the internal charged pion exchange line in $pn \to pne^+e^-$ processes assuming vector dominance, i.e., that the photon couples to dileptons via a ρ^0 meson. This diagram does not exist for the *pp* reaction, so the enhancement should be seen only in *pn* dilepton yield. There is a debate about whether the virtual photon converts fully (i.e., by 100%) to ρ meson ($\gamma^* \to \rho \to e^+e^-$) [95] or by 50% only [96] and the rest decays directly into dileptons ($\gamma^* \to e^+e^-$). In Ref. [96] the electromagnetic pion form factor $F_\pi(M)$ has been parametrized as

$$F_\pi(M^2) = \frac{0.4}{1 - M^2/\lambda^2} + \frac{0.6}{1 - M^2/2m_\rho^2} \frac{m_\rho^2}{m_\rho^2 - M^2 - im_\rho \Gamma_\rho(M^2)}, \quad (18)$$

where $\lambda^2 = 1.9$ GeV^2. The width $\Gamma_\rho(M^2)$ is given in Ref. [96] as

$$\Gamma_\rho^{\rm tot}(M) = \Gamma_{\rho^0 \to \pi\pi} \frac{r_C^2 k^3}{M\left(1 + r_C^2 k^2\right)}, \quad (19)$$

with $k^2 = M^2/4 - m_\pi^2$. The parameter $r_C = 2$ fm is an interaction radius, $\Gamma_{\rho^0 \to \pi\pi} = 0.150$ GeV.

According to the OBE calculations of Ref. [94] for the *pn* reaction at 1.25 GeV, the incorporation of the form factor $F_\pi(M)$ leads to the enhancement of the bremsstrahlung contribution and a better agreement with the HADES data for quasifree *pn* scattering. Following Ref. [94] we have performed a model study by including the form factor from Ref. [96] in our calculations of *pn* bremsstrahlung by simply multiplying the parametrized OBE results from Ref. [41] used in HSD by the form factor of Eq. (18). Indeed, this provides an upper limit because we cannot distinguish the individual diagrams in our parametrization of the bremsstrahlung cross section. We obtain a good agreement with the full OBE calculations from Ref. [94], as shown in Fig. 47, which presents the HSD results for the dilepton differential cross section $d\sigma/dM$ for *pn* [panel (a)] and *pd* [panel (b)] reactions at 1.25 GeV including the electromagnetic pion form factor for the bremsstrahlung channel (denoted as "Brems. NN with F_π") in comparison to the standard HSD calculations without form factor (denoted as "Brems. NN w/o F_π") as in Fig. 6. The

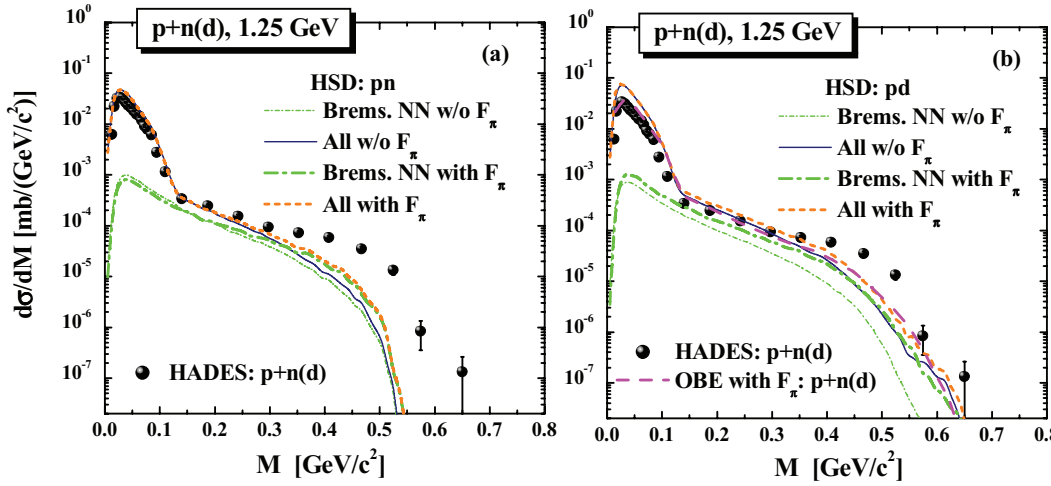

FIG. 47. (Color online) The HSD results for the dilepton differential cross section $d\sigma/dM$ for *pn* (a) and *pd* (b) reactions at 1.25 GeV, including the electromagnetic pion form factor for the bremsstrahlung channel (denoted as "Brems. NN with F_π") in comparison to the standard HSD calculations without form factor (denoted as "Brems. NN w/o F_π") as in Fig. 6. The dashed line [denoted as "OBE with F_π : $p + n(d)$"] shows the OBE results for $p + n(d)$ from Ref. [94].

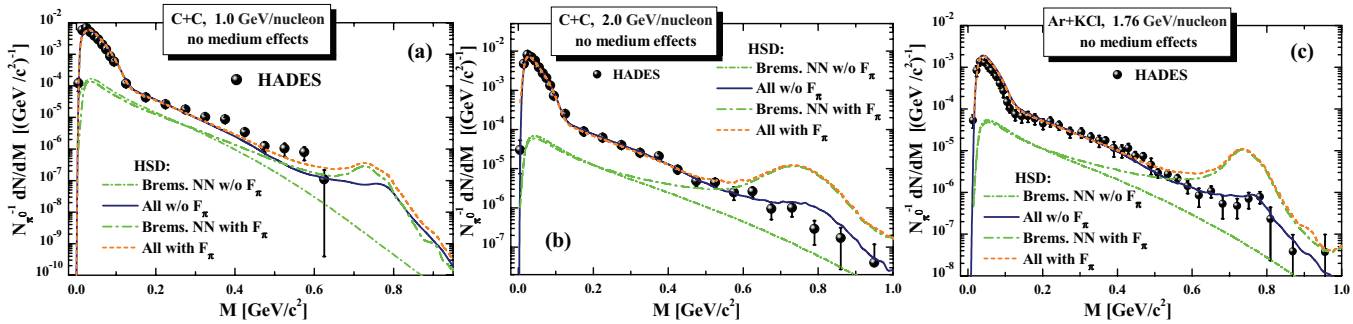

FIG. 48. (Color online) The HSD results for the dilepton differential cross section $d\sigma/dM$ for C + C at 1.0 GeV/nucleon (a), 2.0 GeV/nucleon (b), and Ar + KCl (c) reactions at 1.75 GeV/nucleon. The line descriptions are as in Fig. 47.

dashed line [denoted as "OBE with F_π : $p + n(d)$"] shows the OBE results for $p + n(d)$ from Ref. [94].

As seen from Fig. 47 the inclusion of the form factor does not explain the experimental HADES quasifree $p + n(d)$ data. We check now how the form factor will change the heavy-ion results where we have reliable experimental constraints from the HADES measurements. The HSD results for the dilepton differential cross section $d\sigma/dM$ for C + C at 1.0 GeV/nucleon [panel (a)], 2.0 GeV/nucleon [panel (b)], and Ar + KCl [panel (c)] reactions at 1.75 GeV/nucleon are shown in Fig. 48. One can clearly see a sizable overestimation of the dilepton yields for all systems which brings us to the conclusion that to include a form factor is not supported by the experimental data on heavy-ion collisions.

VII. CONCLUSIONS

We have studied the production of dileptons in pp, pn, pA, and AA collisions at energies between 1 and 3.5 GeV/nucleon by comparing the results of three independent transport approaches—HSD, IQMD, and UrQMD—with all existing data in this energy domain. These data allowed for the first time to study the cycle of creation and absorption of the Δ resonance in heavy-ion reaction, which has been theoretically predicted since long ago.

Despite the common general ideas of transport approaches which are based on the modeling/parameterizations of BB, mB, and meson-meson elementary reactions with further dynamical evolution including the propagation in a self-generated mean-field potential and explicit interactions, the models differ in the actual realization and underlying assumptions where no control from experimental data is available.

Especially for one of the dominant channels for the dilepton production in this energy domain, the Δ-Dalitz decay, the experimental results do not allow for a robust parametrization of the input for these transport theories. Neither the spectral function of the Δ nor the differential decay width of the Δ into dileptons are well known. At energies around 1 GeV/nucleon the Δ production is in agreement with the isospin model, which assumes that the difference Δ states are produced according to the isospin Clebsch Gordon coefficients at higher energies, where two-pion channels contribute substantially, little information is available on population of the different Δ states. This situation will hopefully change with the planned experiments on dilepton production in πN collisions. Such information would substantially improve the predictive power of transport theories for heavy-ion results.

The situation is similar for the bremsstrahlung contribution, which turns out to be the dominant channel for the low-energy collisions at 1 GeV/nucleon. The present OBE models provide different predictions as compared to the soft-photon-approximation and do not agree among each other. More precise data, especially on dilepton production in elementary pp, pn, and especially πN collisions for different energies, are need to reduce this systematic error. They would allow for a more reliable predictions of bremsstrahlung in transport approaches.

We stress the importance of providing such constraint form the experimental side because the transport models constitute the only reliable tool to study the physics of heavy-ion collisions at those energies where neither thermal models nor hydrodynamic models are applicable because the created matter is far from equilibrium.

Despite these uncertainties the results of different transport approaches for the final dilepton yield agree quite well among each other even if there are the deviations in the channel decompositions. The data are between the systematical error of the transport predictions.

We have started our investigation with the dilepton spectra from elementary reactions which can be described as a superposition of the emission from known dilepton sources. In pp collisions at energies of around 1 GeV dileptons stem dominantly from the Δ-Dalitz decay, whereas in pn collisions the bremsstrahlung radiation becomes equally important. At higher energies the η production sets in and contributes to the invariant mass range $M < 0.55$ GeV. At higher invariant masses the vector meson decays dominate but the data are presently not precise enough to allow for firm conclusions. New experimental differential data would be very useful to check the underlying model assumptions.

Our study demonstrates that in heavy-ion reactions the dilepton production for invariant masses below $M < 0.6$ GeV cannot be interpreted as a simple convolution of the average dilepton yield from pn and pp collisions times the number of elementary collisions. The presence of a nuclear medium manifests itself in several ways: First of all, the Fermi motion of nucleons in nuclei smears out the energy distribution of

primary NN collisions substantially. This has a big influence on the particle production at (sub-)threshold energies. The Fermi motion enhances the pion as well as the dilepton yields in AA collisions at threshold energies by up to a factor of two. The enhancement is, however, identical for pions and dileptons. Therefore, if the Fermi motion would be the only difference between AA and NN collisions, one could expect that if one normalizes the dilepton yield to the pion multiplicity, as done in the experimental analysis, no enhancement would be observed.

The real situation is quite different: An enhancement of the dilepton yield in AA relative to NN is observed experimentally even if one normalizes the dilepton yield by the π^0 multiplicity. The experimental enhancement is, however, plagued partly by the use of pd collisions instead of pn collisions because in the interesting kinematical regime the pd collisions are true three-body collisions and cannot be interpreted as quasifree pn reactions. So the "true" enhancement—as compared to elementary collisions—cannot be inferred from present data for invariant masses above 0.5 GeV.

We have analyzed this enhancement in detail and found two origins. The first reason is the bremsstrahlung radiation from pn and pp reactions, which does not scale with the pion number (i.e., the number of participants), but rather with the number of elementary elastic collisions. The second reason is the shining of dileptons from the intermediate Δ's, which take part in the $\Delta \rightarrow \pi N$ and $\pi N \rightarrow \Delta$ reaction cycle. This cycle produces a number of generations of Δ's during the reaction which increase with the size of the system. At the end only one pion is produced but each intermediate Δ has contributed to the dilepton yield because emitted dileptons do not get absorbed. This leads to an enhancement of the dilepton yield as compared to the final number of pions. Thus, the enhancement confirms the predictions of transport theories that in heavy-ion collisions several generations of Δ's are formed which decay and are recreated by $\pi N \rightarrow \Delta$ reactions. Accordingly, the dilepton data from AA reactions shed light on the Δ dynamics in the medium.

In the investigated invariant mass range, $M < 0.5$ GeV, we do not find evidence that the observed enhancement of the dilepton yield in heavy-ion collisions over the elementary reactions requires the assumption of conventional in-medium effects like a modification of the spectral functions of the involved hadrons. Theory predicts such a modification for vector mesons and therefore for invariant masses $M > 0.5$ GeV. More precise data are needed to draw robust conclusions on the in-medium modifications in this invariant mass range.

We summarize with the final remark that the ratio of dilepton yields AA/NN is a sensitive observable that makes it possible to penetrate the intermediate phase of the heavy-ion reaction and sheds light on the Δ dynamics which is not accessible by the hadronic observables. Thus, the HADES data provide the first experimental constraint on this issue in heavy-ion collisions at SIS energies. Moreover, by measuring this ratio at a low bombarding energy one can get access to the bremsstrahlung radiation because it becomes the dominant process there. One expects to observe in this case the scaling of the ratio with the number of binary collisions rather than with the number of pions. A precise measurement of the ratio of dilepton yields in heavy-nuclei collisions (as Au + Au or Pb + Pb) and of that in the light systems (as C + C) for invariant masses $M > 0.5$ GeV will help to obtain information on the in-medium modification of the spectral function of vector mesons.

ACKNOWLEDGMENTS

The authors are grateful for fruitful discussions with W. Cassing, C. Hartnack, S. Endres, L. Fabbietti, M. Gumberidze, F. Krizek, Y. Leifels, O. Linnyk, A. Rustamov, J. Stroth, P. Salabura, H. van Hees, M. Weber, and J. Weil. Our special thanks go to T. Galatyuk and R. Holzmann for the continuous help and useful advice concerning the experimental data and filtering procedure. E.B. and S.V. acknowledge financial support through the "HIC for FAIR" framework of the "LOEWE" program.

[1] Z. Fodor and C. Hoelbling, Rev. Mod. Phys. **84**, 449 (2012).
[2] G. E. Brown and M. Rho, Phys. Rev. Lett. **66**, 2720 (1991).
[3] G. E. Brown, C. H. Lee, M. Rho, and V. Thorsson, Nucl. Phys. A **567**, 937 (1994).
[4] T. Hatsuda, S. H. Lee, and H. Shiomi, Phys. Rev. C **52**, 3364 (1995).
[5] M. Asakawa, C. M. Ko, P. Lévai, and X. J. Qiu, Phys. Rev. C **46**, R1159 (1992).
[6] M. Herrmann, B. Friman, and W. Nörenberg, Nucl. Phys. A **560**, 411 (1993).
[7] G. Chanfray and P. Schuck, Nucl. Phys. A **545**, 271c (1992).
[8] F. Klingl and W. Weise, Nucl. Phys. A **606**, 329 (1996); F. Klingl, N. Kaiser, and W. Weise, *ibid.* **624**, 527 (1997).
[9] G. Chanfray, R. Rapp, and J. Wambach, Phys. Rev. Lett. **76**, 368 (1996).
[10] R. Rapp, G. Chanfray, and J. Wambach, Nucl. Phys. A **617**, 472 (1997).
[11] W. Peters, M. Post, H. Lenske, S. Leupold, and U. Mosel, Nucl. Phys. A **632**, 109 (1998).
[12] S. Leupold, W. Peters, and U. Mosel, Nucl. Phys. A **628**, 311 (1998).
[13] L. Tolós, A. Ramos, and A. Polls, Phys. Rev. C **65**, 054907 (2002).
[14] L. Tolós, R. Molina, E. Oset, and A. Ramos, Phys. Rev. C **82**, 045210 (2010).
[15] G. Agakichiev *et al.* (CERES Collaboration), Eur. Phys. J. C **41**, 475 (2005).
[16] J. Seixas *et al.* (NA60 Collaboration), J. Phys. G **34**, S1023 (2007); S. Damjanovic *et al.*, Nucl. Phys. A **783**, 327c (2007); R. Arnaldi *et al.*, Eur. Phys. J. C **61**, 711 (2009).
[17] H. van Hees and R. Rapp, J. Phys. G **34**, S1051 (2007).
[18] C. Gale and S. Turbide, Nucl. Phys. A **783**, 35 (2007).
[19] T. Renk and J. Ruppert, arXiv:hep-ph/0605130.
[20] E. L. Bratkovskaya, O. Linnyk, and W. Cassing, Phys. Lett. B **670**, 428 (2009).
[21] O. Linnyk, W. Cassing, J. Manninen, E. L. Bratkovskaya, and C. M. Ko, Phys. Rev. C **85**, 024910 (2012).

[22] E. Santini, J. Steinheimer, M. Bleicher, and S. Schramm, Phys. Rev. C **84**, 014901 (2011).
[23] H. S. Matis *et al.* (DLS Collaboration), Nucl. Phys. A **583**, 617C (1995).
[24] W. K. Wilson *et al.* (DLS Collaboration), Phys. Rev. C **57**, 1865 (1998).
[25] W. K. Wilson *et al.* (DLS Collaboration), Phys. Lett. B **316**, 245 (1993).
[26] R. J. Porter *et al.* (DLS Collaboration), Phys. Rev. Lett. **79**, 1229 (1997).
[27] G. Wolf, W. Cassing, and U. Mosel, Prog. Part. Nucl. Phys. **30**, 273 (1993); Nucl. Phys. A **552**, 549 (1993); **545**, 139C (1992).
[28] E. L. Bratkovskaya, W. Cassing, and U. Mosel, Phys. Lett. B **376**, 12 (1996).
[29] L. Xiong, Z. G. Wu, C. M. Ko, and J. Q. Wu, Nucl. Phys. A **512**, 772 (1990).
[30] C. Ernst, S. A. Bass, M. Belkacem, H. Stocker, and W. Greiner, Phys. Rev. C **58**, 447 (1998).
[31] E. L. Bratkovskaya, W. Cassing, R. Rapp, and J. Wambach, Nucl. Phys. A **634**, 168 (1998).
[32] C. Fuchs, A. Faessler, D. Cozma, B. V. Martemyanov, and M. I. Krivoruchenko, Nucl. Phys. A **755**, 499 (2005).
[33] E. L. Bratkovskaya and C. M. Ko, Phys. Lett. B **445**, 265 (1999).
[34] G. Agakishiev *et al.* (HADES Collaboration), Phys. Lett. B **663**, 43 (2008).
[35] Y. C. Pachmayer *et al.* (HADES Collaboration), J. Phys. G **35**, 104159 (2008).
[36] M. Sudol *et al.* (HADES Collaboration), Eur. Phys. J. C **62**, 81 (2009).
[37] G. Agakishiev *et al.* (HADES Collaboration), Phys. Lett. B **690**, 118 (2010).
[38] K. Lapidus *et al.* (HADES Collaboration), arXiv:0904.1128.
[39] G. Agakishiev *et al.* (HADES Collaboration), Phys. Rev. C **84**, 014902 (2011).
[40] E. L. Bratkovskaya and W. Cassing, Nucl. Phys. A **807**, 214 (2008).
[41] L. P. Kaptari and B. Kämpfer, Nucl. Phys. A **764**, 338 (2006).
[42] M. Schäfer, T. S. Biro, W. Cassing, and U. Mosel, Phys. Lett. B **221**, 1 (1989).
[43] M. Thomere, C. Hartnack, G. Wolf, and J. Aichelin, Phys. Rev. C **75**, 064902 (2007).
[44] H. W. Barz, B. Kämpfer, G. Wolf, and M. Zetenyi, arXiv:0910.1541.
[45] E. L. Bratkovskaya and W. Cassing, Nucl. Phys. A **619**, 413 (1997).
[46] W. Cassing and E. L. Bratkovskaya, Phys. Rep. **308**, 65 (1999).
[47] W. Ehehalt and W. Cassing, Nucl. Phys. A **602**, 449 (1996).
[48] K. Weber, B. Blaettel, W. Cassing, H. C. Doenges, V. Koch, A. Lang, and U. Mosel, Nucl. Phys. A **539**, 713 (1992).
[49] B. Andersson, G. Gustafson, and H. Pi, Z. Phys. C **57**, 485 (1993).
[50] E. L. Bratkovskaya, W. Cassing, and U. Mosel, Nucl. Phys. A **686**, 568 (2001).
[51] Gy. Wolf *et al.*, Nucl. Phys. A **517**, 615 (1990).
[52] R. Shyam and U. Mosel, Phys. Rev. C **67**, 065202 (2003).
[53] F. de Jong and U. Mosel, Phys. Lett. B **392**, 273 (1997).
[54] W. Cassing and S. Juchem, Nucl. Phys. A **665**, 377 (2000); **672**, 417 (2000).
[55] W. Cassing, V. Metag, U. Mosel, and K. Niita, Phys. Rep. **188**, 363 (1990).
[56] G. Agakishiev *et al.* (HADES Collaboration), Eur. Phys. J. A **A48**, 64 (2012).
[57] H. Calén *et al.*, Phys. Rev. C **58**, 2667 (1998).
[58] P. Moskal *et al.*, Prog. Part. Nucl. Phys. **49**, 1 (2002).
[59] P. Moskal *et al.*, Int. J. Mod. Phys. A **20**, 1880 (2005).
[60] G. Agakishiev *et al.*, Eur. Phys. J. A **48**, 74 (2012).
[61] Landolt-Börnstein, New Series, edited by H. Schopper, I/12 (1988).
[62] F. Balestra *et al.*, Phys. Rev. C **63**, 024004 (2001); Phys. Rev. Lett. **89**, 092001 (2002).
[63] S. Teis, W. Cassing, M. Effenberger, A. Hombach, U. Mosel, and Gy. Wolf, Z. Phys. A **356**, 421 (1997); **359**, 297 (1997).
[64] S. A. Bass *et al.*, Prog. Part. Nucl. Phys. **42**, 279 (1998).
[65] M. Bleicher *et al.*, J. Phys. G **25**, 1859 (1999).
[66] I. Fröhlich *et al.*, PoS **ACAT2007**, 076 (2007).
[67] J. Weil, H. van Hees, and U. Mosel, Eur. J. Phys. A **48**, 111 (2012).
[68] M. Antinucci *et al.*, Lett. Nuovo Cimento **6**, 121 (1973); M. Gaździcki and D. Röhrich, Z. Phys. C **71**, 55 (1996); J. Bächler *et al.* (NA49 Collaboration), Nucl. Phys. A **661**, 45 (1999).
[69] G. Agakishiev *et al.* (HADES Collaboration), Phys. Rev. C **85**, 054005 (2012).
[70] P. Adlarson *et al.* (WASA-at-COSY Collaboration), Phys. Lett. B **706**, 256 (2012).
[71] L. Alvarez-Ruso, E. Oset, and E. Hernandez, Nucl. Phys. A **633**, 519 (1998).
[72] E. Oset, J. A. Gomez Tejedor, F. Cano, J. C. Nacher, S. Kamalov, L. Alvarez-Ruso, and E. Hernandez, Few-Body Syst. Suppl. **11**, 275 (1999).
[73] X. Cao, B.-S. Zou, and H.-S. Xu, Phys. Rev. C **81**, 065201 (2010).
[74] W. Reisdorf and Y. Leifels (private communication).
[75] W. Reisdorf *et al.* (FOPI Collaboration), Nucl. Phys. A **781**, 459 (2007).
[76] O. Buss, T. Gaitanos, K. Gallmeister, H. van Hees, M. Kaskulov, O. Lalakulich, A. B. Larionov, T. Leitner *et al.*, Phys. Rep. **512**, 1 (2012).
[77] C. Hartnack, R. K. Puri, J. Aichelin, J. Konopka, S. A. Bass, H. Stoecker, and W. Greiner, Eur. Phys. J. A **1**, 151 (1998).
[78] C. Hartnack, H. Oeschler, Y. Leifels, E. L. Bratkovskaya, and J. Aichelin, Phys. Rep. **510**, 119 (2012).
[79] J. W. Harris, G. Odyniec, H. G. Pugh, L. S. Schroeder, M. L. Tincknell, W. Rauch, R. Stock, R. Bock *et al.*, Phys. Rev. Lett. **58**, 463 (1987).
[80] M. Lacombe *et al.*, Phys. Lett. B **101**, 139 (1981).
[81] P. Danielewicz and G. F. Bertsch, Nucl. Phys. A **533**, 712 (1991).
[82] M. Weber *et al.* (HADES Collaboration), J. Phys.: Conf. Ser. **316**, 012007 (2011); G. Agakishiev *et al.*, Phys. Lett. B **715**, 304 (2012).
[83] G. Agakishiev *et al.* (HADES Collaboration), Eur. Phys. J. A **40**, 45 (2009).
[84] D. Schumacher, S. Vogel, and M. Bleicher, Acta Phys. Hung. A **27**, 451 (2006).
[85] K. Schmidt, E. Santini, S. Vogel, C. Sturm, M. Bleicher, and H. Stöcker, Phys. Rev. C **79**, 064908 (2009).
[86] S. Endres and M. Bleicher, J. Phys. Conf. Ser. **426**, 012033 (2013); S. Endres, M. Bleicher *et al.* (unpublished).
[87] The HADES Collaboration website: http://www-hades.gsi.de/

[88] S. A. Bass, M. Hofmann, C. Hartnack, H. Stoecker, and W. Greiner, Phys. Lett. B **335**, 289 (1994).
[89] H. F. Jones and M. D. Scadron, Ann. Phys. **81**, 1 (1973).
[90] M. I. Krivoruchenko and A. Faessler, Phys. Rev. D **65**, 017502 (2001).
[91] M. Zatenyi and Gy. Wolf, Heavy Ion Phys. **17**, 27 (2003).
[92] J. H. Koch, E. J. Monitz, and N. Ohtsuka, Ann. Phys. **154**, 99 (1984).
[93] F. Iachello, A. D. Jackson, and A. Lande, Phys. Lett. B **43**, 191 (1973); F. Iachello and Q. Wan, Phys. Rev. C **69**, 055204 (2004).
[94] R. Shyam and U. Mosel, Phys. Rev. C **82**, 062201 (2010).
[95] T. Ericson and W. Weise, *Pions and Nuclei* (Clarendon, Oxford, 1988).
[96] G. E. Brown, M. Rho, and W. Weise, Nucl. Phys. A **454**, 669 (1986).